
**SEQUENCE VARIANTS IN THE *RYR1*
GENE AND GENETIC DISEASES:
MALIGNANT HYPERTHERMIA AND
CONGENITAL MYOPATHIES**

Giuseppa Perrotta

Dottorato in Scienze Biotecnologiche –XXII ciclo
Indirizzo Biotecnologie Mediche
Università di Napoli Federico II



Dottorato in Scienze Biotecnologiche – XXII ciclo
Indirizzo Biotecnologie Mediche
Università di Napoli Federico II



**SEQUENCE VARIANTS IN THE *RYR1*
GENE AND GENETIC DISEASES:
MALIGNANT HYPERTHERMIA AND
CONGENITAL MYOPATHIES**

Giuseppa Perrotta

Dottoranda:

Dr.ssa Giuseppa Perrotta

Relatore:

Prof.ssa Antonella Carsana

Coordinatore:

Prof. Ettore Benedetti

ACKNOWLEDGEMENTS

I would like to acknowledge my supervisor, Prof. Antonella Carsana, who guided me through this project with her scientific attitude and gave me the opportunity to learn many things. I was very fortunate to work in a friendly research group. I am very grateful to my colleagues that made my Ph.D time a fruitful and joyful experience. Special thanks to Dr. Alberto Zullo for his scientific contribute and also for many relaxing and fun moments. Endless thanks to my parents, my sister, my brother and my grandmother for their love and support through the years.

TABLE OF CONTENTS

	SUMMARY	pag. 1
	RIASSUNTO	pag. 2
1	INTRODUCTION	pag. 6
1.1	Ryanodine receptor 1 (RYR1)	pag. 6
1.1.1	Structure and topology	pag. 6
1.1.2	Gating of RYR1	pag. 8
1.2	RYR1 in excitation-contraction (E-C) coupling	pag. 10
1.3	Modulation of RYR1 activity	pag. 11
1.3.1	RYR1 and regulatory proteins	pag. 12
	<i>Cav 1.1 channel</i>	pag. 12
	<i>Calmodulin (CaM)</i>	pag. 13
	<i>FKBP12</i>	pag. 14
	<i>Calsequestrin, triadin and junction</i>	pag. 14
	<i>Other proteins</i>	pag. 16
1.3.2	Endogenous modulators of RYR1	pag. 16
	<i>Calcium</i>	pag. 16
	<i>ATP and Mg²⁺</i>	pag. 16
	<i>Redox modifications</i>	pag. 16
	<i>Phosphorylation</i>	pag. 16
1.3.3	Exogenous modulators of RYR1	pag. 17
	<i>Ryanodine</i>	pag. 17
	<i>Caffeine</i>	pag. 17
	<i>Local anesthetics</i>	pag. 17
	<i>Volatile anesthetics</i>	pag. 18
	<i>4-Chloro-m-cresol</i>	pag. 18
	<i>Ruthenium red</i>	pag. 18
	<i>Dantrolene</i>	pag. 18
1.4	RYR1-related diseases	pag. 18
1.4.1	Malignant hyperthermia (MH)	pag. 19
	<i>Etiology</i>	pag. 19
	<i>Diagnosis</i>	pag. 20
	<i>Genetic basis</i>	pag. 20
	<i>Genetic testing</i>	pag. 21

1.4.2	Congenital myopathies	pag. 23
1.4.2.1	Central Core Disease (CCD)	pag. 24
	<i>Diagnosis</i>	pag. 25
	<i>Genetic basis</i>	pag. 25
1.4.2.2	Multiminicore Disease (MmD)	pag. 26
	<i>Diagnosis</i>	pag. 27
	<i>Genetic basis</i>	pag. 27
1.4.2.3	Nemaline rod Myopathy (NM)	pag. 28
	<i>Diagnosis</i>	pag. 28
	<i>Genetic basis</i>	pag. 28
1.4.2.4	Centronuclear myopathy (CNM)	pag. 29
	<i>Genetic basis</i>	pag. 29
1.4.2.5	Congenital neuromuscular disease with uniform Type 1 fibers (CNMDU1)	pag. 30
	<i>Genetic basis</i>	pag. 30
1.4.2.6	Congenital fiber type disproportion (CFTD)	pag. 30
	<i>Genetic basis</i>	pag. 30
1.4.3	Molecular mechanisms in RYR1-related core myopathies	pag. 30
1.4.4	Risk of MH associated with core myopathies	pag. 33
2	AIMS OF THE WORK AND EXPERIMENTAL DESIGN	pag. 34
3	MATERIALS AND METHODS	pag. 35
3.1	Patients	pag. 35
3.2	Genomic DNA extraction	pag. 35
3.3	Polymerase Chain Reaction (PCR)	pag. 35
3.4	Denaturing high performance liquid chromatography (dHPLC)	pag. 39
3.5	DNA sequence	pag. 40
3.6	EBV-transformed B-lymphocytes	pag. 40
3.6.1	Production of the Epstein-Barr Virus	pag. 40
3.6.2	Mononuclear cell isolation	pag. 40
3.6.3	EBV infection of human B-lymphocytes	pag. 41
3.7	RNA extraction from EBV-immortalized B-lymphocytes	pag. 41
3.8	cDNA synthesis	pag. 41
3.9	Semi-quantitative PCR	pag. 42
3.10	Capillary gel electrophoresis (CGE)	pag. 43

3.11	Proton release assay	pag. 43
3.12	Calcium release assay	pag. 43
3.13	Statistical analysis	pag. 45
4	RESULTS	pag. 46
4.1	Molecular characterization of DNA sequence variants	pag. 49
4.1.1	Molecular characterization of the double variant S3098I and F4924_V4925insRQGVALLPFF	pag. 50
	<i>Effects of F4924_V4925insRQGVALLPFF insertion on the structure of the RYR1 channel</i>	pag. 51
	<i>Transcription analysis</i>	pag. 53
	<i>mRNA semi-quantitative analysis</i>	pag. 55
4.2	Functional characterization of sequence variants	pag. 57
	<i>Proton release measurements</i>	pag. 57
	<i>Calcium release measurements</i>	pag. 58
5	DISCUSSION	pag. 61
	REFERENCES	pag. 63
	APPENDIX	

LIST OF ABBREVIATIONS

4-CmC	4-chloro-m-cresol
Å	Angstrom
<i>ACTA1</i>	α -actin gene
ATP	Adenosine triphosphate
BSA	Bovine serum albumin
Ca ²⁺	Calcium ion
CaM	Calmodulin
Cav	Voltage-gated calcium
CCD	Central core disease
cDNA	Complementary DNA
CFTD	Congenital fiber type disproportion
CICR	Calcium induced calcium release
CMs	Congenital myopathies
CNM	Centronuclear myopathy
CNMDU1	Congenital neuromuscular disease with uniform Type 1 fibers
<i>CFL2</i>	Cofilin 2
CryoEM	Cryo-electron microscopy
CSQ	Calsequestrin
CY	Cytoplasmic
DHP	Dihydropyridine
dHPLC	Denaturing high performance liquid chromatography
DHPR	Dihydropyridine receptor
EBV	Epstein-Barr virus
E-C	Excitation-contraction
EDTA	Ethylene diamine tetra-acetic acid
EGTA	Ethylene glycol tetraacetic acid
ER	Endoplasmic reticulum
FBS	Fetal bovin serum
FKBP12	12 kDa FK506-binding protein
Fura-2/AM	Fura-2 acetoxymethyl ester
GT	Gomori trichrome
HEK-293	Human embryonic kidney 293 cells
Hepes	4-(2-hydroxyethyl)-1-piperazineethanesulfonic acid
IL	Interleukin
IVCT	<i>In vitro</i> contracture test
K ⁺	Potassium ion
[Ca ²⁺] _i	Intracellular calcium concentration
IP3	Inositol 1, 4, 5-trisphosphate
Mg ²⁺	Magnesium ion
MH	Malignant hypothermia
MHE	Malignant hypothermia equivocal
MHN	Malignant hypothermia normal
MHS	Malignant hypothermia susceptible
MIM	Mendelian inheritance in man
MmD	Multi-minicore disease

MRI	Magnetic resonance imaging
mRNA	Messenger ribonucleic acid
<i>MYH7</i>	β -myosin heavy chain gene
Na ⁺	Sodium ion
<i>NEB</i>	Nebulin gene
NM	Nemalinic myopathy
NO	Nitric oxide
PBS	Phosphate-buffered saline
RYRs	Ryanodine receptors
RYR1	Ryanodine receptor type 1
<i>RYR1</i>	RYR1 gene
RYR2	Ryanodine receptor type 2
RYR3	Ryanodine receptor type 3
<i>SEPN1</i>	Selenoprotein N1 gene
SOC	Store-operated channel
s.e.m.	Standard error of the mean
SR	Sarcoplasmic reticulum
T-tubule	Transverse tubule
TM	Transmembrane
Tn	Troponin
<i>TPM2</i>	β -tropomyosin gene
<i>TPM3</i>	α -tropomyosin gene
<i>TNNT1</i>	Troponin T1
<i>TTN</i>	Titin gene
wt	Wild-type

SUMMARY

This PhD thesis has been focused on the identification and functional characterization of sequence variants in the *RYR1* gene, associated with Malignant hyperthermia (MH) and some congenital myopathies (CMs). MH is an autosomal dominant pharmacogenetic disorder caused by an altered intracellular Ca^{2+} homeostasis. This pathology shows a life threatening hypermetabolic crisis after administration of anaesthetics and/or depolarizing muscle relaxants. MH is syntomatologic silent and until now the only sensitive and specific test for the diagnosis of MH is the *in vitro* contracture test (IVCT), carried out on muscle biopsies. MH presents wide genetic heterogeneity: six genetic *loci* associated with the MH susceptible phenotype (MHS) have been identified. In more than 70% of MHS patients the *locus* segregating with the pathology is MHS-1, where the *RYR1* gene maps. The *RYR1* gene codifies for the ryanodine receptor type 1 (RYR1), a calcium release channel localised in the sarco/endoplasmic reticulum (SR/ER) membrane of skeletal muscle and B-lymphocytes. CMs are a heterogeneous group of inherited neuromuscular disorders characterized by hypotonia and muscle weakness, that usually present at birth or early childhood or rarely adulthood. Myopathies linked to *RYR1* mutations are differentiated on the basis of the histopathological features in: core myopathies (central core disease, multiminicore disease, nemaline rod myopathy, and centronuclear myopathy), characterized histologically by central cores, multi-minicores, nemaline rods, central nuclei in muscle fibers, respectively; and others myopathies (congenital neuromuscular disease with uniform Type 1 fibers, and congenital fiber-type disproportion myopathy) characterized histologically by the almost exclusive presence of Type 1 muscle fiber and relative hypotrophy of type 1 muscle fibers, respectively. Great phenotypic and histopathological overlap and marked phenotypic variability are present in different myopathies. So far more than 200 sequence variants have been identified in the *RYR1* gene, but only 28 variants have been investigated for their functional effect and included in the guidelines for molecular genetic detection of MH susceptibility (www.emhg.org).

In this study, the mutation analysis of the *RYR1* gene was performed by Denaturing High Performance Liquid Chromatography (dHPLC) and automatic sequencing in 24 MHS subjects, one CCD patient and one with minicores. 14 *RYR1* gene sequence variants, an *in-frame* insertion variant and several known and novel polymorphisms have been identified. We characterized the effect of nine *RYR1* variants on the channel function. The functional characterization was performed by two *in vitro* assays, proton and calcium release assays, on Epstein-Barr virus immortalized B-lymphocytes from patients carrying the sequence variants. The results showed alterations in the functional activity of the RYR1 mutated channel.

RIASSUNTO

Questo lavoro di tesi è stato incentrato sull'identificazione e sull'analisi funzionale di varianti di sequenza nel gene *RYR1*, associate all'Ipertermia Maligna (MH) e ad alcune miopatie congenite: miopatia *Central Core* (CCD), miopatia *Multiminicore* (MmD), miopatia nemalinica (NM), miopatia centronucleare (CNM), miopatia congenita neuromuscolare con prevalenza di fibre di tipo 1 (CNMDU1) e miopatia congenita con alterata proporzione dei tipi di fibre (CFTD). L'MH è una malattia neuromuscolare, a trasmissione autosomica dominante nell'uomo, è dovuta ad un'alterata regolazione del calcio intracellulare e si manifesta con una crisi ipermetabolica potenzialmente letale in seguito alla somministrazione dei più comuni anestetici e miorilassanti depolarizzanti in soggetti geneticamente suscettibili (MHS). L'MH mostra un'elevata eterogeneità genetica, sono stati, infatti, identificati sei *loci* genici (MHS1 MIM 180901, MHS2 MIM 154275, MHS3 MIM 154276, MHS4 MIM 600467, MIM MHS5 601887, MHS6 MIM 601888) associati al fenotipo MHS. In più del 70% dei pazienti MHS è stata trovata associazione con il *locus* MHS1, dove mappa il gene *RYR1* che codifica il canale di rilascio del calcio RYR1 presente sul reticolo sarco/endoplasmatico (SR/ER) del muscolo scheletrico e dei linfociti B. L'unico test sensibile e specifico accettato dalla comunità scientifica per la diagnosi di MH è un saggio di contrazione *in vitro* (IVCT) che valuta *ex vivo* la contrazione di fibre muscolari sottoposte a trattamento con alotano e caffeina. La CCD è una rara miopatia congenita raramente progressiva, a trasmissione autosomica dominante, caratterizzata da ipotrofia e ipotonia nell'età infantile. La diagnosi clinica è effettuata mediante analisi istologica di campioni derivati da biopsie muscolari che presentano numerose aree circolari amorphe, definite *cores*, caratterizzate da basso numero di mitocondri, ridotta attività enzimatica ossidativa e disorganizzazione dei sarcomeri nelle fibre di tipo I. La MmD è una condizione clinicamente eterogenea, trasmessa come carattere autosomico recessivo, le cui caratteristiche generali includono ipotonia neonatale, sviluppo ritardato del sistema motorio, debolezza muscolare generale e amiotrofia che può lentamente progredire o rimanere stabile. La biopsia muscolare mostra piccole aree multiple caratterizzate da disorganizzazione dei sarcomeri e perdita di mitocondri a carico sia delle fibre di tipo I che di tipo II. La NM è una rara malattia neuromuscolare ereditaria caratterizzata generalmente da debolezza muscolare non progressiva di gravità variabile. Le principali manifestazioni cliniche comprendono debolezza muscolare, ipotonia e riflessi tendinei profondi, assenti o ridotti. La malattia è ereditata come tratto autosomico dominante e autosomico recessivo. La diagnosi è confermata mediante analisi istologica di campioni derivati da biopsie muscolari che presentano nel citoplasma delle fibre muscolari piccole strutture bastoncellari (*nema* in greco significa proprio bastoncello), costituite da aggregati di proteine (α -actinina), e in alcuni casi anche i *cores*. La CNM è una malattia neuromuscolare ereditaria la cui trasmissione può essere *X-linked* recessiva, autosomica dominante e recessiva. Il quadro clinico è altamente variabile. La biopsia muscolare mostra la presenza di nuclei al centro delle fibre muscolari anziché alla periferia, spesso circondati da un alone chiaro, con disposizione a catenella nelle fibre osservate longitudinalmente. Queste fibre assomigliano ai miotubi, cioè alle fibre muscolari nelle prime fasi dello sviluppo maturativo, che hanno appunto i nuclei centrali. Inoltre, in alcune fibre si evidenziano anche i *cores*. La CNMDU1 è una rara forma di miopatia congenita caratterizzata dalla prevalenza di fibre muscolari di tipo 1 (>99%). Clinicamente, la CNMDU1 mostra le caratteristiche

tipiche di una miopatia congenita, con debolezza muscolare nell'età infantile. La CFTD è una rara miopatia caratterizzata da ipotrofia delle fibre di tipo 1, la cui trasmissione può essere *X-linked* recessiva, autosomica dominante e recessiva. I pazienti con CFTD mostrano ipotonia e debolezza muscolare generalizzata di gravità variabile. Quindi la diagnosi di tutte queste miopatie si basa sull'analisi istopatologica delle biopsie muscolari e sui segni clinici evocativi.

Finora sono state identificate più di 200 mutazioni puntiformi nel gene *RYR1* che segregano con l'MH (la maggior parte), CCD, MmD e in numero minore con le altre miopatie congenite descritte. Solo per alcune mutazioni è stata dimostrata la correlazione con il fenotipo malattia, mediante saggi *in vitro* che valutano le alterazioni nella funzionalità dei canali RYR1 mutati, e 28 di esse sono riportate dalle linee guida 2009 del Gruppo Europeo dell'MH (www.emhg.org) come causative del fenotipo MHS e/o CCD. Tali saggi sono anche per effettuare correlazioni genotipo-fenotipo.

I principali saggi descritti in letteratura valutano il rilascio del Ca^{2+} da parte di RYR1 in risposta ad agenti scatenanti e prevedono l'utilizzo di colture di miotubi o di linfociti B immortalizzati derivati da pazienti portatori di mutazioni in eterozigosi o transfezione ed espressione di cDNA di RYR1 mutati in cellule HEK-293 o in miotubi provenienti da soggetti normali. Per la valutazione del rilascio di calcio citoplasmatico sono stati utilizzati degli indicatori fluorescenti in grado di legare il calcio libero e sistemi microfisiometrici che misurano la variazione di attività metabolica cellulare come rilascio protonico extracellulare.

Nel presente progetto di tesi è stata utilizzata la tecnica della cromatografia in fase liquida ad alte prestazioni in condizioni semi-denaturanti (dHPLC) per l'analisi di mutazioni in 26 soggetti, di cui 24 MHS, uno affetto da CCD e uno da MmD. L'analisi di mutazioni ha portato all'identificazione di 14 varianti di sequenza, un'inserzione *in-frame* e molti polimorfismi. Tutte le varianti di sequenza sono state caratterizzate molecolarmente e nove di esse sono state anche caratterizzate funzionalmente mediante saggi *in vitro*. Nove varianti di sequenza [c.1589G>A (p.R530H), c.1840C>T (p.R614C), c.6488G>C (p.R2163P), c.6502G>A (p.V2168M), c.6635T>A (p.V2212D), c.7025A>G (p.N2342S), c.7361G>A (p.R2454H), c.11708G>A (p.R3903Q) and c.12700G>C (p.V4234L)] sono state precedentemente identificate anche da altri gruppi di ricerca in soggetti MHS. In questo lavoro la variante p.R3903Q è stata identificata in omozigosi in un paziente affetto da MmD, in accordo con la trasmissione autosomica recessiva della patologia. Cinque varianti [c.7112A>G (p.E2371G), c.7035C>A (p.S2345R), c.7355G>C (p.A2452P), c.9293T>A (p.S3098I) and c.13990T>C (p.C4664R)] sono nuove varianti di sequenza. Infine, in un paziente affetto da CCD oltre alla variante *missense* p.S3098I è stata identificata anche la variante-inserzione p.F4924_V4925insRQGVALLPFF. Tale variante consiste in un'inserzione *in frame* di 30 nucleotidi nell'esone 102 e determina a livello proteico l'inserzione 10 aminoacidi nel dominio transmembrana M10 della regione C-terminale di RYR1. La regione C-terminale transmembrana di RYR1 contiene le sequenze che formano il poro, siti di legame per la rianodina, siti multipli di inattivazione del canale ed è fondamentale anche per l'organizzazione tetramerica del canale RYR1. In particolare l'inserzione mutazione cade in un' α – elica adiacente la putativa regione che forma il poro del canale. Gli studi di predizione della struttura secondaria, attraverso il programma Emboss' Garnier, e l'analisi del profilo di idropatia, attraverso il programma Octanol, mostrano che l'inserzione p.F4924_V4925insRQGVALLPFF interrompe l'organizzazione strutturale

ad elica e modifica il profilo di idropatia del dominio M10 del canale RYR1 mutato. Inoltre, lo studio delle sequenze adiacenti l'inserzione ha dimostrato che la sequenza inserita corrisponde ad una porzione dell'introne 105 dello stesso gene *RYR1*, inserita in senso inverso. Per studiare il possibile meccanismo molecolare coinvolto in questa alterazione nucleotidica, è stato eseguito il sequenziamento dell'intera regione genomica dall'introne 102 all'esone 106 del gene *RYR1*. E' stato escluso che l'inserzione fosse dovuta a un evento di trasposizione conservativa in quanto la sequenza dell'introne 105 è conservata. Pertanto, è possibile ipotizzare un evento di trasposizione replicativa come meccanismo responsabile della variante-inserzione. La discriminazione allelica, eseguita mediante una *long range* PCR con un oligonucleotide allele specifico, ha dimostrato che la variante di sequenza p.S3098I e la variante-inserzione sono presenti sullo stesso allele. Inoltre, attraverso studi di espressione è stato dimostrato che nel paziente affetto da CCD la doppia variante nel gene *RYR1* genera un mRNA instabile; infatti, l'espressione dell'allele *RYR1* mutato rappresenta circa il 16% di quella dell'allele *wild type*. Inoltre, lo studio dei livelli di espressione di ciascun allele *RYR1* del paziente affetto da CCD ha mostrato che l'espressione dell'allele *wild type* rappresenta circa il 76% del controllo e quella dell'allele mutato il 13%, quindi i livelli totali di mRNA di *RYR1* nel paziente affetto da CCD sono circa l'89% rispetto al controllo.

Nove varianti di sequenza sono state caratterizzate funzionalmente mediante saggi *in vitro*, in linfociti B immortalizzati con EBV provenienti dai soggetti portatori di tali varianti. L'utilizzo dei linfociti B come sistema cellulare consente di studiare l'attività del canale RYR1 isolato dalle proteine normalmente presenti nel muscolo scheletrico che ne modulano la funzionalità. In particolare, sette varianti di sequenza sono state studiate attraverso un saggio metabolico che misura la risposta cellulare dei linfociti B alle stimolazioni chimiche come rilascio protonico nell'ambiente extracellulare. Le risposte metaboliche alle stimolazioni con il 4-cloro-m-cresolo (4-CmC, un attivatore di RYR1) dei linfociti B portatori delle varianti di sequenza localizzate nelle regioni N-terminale e centrale del canale RYR1 (p.R530H, p.R2163P, p.N2342S, p.S2345R, p.E2371G, p.R2454H) sono significativamente più elevate rispetto a quelle delle linee cellulari di controllo. L'iper-reattività dei canali RYR1 mutati alle stimolazioni con il 4-CmC spiega il fenotipo MHS dei soggetti in cui sono state identificate tali varianti. Invece, la velocità di rilascio protonico in risposta alle stimolazioni con il 4-CmC è significativamente ridotta nei linfociti B portatori della variante p.C4664R, localizzata nella regione C-terminale della proteina, rispetto al controllo. In letteratura è riportato che mutazioni localizzate nella porzione C-terminale di RYR1 conferiscono ai canali ipo-reattività alle stimolazioni chimiche. I canali RYR1 con queste mutazioni sono definiti canali *leaky* perchè liberano Ca^{2+} anche in assenza di stimolazione per cui i depositi dell'ER sono ridotti e liberano minori quantità di Ca^{2+} in seguito a stimolazione di RYR1. Per verificare se la mutazione p.C4664R conferisce al canale un carattere *leaky* è stata misurata la quantità di Ca^{2+} presente come deposito nel ER. Le risposte metaboliche registrate nei linfociti B portatori della variante p.C4664R in risposta al trattamento con la taspigargina (TG), un inibitore delle pompe del Ca^{2+} del SR/ER, sono risultate ridotte di circa il 50% rispetto al controllo. Questo dato indica che i depositi di Ca^{2+} nel ER delle cellule che esprimono la variante di sequenza C4664R sono ridotti. I saggi citfluorimetrici di rilascio di calcio in risposta alla TG eseguiti sui linfociti che esprimono la variante p.C4664R hanno confermato il carattere *leaky* dei canali mutati. Infatti la quantità di Ca^{2+} rilasciata dai linfociti che esprimono questa variante in seguito alle stimolazioni sia con il 4-CmC

sia con la TG è significativamente ridotta rispetto al controllo. Infine, l'alterata funzionalità dei canali RYR1 che esprimono la doppia variante di sequenza p.S3098I/F4924_V4925insRQGVALLPFF è stata dimostrata attraverso i saggi citofluorimetrici di rilascio di calcio; i linfociti che esprimono i canali mutati, estratti dal paziente affetto da CCD e immortalizzati, mostrano un aumento significativo del rilascio di calcio, in seguito a stimolazione con 4-CmC, rispetto ai linfociti controllo. I risultati ottenuti in questo lavoro di tesi, in parte pubblicati su *Human Mutation* (2009), contribuiscono ad arricchire le conoscenze sulle basi molecolari delle malattie genetiche associate a mutazioni del gene *RYR1* e sulle loro diverse caratteristiche fisiopatologiche. Inoltre, lo studio dell'influenza di una determinata mutazione sulla struttura e funzione della proteina potrebbe fornire un considerevole contributo alla diagnosi. Infatti, le linee guida per l'analisi molecolare genetica della suscettibilità all'MH indicano che una mutazione del gene *RYR1* può essere considerata causativa di MH solo quando è stato dimostrato, mediante saggi *in vitro*, che essa altera le proprietà di rilascio del calcio del canale RYR1. Pertanto, un individuo che ha una mutazione causativa può essere considerato MHS sulla sola base dei dati biomolecolari, anche in assenza del risultato dell'IVCT. Quindi, in questi casi, l'analisi genetica dà risultati diagnostici conclusivi e il vantaggio per le famiglie MH, specialmente per grandi famiglie o quando i parenti rifiutano di sottoporsi a biopsia muscolare, appare evidente. Inoltre, l'analisi genetica può fornire anche ulteriori dati alla diagnosi strumentale. Infatti, sebbene l'IVCT sia il test di riferimento per l'MH, sono stati identificati rari casi di discordanza tra genotipo, caratterizzato dalla presenza di una mutazione causativa, e fenotipo, tipizzato MHN mediante IVCT. Sulla base di queste osservazioni è stato proposto che tali soggetti, in quanto portatori di una mutazione causativa, debbano essere considerati MHS ai fini clinici. Quindi l'analisi genetica permette di individuare questi rari ma pericolosi casi di falsi negativi e può contribuire alla definizione della sensibilità diagnostica dell'IVCT.

1. INTRODUCTION

1.1 Ryanodine receptor 1 (RYR1)

RYR1 is the skeletal isoform of the ryanodine receptors (RYRs), intracellular ligand-gated Ca^{2+} release channels. RYRs are large homo-tetrameric proteins (molecular weight of 2.26 MDa) present in the sarco/endoplasmic reticulum (SR/ER) membranes, an intracellular calcium storage organelle. RYRs are involved in the control of Ca^{2+} homeostasis by releasing calcium ions from intracellular stores into the cytoplasm [Fill *et al.*, 2002]. Three mammalian isoforms have been identified and named according to the tissue where they were first identified:

- § the skeletal ryanodine receptor, or type 1 (RYR1), the predominant isoform in skeletal muscle [Zorzato *et al.*, 1990], but also expressed in the lymphocyte cells [Sei *et al.*, 1999];
- § the cardiac ryanodine receptor, or type 2 (RYR2), the most abundant isoform in cardiac muscle [Nakai *et al.*, 1990], also present in the cerebellum;
- § the ryanodine receptor 3 (RYR3), expressed in many tissues but originally purified from the brain [Hakamata *et al.*, 1992].

RYRs are encoded by three different genes located on human chromosomes 19q13.1 (*RYR1*), 1q42.1-q43 (*RYR2*) and 15q14-q15 (*RYR3*) [Sorrentino *et al.*, 1993; Otsu *et al.*, 1990; Philips *et al.*, 1996]. At the amino acid level, the three mammalian isoforms share about 70% sequence identity [Rossi and Sorrentino, 2002].

1.1.1 Structure and topology

The RYR1 is encoded by the *RYR1* gene, a large gene organized in 106 exons. RYR1 is made up of four 565-kD subunits which form a Ca^{2+} channel of SR/ER. Each subunit is organized into two principal regions, a transmembrane (TM) region and a cytoplasmic (CY) region. Membrane-spanning portions of each subunit form an ion-conducting pore, whereas the CY region regulates gating *via* interaction with a variety of intracellular messengers. The C-terminal region is on the SR/ER lumen side and contains the hydrophobic pore-forming region, while the remaining 70–80% of the molecule has been assigned to the SR/ER cytoplasmic side and forms a large hydrophilic region, called “foot region”, that contains most ligand binding sites [Sutko *et al.*, 1996]. The topology of the C-terminal region has not yet been elucidated. Depending on the model, the exact number of transmembrane (TM) domain ranges between 4 and 12. Primary sequence and hydropathy plot analysis by Takeshima *et al.* [1989] suggest an arrangement of four transmembrane spanning α -helices (M1 corresponding to the amino acids F4564-Y4580, M2 to P4641-L4664, M3 to Q4836-F4859, and M4 to I4918-I4937) and a final tail facing the SR/ER lumen. In a second model, Zorzato *et al.* [1990] proposed 12 transmembrane domains: M^I (G3124-F3144) and M^{II} (P3188-L3206), both considered to be tentative, and M1 (L3985-A4004), M2 (M4023-A4041), M3 (G4277-A4300), M4 (A4342-F4362), M5 (F4559-Y4580), M6 (L4648-F4671), M7 (F4789-V4820), M8 (L4837-F4856), M9 (M4879-G4898), and M10 (V4914-I4937). M1–M4 in the Takeshima model correspond to M5, M6, M8, and M10 in the Zorzato model. More recently, Du *et al.* [2002] demonstrated that the M^I, M^{II}, M1, M2, and M3 sequences are not membrane-associated. In the Du

model, RYR1 contains eight transmembrane helices and M9 is not a transmembrane helix, but it might form a selectivity filter between M8 and M10 (Fig. 1).

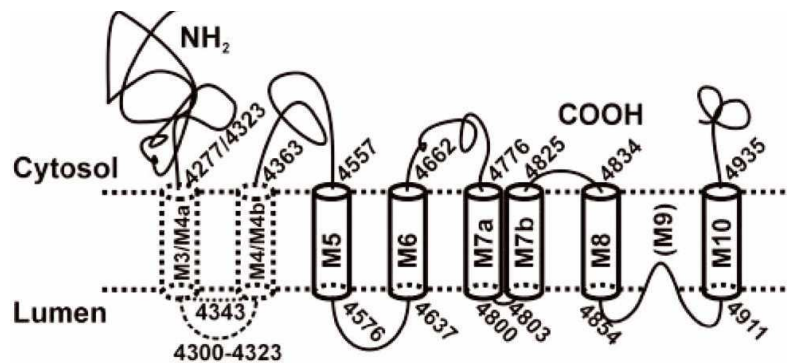


Fig. 1 Transmembrane topology of rabbit skeletal muscle RYR1 [Du model, Du *et al.*, 2002]. The first two cylinders with dashed lines indicate the tentative nature of the composition of the first predicted helical hairpin loop (M3–M4 or M4a–M4b) in the transmembrane sector of RYR1. The numbers, M3–M10, inside each transmembrane sequence are those proposed in the Zorzato model [Zorzato *et al.*, 1990]. The long M7 sequence of the Zorzato model is designated as M7a and M7b. The proposed selectivity filter between M8 and M10 is designated as (M9) and is clearly not a transmembrane sequence (figure from Du *et al.*, 2002). The structure of RYR1 in a closed conformation was determined to 9.6 Å resolution by using cryo-electron microscopy (cryoEM) and computer reconstruction techniques. In the CY region of each RYR1 monomer, 36 α -helices and 7 β -sheets can be resolved (Fig. 2). Several α -helices with various inclination angles to the membrane plane are found in the stem region and could be involved in maintaining the connection between the membrane-spanning and the cytoplasmic regions [Serysheva *et al.*, 2008].

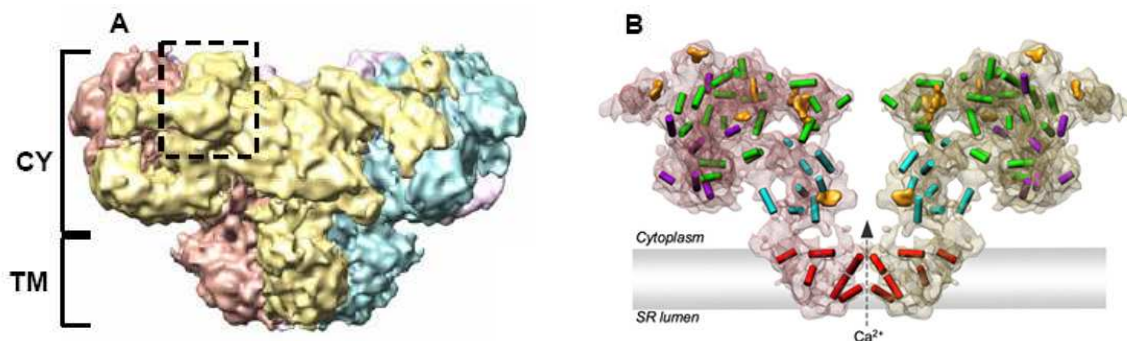


Fig. 2 A. 9.6 Å resolution 3D map of RYR1 in its closed conformation is shown in a side view. CY and TM regions are indicated. Segmented individual RYR1 subunits are shown in different colors. The map is displayed at the threshold level corresponding to channel molecular mass of about 2.3 MDa. **B.** Two opposing RYR1 subunits from the channel tetramer are displayed as semi-transparent surfaces. 36 α -helices are annotated as cylinders colored according to their locations in the map. 7 β -sheets are shown as yellow surfaces (figure from Serysheva *et al.*, 2008).

An atomistic model of the pore-forming region of the tetrameric RYR1 was presented by Ramachandran *et al.*, [2009]. Figure 3 A shows two of the four inner helices and pore helices connected by a long luminal loop. Site-directed mutagenesis [Gao *et al.*, 2000] predicts that RYR1 has a selectivity filter (4894GGGI_{GD}) (Fig. 3 B), which is analogous to K^+ channels [Ludtke *et al.*, 2005]. In fact, mutations in the 4894–4899 sequence of RYR1 alter the conductance of the channel, supporting the assignment

of this sequence as the selectivity filter. Both the cytoplasmic and luminal faces of the pore are highly negatively charged (as seen in the surface representation in Fig. 3C and 3D), which may allow cations to concentrate around the mouths of the pore. The model exhibits structural similarities with the K^+ channel MthK, such as the positioning of the pore helix and the inner helix and the bending of the inner helix, although in RYR1 the pore is significantly wider [Ramachandran *et al.*, 2009].

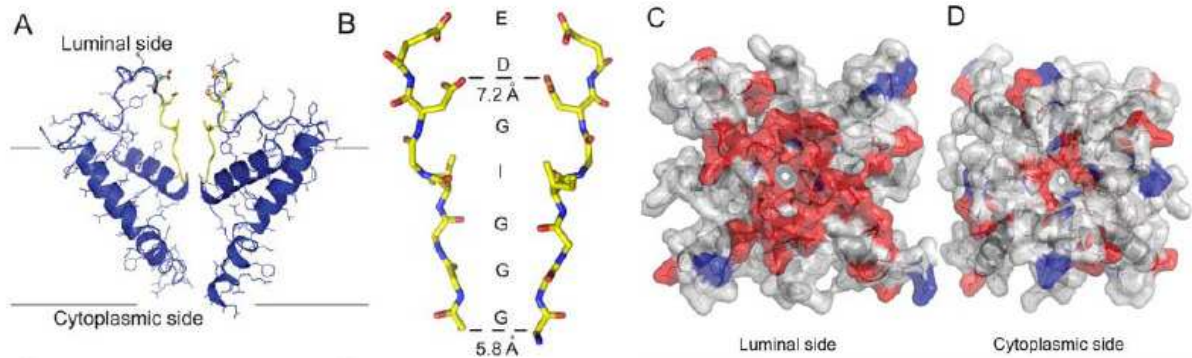


Fig. 3 The pore model. **A.** Two opposing RYR1 monomers shown in cartoon representation. The selectivity filter (the motif 4894GGGIGDE) is shown in yellow. **B.** Selectivity filter region of two opposing RYR1 monomers shown in stick representation. The sequence of the fragment is shown along the path of the ions. The molecular surface of the luminal face (**C**) and the cytoplasmic face (**D**) of RYR1 pore tetramer. Negative residues are shown in red while positive residues are shown in blue and the neutral residues are shown in white (figure from Ramachandran *et al.*, 2009).

1.1.2 Gating of RYR1

Cryo-electron microscopy (cryoEM) and single-particle image analysis of frozen-hydrated RYR1 revealed the 3D structure of RYR1 at approximately 25–30 Å resolution [Serysheva *et al.*, 1995; Radermacher *et al.*, 1994; Wagenknecht and Samsò, 2002]. The cytoplasmic domain is shaped like a flat square prism of 290 Å side and 120 Å high, with at least 12 reproducible domains that have been assigned numerals 1–12 [Samsò *et al.*, 2005]. Recently, Samsò *et al.*, [2009] demonstrated that the ion pathway of RYR1 is formed by two sets of bundles, each containing four rods along a common axis. One set (inner helices) stretches from the lumen to the ion gate, whereas the second (inner branches) stretches from the ion gate to the peripheral cytoplasmic domains. The configuration of the two bundles is clearly different in the two physiological states (closed and open), allowing a 4 Å increase in diameter of the ion gate upon opening. This diameter increase is sufficient to ensure flow of calcium ions. Upon gating, the cytoplasmic domains undergo a conformational change that converges on the inner branches, revealing a long-range allosteric mechanism that directly connects effectors acting on the cytoplasmic moiety with the ion gate. Samsò *et al.*, [2009] proposed that three structures, the inner branches, the inner helices, and horizontal rod-like structure (h1) densities, by forming a mobile axial structure, are the three main gating effectors (Fig. 4). In the closed state (Fig. 4 A), the two right-handed bundles (inner helices, inner branches) form the high-density constriction (ion gate) at their meeting point. In going from the closed to the open state, both sets of bundles relax and appear to contribute equally to lowering the density of the ion gate (see arrows in Fig. 4 A). The h1 densities also contribute

to the constricting effect in the closed state and move outwards as the gate opens. In the closed state, the inner helices form a right-handed helical bundle constricting towards the cytoplasm (Fig. 4 A). A slight decrease in density in the region closest to the cytoplasmic side of the membrane indicates a point of flexibility. In the open conformation (Fig. 4 B), the bottom halves of the inner helices (proximal to the lumen) are reoriented in four ways with respect to the closed state. They are shifted 3 Å along the 4-fold axis towards the cytosol, they are in a more vertical position with respect to the 4-fold axis causing the portion facing the ion gate to move farther away from each other, and they are slightly bent outwards (Fig. 4 B). After this bend, the electron density of the inner helices becomes very weak. The inner helices clearly point to a ring of density that has a larger diameter and is less thick in the open state than in the closed state (Fig. 4 A and 4 B). These data confirm that this ring of density is the ion gate. The outward movement of the h1 densities is concomitant with the outward and upward (toward the cytoplasm) movement of the inner helices upon opening (arrows in Fig. 4 A), which accounts for the slightly wider and shorter appearance of the transmembrane domain in the open state.

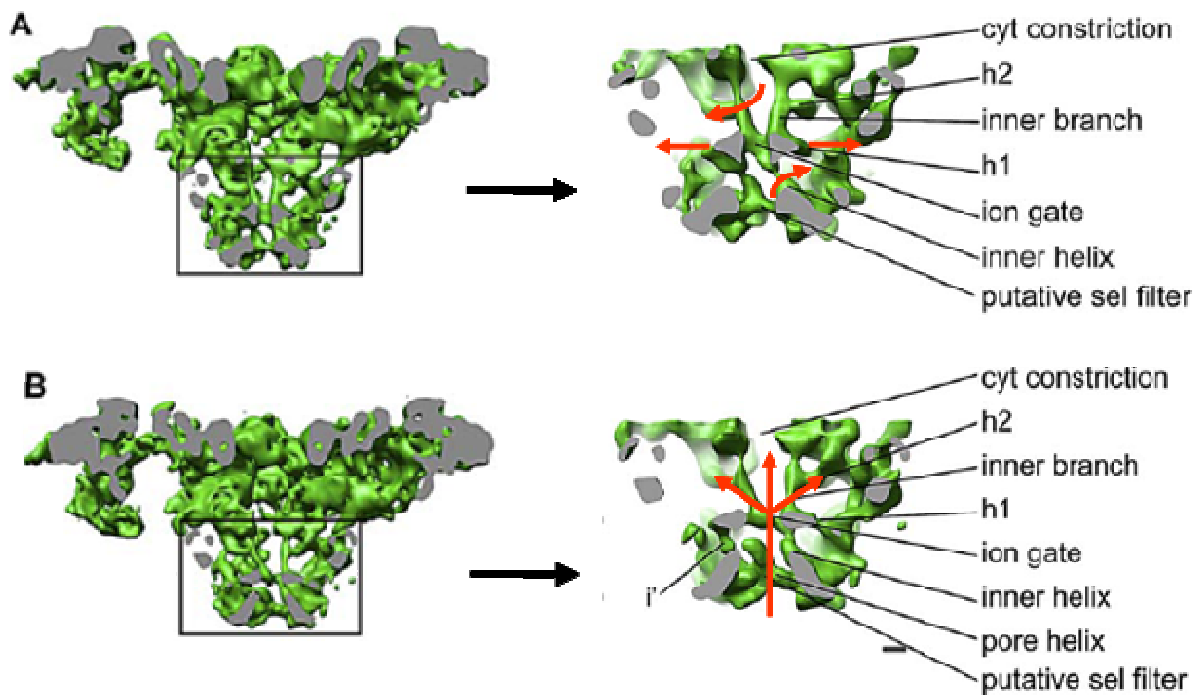


Fig. 4 Stereo view of RYR1 in the closed and open states. Side view of RYR1 in the closed (**A**) and open (**B**) states, respectively, with the region indicated with a square magnified. The two bundles formed by the inner branches and the inner helices define the ion gate at their meeting point. **A.** The arrows indicate how the different structures move upon opening. **B.** The arrows indicate the pathway of the ion flow. The identifiable features are indicated, and the abbreviations are as follows: cytosolic constriction (cyt constriction), horizontal rod-like structures (h1, h2), possible continuation of the inner helices (i'), and putative selectivity filter (putative sel filter). The gray dashed lines indicate the approximate boundary of the SR membrane. Scale bar indicates 10 Å (figure modified from Samsò *et al.*, 2009).

The inner branches become bulkier approximately 25 Å away from the ion gate, and in the closed conformation, they contact each other forming a 10 Å -diameter ring, that represents the cytosolic constriction (Fig. 4). The cytosolic constriction is situated

after the putative ion gate and it does not appear to have a direct role in gating. However, it is conceivable that the cytosolic constriction has a role in stabilizing the closed conformation. The inner branches are probably formed by part of the 4938-5037 C-terminal sequence downstream of the inner helices since one of the predicted α helical segments of this region (Fig. 5) has an estimated length of 21 residues, which is compatible with its physical measurements of 25 Å [Samsò *et al.*, 2009].

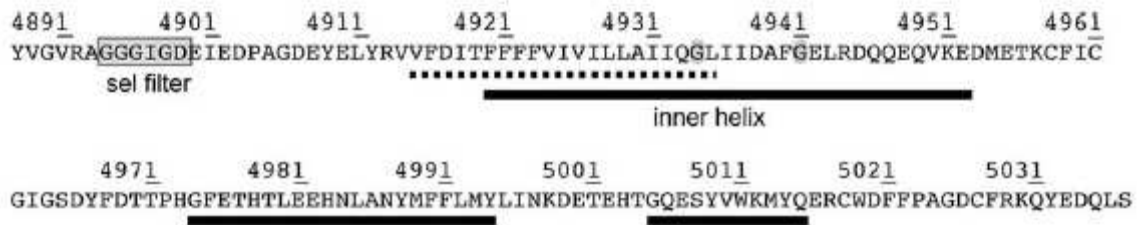


Fig. 5 Secondary Structure Prediction. Predicted regions of hydrophathy (dashed line) and a helix (continuous line) for the C-terminal region of RYR1. The position of the selectivity (sel) filter is also indicated. The G residues (highlighted in gray) are possible points of flexibility (figure from Samsò *et al.*, 2009).

Through the mechanism to open and close the ion gate, RYR1 mediates the Ca^{2+} release from SR stores into the cytoplasm during muscle contraction.

1.2 RYR1 in excitation-contraction (E-C) coupling

Skeletal muscles are made up of individual components known as muscle fibers (Fig. 6). Each muscle fiber is delimited by the plasma membrane (sarcolemma) that through tubular invaginations called transverse tubules (T-tubules) propagates action potentials in the muscle fiber. Muscle fibers are in turn composed of numerous smaller myofibrils which make up the contractile element. Myofibrils are divided into repeating functional units, the sarcomeres. This repeating pattern gives skeletal muscle its striated appearance. A system of membranous sacs, called SR, surrounds the myofibrils.

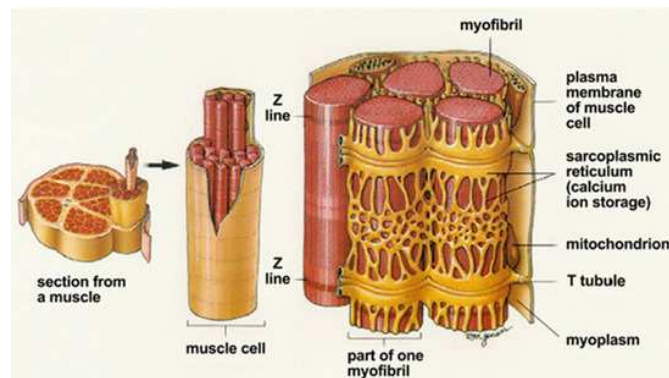


Fig. 6 Illustration of the structure of a skeletal muscle.

The action potential generated by the central nervous system propagates to the motorneuron innervating the muscle cell. At the neuromuscular junction, the

presynaptic terminal nerve releases the transmitter acetylcholine (ACh). ACh diffuses across the synaptic cleft and binds to nicotinic receptors localized on the sarcolemma, opening the voltage-gated Nav1.4 channels, which elicit a Na⁺ inward current with rapid activation kinetics (Fig. 7). Repolarization of the membrane by fast Na⁺ channel inactivation is supported by opening of delayed rectifier K⁺ channels that mediate an outward K⁺ current. Buffering of after potentials is achieved by a high Cl⁻ conductance near the resting potential, resulting from the Cl⁻ channel CIC-1 [Lehmann-Horn *et al.*, 1999]. At specialized junctions in the transverse tubular system, the signal is transmitted from the tubular membrane to the SR, causing the release of Ca²⁺ ions into the myoplasm, which activate the contractile apparatus [Leong *et al.*, 1998]. This process is called E-C coupling, which transform electrical signals into mechanical signal. The combination of one T-tubule and two adjacent terminal cisternae of SR defines a triad, the anatomical site for E-C coupling. Two Ca²⁺ channel complexes are chiefly involved in this process: the ligand-gated homo-tetrameric RYR1, present in the terminal cisternae of SR, and the voltage-gated hetero-pentameric Cav 1 (also called the dihydropyridine (DHP) receptor, DHPR), present in the T-tubule membranes. Cav 1.1 senses the membrane depolarization, alters its conformation, and activates RYR1, which releases Ca²⁺ from the SR. Ca²⁺ binds to troponin C and allows myosin and actin to form cross-bridges leading to the sliding of actin and myosin filaments with respect to each other and the shortening of the sarcomere. The result is muscle contraction [Jurkat-Rott and Frank Lehmann-Horn, 2005].

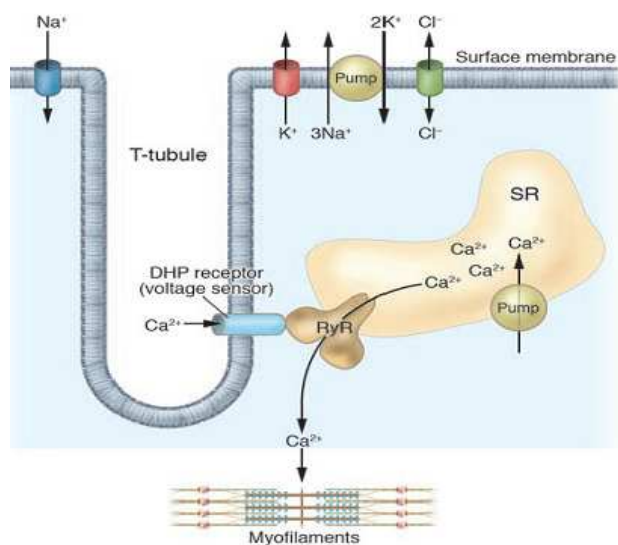


Fig. 7 E-C coupling of skeletal muscle. Depolarization of the T-tubule membrane activates Cav1.1, triggering SR Ca²⁺ release through RYR1 and leading to sarcomere contraction (figure from Jurkat-Rott and Frank Lehmann-Horn, 2005).

1.3 Modulation of RYR1 activity

The RYR1 channels are modulated by several proteins (e.g., Cav 1.1, calmodulin, FKBP12, calsequestrin, triadin, junctin and other proteins), numerous endogenous (e.g., Ca²⁺, ATP, and Mg²⁺, redox modifications, and phosphorylation) and exogenous (e.g., ryanodine, caffeine, local anesthetics, volatile anesthetics, 4-chloro-m-cresol, ruthenium red, and dantrolene) modulators [Fill *et al.*, 2002; Sutko *et al.*, 1997; Zucchi and Ronca-Testoni., 1997].

1.3.1 RYR1 and regulatory proteins

Cav 1.1 channel is the skeletal isoform of the L-type calcium channel alpha subunit Cav 1 and can function both as a voltage sensor and a calcium channel by responding to variation in membrane potential. The several isoforms are classified on the basis of α_1 subunit, e.g. α_{1s} and α_{1c} are skeletal and cardiac isoforms in the Cav 1.1 and Cav 1.2 channels, respectively. Cav 1.1 is a large heteropentamer (435 kDa) containing several subunits: α_{1s} (175-212 kDa), α_2 (140 kDa), β (55 kDa), γ (33 kDa) subunits and the small δ (24-33 kDa) polypeptide chain connected to α_2 . The α_2 , β , γ and δ subunits have regulatory functions, whereas the α_{1s} subunit contains the voltage sensor, the DHP-binding sites and the pore-forming region. The α_{1s} subunit, encoded by *CACNA1S* gene, consists of 4 highly homologous domains, (I-IV), each containing six transmembrane segments (S1-S6) arranged in α -helices (Fig. 8).

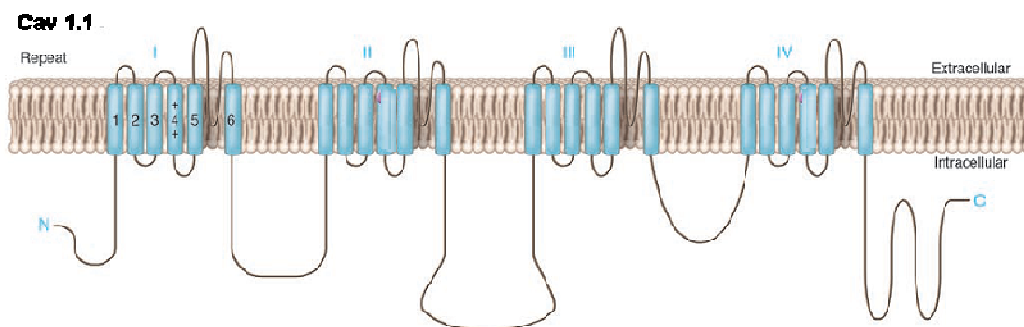


Fig. 8 Structure of voltage-gated Ca^{2+} channel Cav 1.1 (figure from Jurkat-Rott and Frank Lehmann-Horn, 2005).

S4 is positively charged, while the others are hydrophobic. S4 fragment is the voltage-sensor, while the regions between the II-III loop are crucial for E-C coupling [Jurkat-Rott and Frank Lehmann-Horn, 2005]. Bannister *et al.*, [2008] demonstrated that the regions between the III-IV loop are not directly involved in E-C coupling but influence Cav 1.1 gating transitions important both for E-C coupling and activation of L-type conductance.

In skeletal muscle (Fig. 9 B), the T tubule contains the Cav 1.1 channels arranged in clusters of four (tetrads). RYR1 channel is physically coupled with a Cav 1.1 tetrad. The T-tubule membrane depolarization alters the Cav 1.1 conformation. A specific cytosolic loop of the Cav 1.1 is involved in a physical communication with RYR1. As a consequence, the coupling between Cav 1.1 and RYR1 is bidirectional: an orthograde signal from the Cav 1.1 to the RYR1 occurs when depolarisation of the membrane triggers a conformational change of α_{1s} subunit of Cav 1.1 and is translated into the opening of RYR1 and generation of a retrograde signal from RYR1 to the Cav 1.1. In cardiac muscle (Fig. 9 B), there is about one Cav 1.2 for every five-ten RYR2 channels, and the Cav 1.2 and RYR2 channels are not aligned in such a highly ordered fashion. The T-tubule membrane depolarization activates the Cav 1.2, and the resulting Ca^{2+} entry triggers underlying RYR2 channels to open and release Ca^{2+} from the SR. This process is named calcium-induced calcium release (CICR) [Fill *et al.*, 2002].

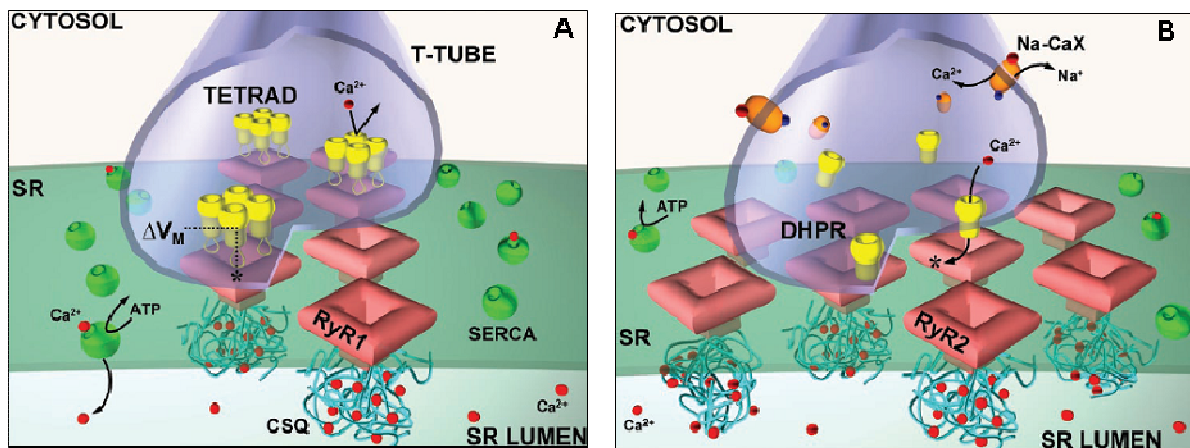


Fig. 9 Environment of the ryanodine receptor channel in skeletal (A) and cardiac (B) muscle (figure from Fill *et al.*, 2002).

Calmodulin (CaM) is a small cytoplasmic Ca^{2+} binding protein that is comprised of two globular domains separated by a central α helical domain. Each of the N and C-terminal domains contains two EF-hand Ca^{2+} binding sites [Zhang *et al.*, 1995]. The two Ca^{2+} binding sites in the C-lobe have a higher Ca^{2+} affinity than the two sites in the N-lobe, resulting in nearly full occupancy at $100 \mu\text{M}$ Ca^{2+} and little binding at $<0.01 \mu\text{M}$ free Ca^{2+} . CaM modulates channel activity in response to changing Ca^{2+} intracellular concentrations, binding to the RYR1 with a stoichiometry of four per channel tetramer. CaM has a bimodal action on channel activity depending on its association with Ca^{2+} [Samsò *et al.*, 2002]. The Ca^{2+} bound form (CaCaM, in micromolar Ca^{2+} concentrations) inhibits RYR1 in the absence of ATP, whereas at low Ca^{2+} concentrations (ApoCaM, in submicromolar Ca^{2+} concentrations) activates RYR1. RYR1 proteolysis and mutagenesis experiments have identified a single CaM-binding domain in the RYR1 channel, corresponding to the amino acid residues 3614–3643, that interacts with both the Ca^{2+} -free (apoCaM) and Ca^{2+} -bound (CaCaM) forms of CaM. [Moore *et al.*, 1999]. Moreover, synthetic peptides corresponding to this region were drawn to bind both apo-CaM and CaCaM [Yamaguchi *et al.*, 2001]. Recently, Cornea *et al.*, [2009] investigated Ca^{2+} -dependent rearrangements of CaM bound to the RYR1 channel by using fluorescence resonance energy transfer (FRET). Small FRET acceptors were covalently attached to single cysteine residues introduced into N lobe of the CaM, central linker, or C lobe. The targeting of FRET donors was a single-cysteine fluorescent labeled of FKBP12 (see next paragraph). Cornea *et al.*, [2009] suggested new insights into the location and orientation of CaM on the RYR1 channel when considered in context with existing structural models. In figure 10 A is shown a recent cryo-EM model of the RYR1 [Serysheva *et al.*, 2008] and the atomic model of CaCaM in complex with the RYR1_{3614–3640} target [Maximciuc *et al.*, 2006]. In figure 10 B is shown a space-filling representation of the CaM-RYR1_{3614–3640} complex, as indicated by cryo-EM mapping of CaCaM [Wagenknecht *et al.*, 1997; Samsò *et al.*, 2002]. The placement of CaM in figure 10 B is consistent with the position of CaCaM in RYR1 cryo-EM models [Wagenknecht *et al.*, 1997]. In the Cornea model, the domain of CaM nearest to FKBP12 and adjacent to the handle region is identified as the N lobe, whereas the C lobe is placed beneath the clamp region. This model thus positions N and C lobe of CaM Ca^{2+} -binding sites within distinct microdomains of the

channel. The location of the RYR1_{3614–3643} target helix within the domain structure of the channel is not defined in existing structural models. In this model, the target helix is placed near the outer edge of domain 3 (Fig. 10 A). Alternatively, the target helix may also lie along the edge of domain 8 without significantly changing distance relationships between CaM and FKBP.

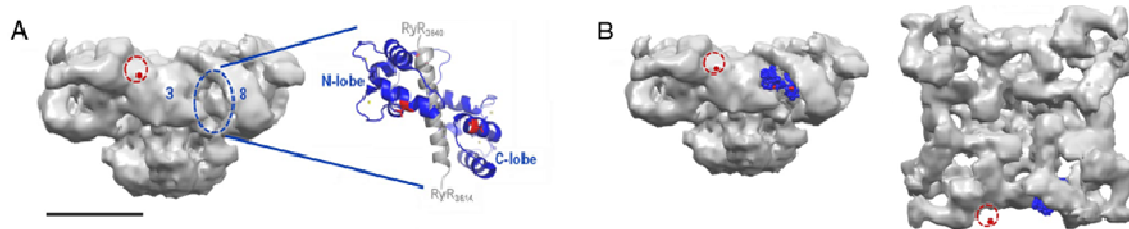


Fig. 10 Suggested placement of CaM within the RYR1 3D architecture. **A. Left** The RYR1 cryo-EM structure is shown in side view. (Scale bar: 100 Å.) The dashed red circle indicates the FKBP12-binding site, and the red dot approximates the predicted position of donor fluorophore attachment based on the model of Samsò *et al.* [2002]. The dashed blue oval approximates the site of CaCaM binding within the cleft separating cytoplasmic domains 3 and 8. **Right** Atomic structure of CaCaM in complex with RYR1_{3614–3640}. Positions of acceptor attachment within N lobe and C lobe of CaM are highlighted in red (labeling site within the central linker is obscured). **B.** Proposed placement of CaM. A space-filling representation of CaM–RYR1_{3614–3640} is positioned within the channel cleft and oriented such that the N lobe is nearest and C lobe farthest from FKBP12, as indicated by FRET (figure from Cornea *et al.*, 2009).

FKBP12 is the 12 kDa FK506-binding protein, a cytosolic receptor for the immunosuppressant drugs FK506 and rapamycin, that constitutively binds to the RYR1. Removal of FKBP12 using FK506 or rapamycin causes an increased open probability and an increase in the frequency of sub-conductance states in RYR1. FKBP12 facilitates the coordination of channel opening to full conductance [Brillantes *et al.*, 1994]. Binding sites for FKBP12 have been localised by cryo EM and this approach has yielded a model of four symmetrically related binding sites about 10 nm apart from the cytoplasmic assembly of the RYR1 [Wagenknecht *et al.*, 1996]. Q3, R18 (N-terminal regions), and M49 residues of FKBP12 are essential and unique for binding of FKBP12 to RYR1 in skeletal muscle [Lee *et al.*, 2006]. Using cryo EM and single-particle image processing, also Samsò *et al.*, [2006] have determined that N-terminal region (Q3 residue) of FKBP12 participates directly in the interaction with RYR1. The orientation of RYR1-bound FKBP12, with part of its FK506 binding site facing towards RYR1, suggests how FK506 is involved in the dissociation of FKBP12 from RYR1.

Calsequestrin, triadin and junctin. Calsequestrin (CSQ) is the major Ca²⁺-binding protein in the lumen of the SR where it forms a linear polymer closely associated with the junctional face membrane [Franzini-Armstrong *et al.*, 1987]. The inhibiting action of CSQ on the RYR1 channel depends on the presence of triadin and junctin [Gyorke *et al.*, 2004] both transmembrane SR proteins which bind to CSQ and the RYR1 forming a quaternary complex (Fig. 11).

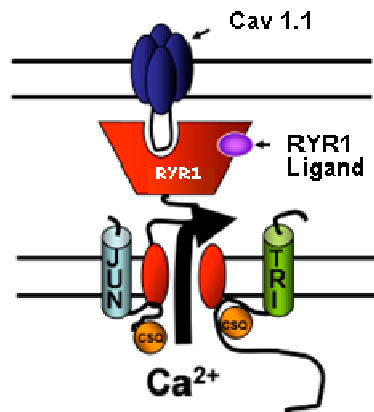


Fig. 11 The quaternary complex: CSQ–triadin (TRI)–RyR1–junction (JUN) [figure from Goonasekera *et al.*, 2007].

CSQ is highly acidic and contains up to 50 Ca^{2+} -binding sites, which are formed simply by clustering of two or more acidic residues. The protein polymerises when Ca^{2+} concentrations approach 1mM. CSQ was considered the main candidate for a luminal Ca^{2+} concentration-detector because Ca^{2+} stabilizes CSQ conformation and the CSQ polymer [Wang *et al.*, 1998]. The response of RyR1 channels to a decreased luminal Ca^{2+} concentration differs in the presence/absence of the CSQ, and thus provides evidence that CSQ is a dominant luminal Ca^{2+} sensor for the RyR1. Recently Qin *et al.*, [2009] demonstrated that no significant luminal Ca^{2+} -sensitivity of RyR1 was detected in the presence of CSQ added to the luminal side of single RyR1 channels over the physiologically relevant range (0.05-1 mM Ca^{2+}). These results indicate that CSQ-dependent luminal Ca^{2+} regulation in skeletal muscle likely plays a relatively minor role in regulating the RyR1 channel activity and that the main role of CSQ1 in this tissue is as an intra-SR Ca^{2+} buffer. In contrast, the luminal Ca^{2+} sensitivity of single RyR2 channels was substantial when CSQ was present.

Triadin was first identified in skeletal muscle as a 95 kDa transmembrane protein [Brant *et al.*,1990] that is abundantly expressed on the junctional SR, where it colocalizes with RyR1 and Cav 1.1 and binds to CSQ and the RyR1 [Guo and Campbell, 1995]. Shen *et al.*, [2007] indicated an indirect role for triadin in regulating myoplasmic Ca^{2+} homeostasis and organizing the molecular complex of the triad but not in regulating skeletal E-C coupling.

Junctin was later discovered and thought to have a comparable function to triadin, due to its similar structure and its ability to also bind CSQ and the RyR1 [Tijskens *et al.*, 2003]. A putative triadin binding site was identified in the terminal intraluminal loop of RyR1 between amino acid residues 4860 and 4917 [Lee *et al.*, 2004]. Alanine substitution of three specific negatively charged residues within this region (D4878, D4907, and E4908) was found to disrupt triadin binding to RyR1 [Lee *et al.*, 2006]. Goonasekera *et al.*, [2007] demonstrated a single mutation to any of these three negatively charged residues is not sufficient to modify RyR1–triadin association and the combination of the different mutations indicates that each residue contributes unequally (D4907 > E4908 > D4878) to triadin to RyR1. This interaction is an important regulator of both voltage- and ligand-induced SR Ca^{2+} release in skeletal muscle. They proposed a model where by triadin binding to RyR1 enhances release channel opening in response to both voltage- and ligand-induced activation and that this activity is important for ensuring robust and rapid calcium release during E-C coupling.

Other proteins interact with the RYR1: sarcoplasmic reticulum protein 35 (SRP35) [Zorzato *et al.*, 2009], sarcoplasmic reticulum protein 27 (SRP27) [Bleuven *et al.*, 2008], JP-45 [Anderson *et al.*, 2003], sorcin [Meyers *et al.*, 1995], S-100 [Treves *et al.*, 1997], mistugumin-29 [Takeshima *et al.*, 1998], junctate [Treves *et al.*, 2000], junctophilin [Takeshima *et al.*, 2000], homer [Feng *et al.*, 2002]. Some proteins, JP-45, SRP27, SRP35, and junctate, are components of the EC-coupling machinery. JP-45 is mainly expressed in skeletal muscle, down regulated during ageing and a component interacting with the subunit of α_{1s} of Cav 1.1 and CSQ. JP-45 appears to be important for the functional expression of the Cav 1.1.

1.3.2 Endogenous modulators of RYR1

Calcium. RYR1 channels are activated by low Ca^{2+} concentrations (1–10 μM) and inhibited by high Ca^{2+} concentrations (1–10 mM). Trypsin digestion of the luminal side of the RYR1 channel suggested the presence of both activating and inactivating divalent sites [Ching *et al.*, 2000]. Ca^{2+} release studies suggested that Ca^{2+} binding to the luminal surface of the RYR1 channel may regulate the channel [Donoso *et al.*, 1996; Donoso *et al.*, 1995]. Sensitivity of RYR1 channel to certain cytosolic agonists increases at high luminal Ca^{2+} levels [Gyorke I and Gyorke S 1998]. Probably, the luminal Ca^{2+} effects are mediated by associated proteins like calsequestrin [Beard *et al.*, 2002] or junctin [Zhang *et al.*, 2001].

ATP and Mg^{2+} . Cytosolic ATP and Mg^{2+} are an effective RYR1 channel activator and inhibitor, respectively. The cytosol of most cells contains ~5 mM total ATP and ~1 mM free Mg^{2+} . The action of ATP and Mg^{2+} on single RYR channel function is isoform specific. Free ATP is a much more effective activator of the RYR1 channel than of the RYR2 channel [Copello *et al.*, 2002], and of the RYR3 channel [Chen *et al.*, 1997]. Mg^{2+} may compete with Ca^{2+} at the Ca^{2+} activation site, shifting the Ca^{2+} sensitivity of the channel. Moreover, Mg^{2+} competes with Ca^{2+} at the high Ca^{2+} inhibition site. The high Ca^{2+} inhibition site does not discriminate between different divalent cations. In the presence of physiological levels of Mg^{2+} and ATP, the RYR1 channel requires less Ca^{2+} to activate than the RYR2 or RYR3 channel [Copello *et al.*, 2002].

Redox modifications. Reactive oxygen species and nitric oxide (NO) derivatives are synthesized by skeletal muscle. Reversible redox modifications of RYR1 are S-nitrosylation, S-glutathionylation, and disulfide oxidation. Each subunit of RYR1 contains 101 cysteines [Sun *et al.*, 2001 a], but one redox-sensitive cysteine (C3635) has been proposed as functionally relevant to the redox sensing properties of the channel. C3635 is selectively nitrosylated [Sun *et al.*, 2001 b], and this modification regulates the interaction of calmodulin with RYR1 [Oba *et al.*, 2002] and is likely to play a modulatory role in voltage-gated E-C coupling. By using mass spectrometry, Voss *et al.*, [2004] identified in RYR1 seven hyper-reactive cysteines (C1040, C1303, C2436, C2565, C2606, C2611, and C3635) that are thought to be targets for disulfide cross-linking, S-nitrosylation, and/or S-glutathionylation. These modifications increase channel activity, but appear to do so by different mechanisms. Both S-nitrosylation and oxidation increase the sensitivity of the channel to Ca^{2+} activation, whereas S-glutathionylation decreases selectively the sensitivity of the channel to

inhibition by Mg^{2+} [Salama *et al.*, 1992] and the response of the channel to nitrosylating agents [Xia *et al.*, 2000].

Phosphorylation. The cAMP-dependent protein kinase PKA and the protein phosphatase 1 (PP1) regulate the phosphorylation/dephosphorylation of the RYR1 channel [Marx *et al.*, 2001]. Reiken *et al.*, [2003] identified the S2843 as unique PKA phosphorylation site on RYR1 using site directed mutagenesis; this PKA phosphorylation site was previously identified by Sutko *et al.*, [1993] using phosphopeptide mapping. PKA phosphorylation of RYR1 at S2843 activates the channel by releasing FKBP12. Recently, Blayney *et al.*, [2009] studied the interaction between RYR1 and FKBP12 by using the experimental inhibitory drug K201, a multi-channel blocker. They demonstrated that phosphorylation and K201 behave similarly to change the conformation of RYR1 and regulate FKBP12 binding. K201 stabilizes the closed conformation, whereas phosphorylation facilitates a subsequent molecular event that might increase the rate of an open/closed conformational transition.

1.3.3 Exogenous modulators of RYR1

Ryanodine gives the name to receptor that specifically binds, RYR channel. Ryanodine is an alkaloid extract from the plant *Ryania speciosa*. Low doses of ryanodine (~10 nM) increase the frequency of single RYR channel openings to the normal conductance level [Buck *et al.*, 1992]. Intermediate ryanodine doses (~1 μ M) induce very-long-duration open events and simultaneously reduces ion conductance through the pore. High doses of ryanodine (~100 μ M) lock the channel in a closed configuration [Zimanyi *et al.*, 1992]. The ryanodine-binding site has been localized to the C-terminus of the protein the region of the RYR1 protein thought to contain the structural determinants of the pore. Each RYR1 monomer contains one high-affinity ryanodine binding site and the additional lower affinity ryanodine binding sites. RYR1 monomers are not able to bind ryanodine, but the tetrameric structure is necessary for ligand binding. The ryanodine binding changes the effective diameter of the RYR1 channel pore [Fill *et al.*, 2002].

Caffeine is an activator of RYR1. Caffeine has been shown to activate Ca^{2+} release from SR by increasing the apparent affinity of the Ca^{2+} activation site for Ca^{2+} . The caffeine causes an increase in the open probability of RYR1 [Rousseau *et al.* 1988] and renders it more sensitive to voltage sensor activation and physiological activators such as Ca^{2+} and ATP [Herrmann-Frank *et al.* 1999].

Local anesthetics. Procaine and tetracaine inhibited SR Ca^{2+} release induced by Ca^{2+} or caffeine [Garcia and Schneider, 1995]. A similar action has been observed with other local anesthetics, such as the tertiary amines etidocaine, bupivacaine, prilocaine, lidocaine, and mepivacaine, the quaternary amines QX 572 and QX 314, and the neutral anesthetic benzocaine. Local anesthetics show at least two different actions. 1) Channel inhibition associated with reduced ryanodine binding. Such action, produced by tetracaine and procaine, is likely to be mediated by a high-affinity binding site, corresponding to or interacting with the Ca^{2+} -binding and adenine nucleotide binding sites. 2) Voltage-dependent channel blockade, characterized by reduced channel conductance. This action occurred with lidocaine, with quaternary

amines, and, possibly, with high concentrations of procaine and tetracaine; it was associated with increased affinity for ryanodine, and it is supposed to be mediated by a lower-affinity site, located close to the conductive pathway. Additional effects cannot be excluded. In particular high concentrations of local anesthetics might affect SR Ca^{2+} release by a nonspecific action on membrane permeability.

Volatile anesthetics. In skeletal muscle and cardiac SR preparations, halothane increased SR Ca^{2+} release at gas concentrations ranging from about 0.002% to 3.8% (v/v) [Beltran *et al.*, 1996]. The response to halothane was Ca^{2+} -dependent and pH-dependent. At a pH of 7.4, halothane increased the rate of Ca^{2+} release at all Ca^{2+} concentrations. At a pH of 6.8, no significant Ca^{2+} release occurred in the absence of halothane, at any Ca^{2+} concentration, and the stimulation produced by halothane was Ca^{2+} -independent [Beltran *et al.*, 1996]. The response to halothane was not affected by adenine nucleotides, and it was inhibited by ruthenium red [Frazer and Lynch, 1992]. Similar effects have been observed with isoflurane and enflurane (2.5 to 4%).

4-Chloro-m-cresol (4-CmC) is a clinically relevant activator of RYR1. It is a structural analog of phenol and activates RYR1 with an EC_{50} ~50-200 μM [Zorzato *et al.*, 1993]. The structural determinants on RYR1 required for 4-CmC activation have been localized to a 173 amino acid region between amino acid residues 4007-4180 [Fessenden *et al.*, 2003]. Jacobson *et al.*, [2006] suggest that the 4-CmC binding site on RYR1 contains two critical components: 1) hydrophilic side chains of amino acids to stabilize the 1-hydroxyl on 4-CmC *via* hydrogen binding and/or electrostatic interactions and 2) a hydrophobic surface to interact with hydrophobic groups on the 3, 4, and/or 5-positions on the benzene ring.

Ruthenium red is a polycationic dye with a structure that includes 14 amino groups. Ruthenium red has been shown to inhibit SR Ca^{2+} release. The inhibition was incomplete, because a complete block requires the addition of Mg^{2+} . On the basis of single-channel results, it has been demonstrated that the binding site is located within the transmembrane region of RYR1, probably close to the pore of the channel, and that ruthenium red cannot permeate through the open channel [Ma, 1993].

Dantrolene, a hydantoin derivative, has structural similarities to both hydantoin and some local anaesthetics, but has neither anticonvulsant nor anaesthetic properties. In skeletal muscle dantrolene inhibits the RYR1-mediated Ca^{2+} release [Paul-Pletzer *et al.*, 2002]. The dantrolene binding site on RYR1 is located at the N-terminal region (amino acids 590–609). Dantrolene reduced the maximum rate of Ca^{2+} release without affecting the Ca^{2+} -sensitivity of the process, and its action was much more evident in the presence of caffeine and adenine nucleotides than in their absence [Zucchi and Ronca-Testoni 1997].

1.4 RYR1-related disease

The RYR1 channel, which is encoded by the *RYR1* gene, plays an essential role in the sarco/endoplasmic Ca^{2+} regulation and in the generation of Ca^{2+} signals that triggers muscle contraction. Mutations in the *RYR1* gene, resulting in dysfunctions in RYR1 channel activity and defects in sarco/endoplasmic Ca^{2+} regulation, are linked

to malignant hyperthermia and to some congenital myopathies among which the most common are core myopathies.

1.4.1 Malignant hyperthermia (MH)

MH (MIM 145600) is a potentially lethal pharmacogenetic disorder that affects genetically predisposed individuals when they are exposed to volatile anesthetics (halothane, enflurane, isoflurane, desflurane, sevoflurane) or depolarizing neuromuscular myorelaxants (e.g. succinylcholine). Volatile anesthetics trigger a sustained release of Ca^{2+} from the SR that leads to hypermetabolism, muscle rigidity, rhabdomyolysis, and death. First reported in 1960 (Denborough and Lovell, 1960), MH is a major cause of anaesthetic related deaths in young, fit individuals [Kaus and Rockoff, 1994]. MH exhibits an autosomal dominant mode of inheritance in man with an estimated frequency varying from 1:15,000 anesthetic administrations in children to 1:50,000 anesthetics in adults [Jurkat-Rott *et al.*, 2000]. The actual frequency is difficult to establish since many susceptible individuals will never be exposed to the anesthetic triggers. Although the mechanism of MH triggering is specific, the resulting clinical features are not. Thus, patients with a variety of neuromuscular disorders are sporadically reported to have developed one or more of the clinical features of MH (such as pyrexia, tachycardia, hypercapnia, and hyperkalemia) in the perioperative period. It is important to distinguish such nonspecific problems from MH, because different underlying pathophysiological mechanisms are likely to require different treatments and have different implications for the anesthetic management of the patient and their family. Therefore, except in conditions where SR Ca^{2+} release is specifically sensitized to volatile anesthetics, as in MH, triggering drugs should not be absolutely avoided [Klingler *et al.*, 2009].

Etiology. MH is a skeletal muscle disorder related to sustained release of Ca^{2+} from the SR with increased intracellular Ca^{2+} levels. The enhanced intracellular calcium results in activation of muscle contraction, oxygen consumption, carbon dioxide production. The processes of muscle contraction and of reabsorbing this excess Ca^{2+} accumulation, consumes large amounts of ATP and generates the excessive heat (hyperthermia) that is the hallmark of the disease. The muscle cell is damaged by the depletion of ATP and by the high temperatures, and cellular constituents are poured into the circulation, including potassium, myoglobin, creatine, phosphate and creatine kinase. The low ATP concentration causes muscle rigidity, since the presence of ATP is normally required to allow muscle relaxation. ATP depletion causes association of actin and myosin filaments so that the muscle becomes rigid and inextensible. This is really a premature rigor mortis and explains why the rigidity persists up to and after death [Furniss, 1971]. The treatment of a MH crisis consists in the administration of the skeletal muscle relaxant dantrolene, an inhibitor of Ca^{2+} release from intracellular stores. After its introduction, the mortality of malignant hyperthermia decreased from 80% in the 1960s to < 10% today. Dantrolene depresses the intrinsic mechanisms of E-C coupling in skeletal muscle by inhibiting RYR1-mediated Ca^{2+} release [Paul-Pletzer *et al.*, 2002].

Diagnosis. The *in vitro* contracture test (IVCT) is the “gold standard” for diagnosis of MH. The European MH Group (EMHG, www.emhg.org) has developed a

standardized protocol for the IVCT [European Malignant Hyperpyrexia Group, 1984]. Using this assay patients are assigned MH susceptible (MHS), MH normal (MHN) or MH equivocal (MHE) according to the *in vitro* contracture response of viable muscle tissue strips following exposure to halothane and to caffeine. An increase in contracture of ≥ 0.2 g at a threshold dose of 2 mM caffeine and 2% halothane is considered a positive test result (MHS). A MHN diagnosis is obtained when both drug-responses are below the threshold. The MHE class includes patients who react to only one of triggering agents used in the test. The IVCT involves an invasive open muscle biopsy and is carried out only on patients who had an MH episode or on their family members. The IVCT exhibits good diagnostic sensitivity (99%) and specificity (93.6%) [Ording *et al.*, 1997]. A slightly different protocol for testing MH susceptibility was developed by the North America Malignant Hyperthermia Group (www.mhaus.org) and is referred as the caffeine-halothane contracture test (CHCT) [Larach, 1989]. The test is associated with lower diagnostic specificity (78%) and sensitivity (97%) than the European protocol [Larach *et al.*, 1992]. Modifications of the EMHG protocol include the use of ryanodine [Bendahan *et al.* 2004], which binds selectively to RYR1 or 4-CmC [Rueffert *et al.*, 2002], but to date these agents have not been included in the standard protocol. Anetseder *et al.*, [2002] proposed a less invasive open muscle biopsy in which intramuscular injections of caffeine lead to an increase in carbon dioxide pressure only in MHS subjects. At present, the clinical approach for MHS subjects involves the use of non-triggering anesthetic agents, thus bypassing the need for an extensive preoperative workup. The anesthesia is managed with a combination of non-triggering anesthetics (barbiturates, nitric oxide, propofol, narcotics) and local anesthetics. On the day of the operation, the patient is carefully monitored. If a MH episode occurs, the dantrolene is administered (2-2.4mg/kg of body weight) and injection are repeated until symptoms persist (10mg/kg is maximal dose).

Genetic basis. Sequence variants of *RYR1* gene have been identified in up to 70% of MH families [Klingler *et al.*, 2009]. MHS1 *locus* (MIM 180901), located on chromosome 19q13.1, is a main site where the *RYR1* gene maps [McCarthy *et al.*, 1990]. However, a considerable genetic heterogeneity has been reported for MH; in fact, other five MH susceptibility *loci* have been mapped to specific chromosome intervals. The nomenclature of the MHS *loci* followed the order of their appearance (Tab. 1). The MHS2 *locus* (MIM 154275) has been linked to chromosomal *locus* 17q11.3-q24 where the *SCN4A* gene maps [Levitt *et al.*, 1992]. This gene encodes α subunit of voltage-dependent sodium channel expressed in the skeletal muscle. The MHS3 *locus* (MIM 154276), assigned to chromosome 7q21-q22, contains the *CACNL2A* gene that encodes the $\alpha 2/\delta$ subunit of the calcium channel Cav 1 [Illies *et al.*, 1994]. The MHS4 *locus* (MIM 600467) was mapped to chromosome 3q13.1 and a candidate gene was not identified yet [Sudbrak *et al.*, 1995]. The MHS5 *locus* (MIM 601887), located on chromosome 1q32, contains the *CACNA1S* gene that encodes the $\alpha 1_s$ subunit of Cav 1.1. Sequence variants have been identified in this gene in Italian, German and French MH families [Pirone *et al.*, 2007; Jurkat-Rott *et al.*, 2000; Monnier *et al.*, 1997]. It was estimated that sequence variants in this gene account for 1% of all MH cases. Finally, the MHS6 *locus* (MIM 601888) was located on chromosome 5p [Robinson *et al.*, 1997].

Locus	Chromosomal location	Gene
MHS1	19q13.1	<i>RYR1</i>
MHS2	17q11.3-q24	<i>SCN4A</i>
MHS3	7q21-q22	<i>CACNL2A</i>
MHS4	3q13.1	Unidentified
MHS5	1q32	<i>CACNA1S</i>
MHS6	5p	Unidentified

Tab. 1 MH susceptibility *loci* and their chromosomal location.

Thus far, more than 200 sequence variants have been identified in the *RYR1* gene, the main *locus* of MH susceptibility [Anderson *et al.*, 2008; von der Hagen *et al.*, 2008; Monnier *et al.*, 2008; Sato *et al.*, 2008; Kossugue *et al.*, 2007; Lyfenko *et al.*, 2007; Rossi *et al.*, 2007; Zhou *et al.*, 2007; Robinson *et al.*, 2006]. The majority of variants (96%) linked to MH so far detected in the *RYR1* gene are missense changes [Robinson *et al.*, 2006] and are clustered in three main “hotspot” regions of the RYR1 protein: residues 35-614 (region 1), residues 2117-2787 (region 2) and residues 4136-4973 (region 3). Almost all mutations occur at the heterozygous state, and homozygotes was rarely reported [Lynch *et al.* 1997].

Genetic testing. According to guidelines of EMHG, mutation analysis of *RYR1* gene is used in predictive genetic testing of MH susceptibility and is offered to IVCT-positive patients and their relatives, as well as to patients who suffered from suspected MH episodes and their relatives. So far, only 28 sequence variants of *RYR1* (Tab. 2), investigated for their functional effect, fulfil the criteria to be included in the guidelines for molecular genetic detection of MH susceptibility.

EXON	NUCLEOTIDE	AMINO ACID
2	c.103T>C	p.C35R
6	c.487C>T	p.R163C
6	c.488G>T	p.R163L
9	c.742G>A	p.G248R
11	c.1021G>A	p.G341R
12	c.1209C>G	p.I403M
14	c.1565A>C	p.Y522S
15	c.1654C>T	p.R552W
17	c.1840C>T	p.R614C
17	c.1841G>T	p.R614L
39	c.6487C>T	p.R2163C
39	c.6488G>A	p.R2163H
39	c.6502G>A	p.V2168M
40	c.6617C>T	p.W2206M
40	c.6617C>G	p.W2206R
44	c.7048G>A	p.A2350W
44	c.7124G>C	p.G2375A
45	c.7282G>A	p.A2428W
45	c.7300G>A	p.G2434R
45	c.7304G>A	p.R2435H
46	c.7360C>T	p.R2454C
46	c.7361G>A	p.R2454H
46	c.7372C>T	p.R2458C
46	c.7373G>A	p.R2458H
100	c.14387A>G	p.Y4796C
101	c.14512C>G	p.L4838V
101	c.14582G>A	p.R4861H
102	c.14693T>C	p.I4898W

Tab. 2 Causative *RYR1* gene mutations included in the guidelines for molecular genetic detection of MH susceptibility.

The following criteria have been adopted.

1) Genetic characterization. Each mutation should be characterised at the genetic level, including a full description at the DNA and protein level, considering aspects of evolutionary conservation and change in charge, polarity or structure introduced by the amino acid replacement, co-segregation of the mutation with the disease in at least 2 pedigrees, absence of the sequence change from 100 normal chromosomes of the same ethnic group for exclusion of polymorphisms.

2) Functional characterisation. The effect of each mutation on RYR1 function should be assayed in the following cell system:

- assays on HEK293 cells, myotubes of the dyspedic mouse. The standard system is based on the expression of a rabbit mutant RYR1 cDNA construct in HEK293 cells. Calcium release is measured fluorimetrically in response to triggering agents (Tong *et al* 1997, Lynch *et al.* 1999, Tong *et al.* 1999, Monnier *et al.* 2000, Sambuughin *et al.* 2001, Oyamada *et al.* 2002). The advantage of the system is the standardised genetic background of the recipient cell line. This cell system allows for direct comparison between mutations and eliminates the potential influence of mutations in other genes which could modify the RYR1 function in cells taken from patients. Alternatively, myotubes of the dyspedic mouse (RYR1-knock out) have been used as recipients for the expression of cDNA constructs (Avila *et al.* 2001). In this cell system both Ca²⁺ release and E-C coupling can be studied. Again, cDNA construct and genetic background are well defined and standardised. The genetic expression

profile of myotubes may be closer to those of mature muscle. For this reason, results may not be directly comparable to the HEK293 cell system.

- assays on cells derived from patient tissues. Calcium measurements ligand binding studies have been performed on tissues from MHS patients (in myotubes [Brinkmeier *et al.* 1999, Wehner *et al.* 2002], in microsomal SR preparations from muscle biopsies [Richter *et al.* 1997], and in lymphoblasts [Zullo *et al.*, 2009; Girard *et al.* 2001, Tilgen *et al.* 2001]) carrying the *RYR1* gene variants. The parameters analyzed were Ca^{2+} release and resting $[\text{Ca}^{2+}]$, proton release, ryanodine binding to SR RYR1 preparations. Moreover, the responses to electrical stimulation can be studied in myotubes. Since the tissue were derived from patients, the potential influence of other individual genetic factors cannot be excluded. Therefore, in order to remove the interference of other genetic factors, the assays should be performed on samples from at least two independent patients with the same mutation.

The study of the impact of a given mutation on the structure and function of the protein could have important implications also for MH diagnosis. In fact, according to the EMHG guidelines (Urwyler *et al.*, 2001), once a mutation has been detected in the proband or index patient, that fulfils the criteria to be included in the guidelines as MH causative mutation, it can be used to test relatives who have not yet been tested by the IVCT. The individual carrying such a mutation should be regarded as MHS; therefore, the genetic analysis may provide conclusive diagnostic information, even in the absence of IVCT result. This is useful for large families or if relatives refuse a muscle biopsy. However, family members who do not carry the mutation observed in the pedigree should still undergo IVCT investigation. The reason for such caution is the of discordance between genetic and IVCT results, implicating a second MH susceptibility gene segregating in the kinship. Furthermore, genetic analysis may also provide adjunctive information to the instrumental diagnosis. Although the IVCT is the gold standard test with which to establish the risk for MHS, there have been some rare cases of discordance between genotype, characterised by a causative mutation, and phenotype, typed MHN by the IVCT [Robinson *et al.*, 2003; Fortunato *et al.*, 1999; Brandt *et al.*, 1999; Deufel *et al.*, 1995]. On the basis of these observations, it has been proposed that subjects who carry a causative mutation should be regarded MHS for clinical purposes [Fortunato *et al.*, 1999]. Therefore, genetic analysis will contribute to the definition of the sensitivity of the IVCT, since it reveals these rare but nevertheless high-risk cases of subjects falsely typed "normal".

1.4.2 Congenital myopathies

Congenital myopathies (CMs) are a heterogeneous group of inherited neuromuscular disorders characterized by hypotonia and muscle weakness, that usually present at birth or early childhood or rarely adulthood [Goebel, 2005]. The incidence of all congenital myopathies is estimated at around 6.0/100.000 live births, or one-tenth of all cases of neuromuscular disorders [Wallgren-Pettersson, 1990]. Myopathies linked to *RYR1* mutations are differentiated on the basis of the histopathological features in:

- core myopathies (central core disease, multimicore disease, nemaline rod myopathy, and centronuclear myopathy), characterized histologically by central cores, multi-minicores, nemaline rods, central nuclei in muscle fibers, respectively;

- others myopathies (congenital neuromuscular disease with uniform Type 1 fibers, and congenital fiber-type disproportion myopathy) characterized histologically by almost exclusive presence of Type 1 muscle fiber, relative hypotrophy of type 1 muscle fibers, respectively.

Jungbluth *et al.* [2003] reported genetic, phenotypic and histopathological overlaps between different myopathies, and marked phenotypic variability. In particular, defects in more than one gene are associated with the presence of the same pathological feature, while defects in the same gene can result in more than one pathological feature (Tab. 3).

Disease	Gene	MH risk
Central core disease (CCD)	<i>RYR1</i>	High*
	<i>ACTA1, MYH7</i>	Low
Multiminicore disease (MmD)	<i>SEPN1, TTN</i>	Low
	<i>RYR1</i>	High*
Nemaline rod myopathy (NM)	<i>NEB, TPM3, TNNT1, TPM2, ACTA1, CFL2</i>	Low
	<i>RYR1</i>	High*

Tab. 3 Genes involved in core myopathies and estimated risk of MH (given there isn't cases of MH in the family)

1.4.2.1 Central Core Disease (CCD)

CCD (MIM 11700) is a rare hereditary myopathy, characterized clinically by muscle weakness of variable degree and histologically by central cores generally in the type I muscle fibers. The term central cores indicates areas with characteristic absence of oxidative enzyme activity in the muscle fiber as detected by NADH reductase staining (Fig. 12) [Dubowitz *et al.*, 1960].

The classic phenotype is characterized by mild hypotonia during early childhood, delayed motor milestones, and diffuse and moderate muscle weakness that frequently involves axial muscles. Congenital hip dislocation, early-onset scoliosis, arched feet, and pectus excavatus may also be present, whereas bulbar involvement, ophthalmoplegia, and diaphragmatic weakness are very rare. In adulthood, the syndrome usually is nonprogressive. Functional improvement can occur and approximately 40% of affected adults are considered asymptomatic. However, the evolution is unpredictable, and weakness may cause severe disability in daily life [Fischer *et al.*, 2006; North *et al.*, 2004].

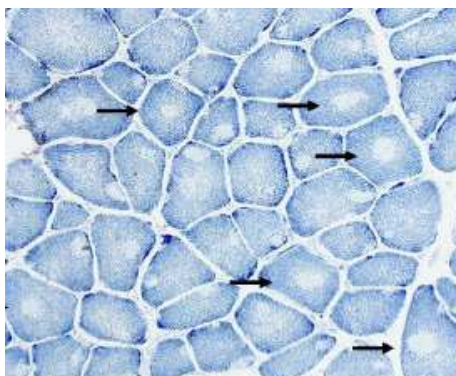


Fig. 12 Histopathologic appearance of typical central core disease: type 1 fibers containing unstructured cores (arrow) and no mitochondria (NADH reductase staining). Cores are typically well demarcated and centrally located, but may occasionally be multiple and of eccentric location (figure from Jungbluth *et al.*, 2007).

Diagnosis. The diagnosis of CCD is based on the presence of suggestive clinical features and on histochemical staining of muscle biopsy samples that shows areas with reduced/absence oxidative activity, called central cores (Fig 12). The clinical severity of CCD and the number of cores can vary with age, making uncertain the diagnosis. Muscle magnetic resonance imaging (MRI) may show a characteristic pattern of selective muscle involvement and helps to confirm the diagnosis in cases with equivocal histopathologic findings [Jungbluth *et al.*, 2004]. No curative therapy is currently available for congenital myopathies. The therapy of congenital myopathies is essentially supportive and/or rehabilitative. Physiotherapy is utilized for the maximum preservation of muscle power and function and the prevention of contractures, with particular care after surgical procedures. β -agonists, as the salbutamol, have been shown to be beneficial on muscle strength in patient affected by congenital myopathy [Messina *et al.*, 2004]. Therapeutic assays with the salbutamol administration have been proven to significantly increase muscle strength in CCD patients. Salbutamol is also able to reduce muscle pain when present. In addition, patients affected by a CCD should be given general anesthesia cautiously because they can develop life-threatening MHS.

Genetic basis. CCD is caused in the majority of cases by mutations in the *RYR1* gene, also implicated in the MH susceptibility. CCD is usually inherited as an autosomal dominant trait [Jungbluth, 2007] but autosomal recessive forms have been recently reported [Kossugue *et al.*, 2007; Wu *et al.*, 2006; Zhou *et al.*, 2006b; Zhou *et al.*, 2007]. Dominant *RYR1* mutations affecting the cytoplasmic N-terminal and central regions (domains 1 and 2) of the RYR1 protein give rise predominantly to the MHS phenotype characterized by highly responsive channels with massive Ca^{2+} release (Fig. 13 A), whereas the classical CCD phenotype, with few exceptions, is associated with dominant *RYR1* mutations clustered in the hydrophobic C terminal pore-forming region of the protein (domain 3) [Robinson *et al.*, 2006; Treves *et al.*, 2005]. There is a clear association between CCD and MH susceptibility: patients with CCD may be prone to MH episodes [Eng *et al.*, 1978; Frank *et al.*, 1980; Shuaib *et al.*, 1987] and individuals with MHS may have central cores on muscle biopsy [Denborough *et al.*, 1973]. Cases of the MH (~70%) and CCD (~50%) linkage to mutations in *RYR1* gene suggested that the two conditions are allelic disorders [Zhang *et al.*, 1993; Quane *et al.*, 1993; Gillard *et al.*, 1991].

In vitro studies demonstrated that two distinct cellular mechanisms can generate the muscle weakness in CCD patients. The leaky-channels hypothesis [Du *et al.*, 2001] proposes that mutations in the RYR1 protein generate channels that are excessively leaky to Ca^{2+} and lead to depletion of SR Ca^{2+} stores, generating consequently muscle weakness (Fig. 13 B and C). The E-C uncoupling hypothesis [Dirksen and Avila, 2002] proposes instead that a deficit in E-C coupling, i.e., a reduced voltage-gated release in the absence of detectable store depletion, lies at the base of muscle defects. The two hypotheses are not necessarily mutually exclusive. The discrepant results obtained so far indicate that the two mechanisms could coexist. However, these two hypotheses clearly do not explain all cellular and pathological phenotypes, that are overlapping in different congenital myopathies (see 1.4.3 for deepening).

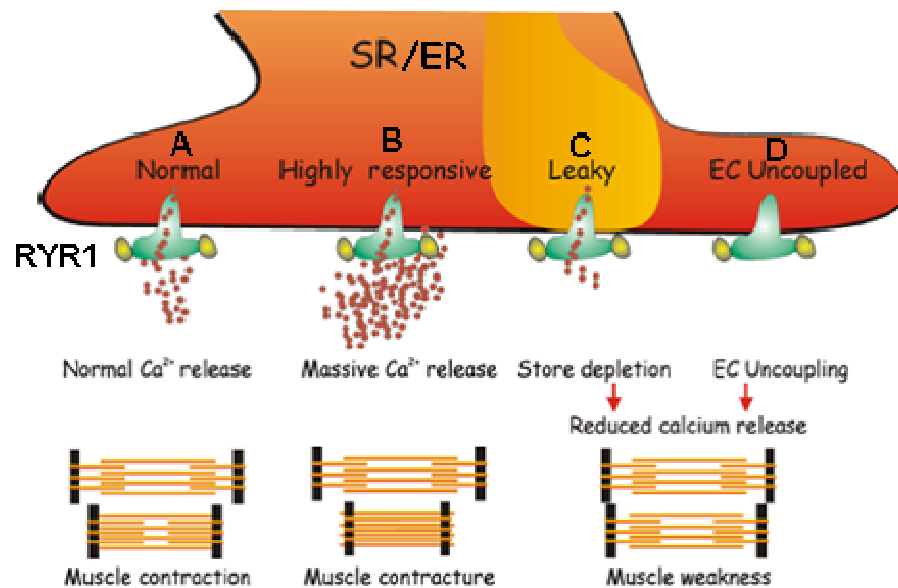


Fig. 13 Schematic model of distinct cellular mechanisms generating MH (B) and CCD (C and D) phenotypes (figure modified from Brini *et al.*, 2004).

Central cores on muscle biopsy have been observed in a group of patients with hypertrophic cardiomyopathy secondary to mutations in the β -myosin heavy chain (*MYH7*) gene, however, these patients typically do not have associated muscle weakness or any other features of typical CCD [Fananapazir *et al.*, 1993]. Central and minicores in association with a dilated cardiomyopathy may also rarely be observed in patients with mutations in the skeletal muscle α -actin (*ACTA1*) gene [Kaindl *et al.*, 2004], more frequently associated with nemaline myopathy.

1.4.2.2 Multiminicore Disease (MmD)

MmD (MIM 255320) is a recessively inherited congenital myopathy morphologically defined by localized multiple areas of mitochondrial depletion and sarcomere disorganization, called minicores, running to a limited extent along the longitudinal axis of both type 1 and type 2 muscle fibers (Fig. 14) [Jungbluth *et al.*, 2004]. Presentation of MmD is usually in infancy or childhood with hypotonia or proximal weakness; prenatal onset with reduced fetal movements and polyhydramnios has also been recognized [Jungbluth *et al.*, 2000]. At least four clinical phenotypes have been associated with the presence of minicores: 1) the classic phenotype characterized by axial muscle weakness, commonly leading to severe scoliosis; 2) the classic MmD phenotype with also ophthalmoplegia; 3) predominant hip-girdle involvement, occasionally associated with arthrogryposis at birth, and 4) moderate forms with marked distal weakness and wasting predominantly affecting the upper limbs [Ferreiro *et al.*, 2000].

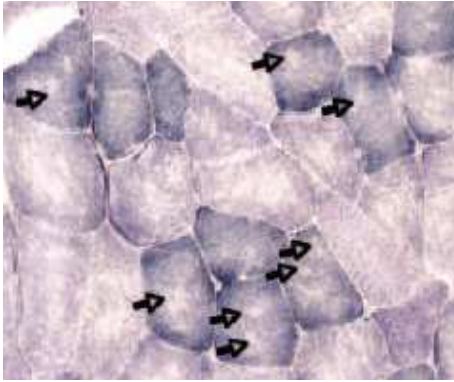


Fig. 14 Histology of multiminiore disease (NADH-TR staining). The cores (arrows) are multiple, poorly defined (figure from Klingler *et al.*, 2009).

Diagnosis. The diagnosis of MmD is based on histochemical staining of muscle biopsy. MmD is characterized by multifocal, well-circumscribed areas with reduction of oxidative staining and low myofibrillar ATPase [Naguib *et al.*, 2002]. In contrast to central cores, minicores extend only for a short distance along the longitudinal axis of the muscle fibre, are typically unstructured and may affect both type 1 and type 2 fibres (Fig. 14) [Dubowitz *et al.*, 2006]. As for CCD, the salbutamol has been used in some MmD patients with encouraging results [Messina *et al.*, 2004], however, results of this pilot study will have to be validated in a larger randomized controlled.

Genetic basis. MmD is genetically heterogeneous. The classic form of MmD is most frequently associated with mutations in the selenoprotein N1 (*SEPN1*) gene [Ferreiro *et al.*, 2002a]. Selenoprotein, a glycoprotein localized in the ER, has recently been shown to be required for RYR1 Ca^{2+} release [Jurynek *et al.*, 2008]. The *SEPN1* gene mutations account for about 50% of cases with the classic MmD phenotype. Clinical subgroups other than the classic phenotype of MmD have now been associated with mutations in the *RYR1* gene [Jungbluth *et al.*, 2005] (Tab. 3). These can be homozygous, compound heterozygous, or heterozygous with monoallelic expression [Zhou *et al.*, 2006; Jungbluth *et al.*, 2005; Monnier *et al.*, 2003]. The *RYR1* gene is also a likely candidate for the severe form of MmD with neonatal onset and arthrogryposis. The majority of MmD-related *RYR1* mutations are missense mutations and are spread across the *RYR1* gene; few intronic splicing mutations have been recently reported [Zhou *et al.*, 2007; Jungbluth *et al.*, 2005; Monnier *et al.*, 2003]. Few functional data are available to understand the pathogenetic mechanisms of MmD-related *RYR1* mutations and suggest a wide variety of alterations [Ducreux *et al.*, 2006; Zhou *et al.*, 2006b; Zorzato *et al.*, 2007]. Studies of Ca^{2+} homeostasis in EBV-immortalized lymphoblasts from patients carrying the RYR1 p.P3527S substitution [Ducreux *et al.*, 2006] suggested uncoupling defects, whereas the p.V4849I substitution [Jungbluth *et al.*, 2002] was associated with a small but significant effect on resting Ca^{2+} concentrations. E-C uncoupling was also indicated by complete loss of Ca^{2+} conductance in recombinant mutant RYR1 channels expressing the p.R109Y substitution [Zhou *et al.*, 2006b] previously associated with a MmD and ophthalmoplegia phenotype [Jungbluth *et al.*, 2005]. Marked reduction of the amount of the RYR1 protein suggests that some *RYR1* mutations identified in MmD patients may affect the expression and stability of the protein [Monnier *et al.*, 2003, Zhou *et al.*, 2007]. Additional work will be required to further elucidate the molecular mechanisms underlying RYR1-related MmD.

Finally, autosomal recessive mutations in the titin (*TTN*) gene were identified in a novel early-onset myopathy with minicores, increased central nuclei, dystrophic features and a fatal cardiomyopathy [Carmignac *et al.*, 2007].

1.4.2.3 Nemaline rod Mopathy (NM)

NM (MIM 161800) is a rare congenital myopathy with an incidence of about two cases per 100,000 live births [Sanoudou *et al.*, 2001]. It is characterized by the presence of rods or nemaline bodies, which are purple inclusions in myofibers detected by modified Gomori trichrome (GT) technique (Fig. 15) [Fardeau *et al.*, 2004]. The distribution of rod bodies may be random, but they generally clustered under the sarcolemma, around nuclei, or inside nuclei. The rods lack ATPase histochemical activity cores. The clinical features are heterogeneous, ranging from severe neonatal cases to mildly affected adults. NM can be divided into the following forms: 1) severe congenital; 2) intermediate congenital; 3) typical; 4) mild, childhood-, or juvenile onset; 5) adult-onset; and 6) others rarely associated with cardiomyopathy. NM is characterized by generalized muscle weakness with facial involvement or predominant involvement of proximal limb and respiratory muscles. Feeding difficulties, severe respiratory impairment, and skeletal involvement (including arthrogryposis, scoliosis, or spinal rigidity) have been observed in the congenital or very early-onset forms.

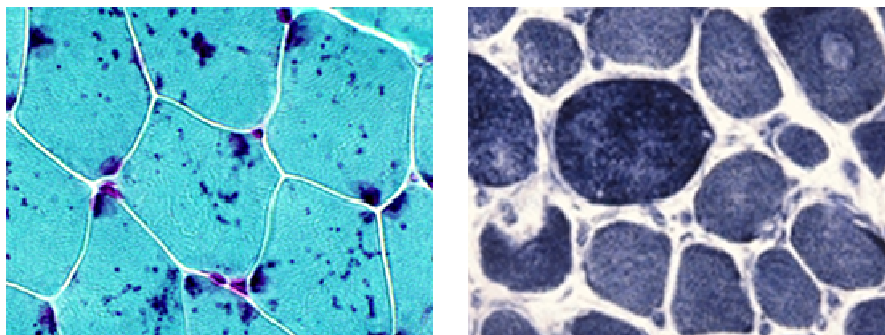


Fig. 15 Skeletal muscle fibers of patient with NM. **A.** Accumulations of rod-shaped nemaline bodies are clearly present (GT stain). **B.** Few cores are seen in NADH-TR staining.

Diagnosis can only be made by detecting the specific structural abnormality on a muscle biopsy. Accumulation of sarcomeric components (α -actinin and tropomyosin) and formation of nemaline bodies (rods) are seen as dark purple structures with GT stain (Fig. 15), and the NADH-TR stain reveals the cores as white unstained areas.

Genetic basis. NM is inherited as an autosomal recessive or autosomal dominant trait [Wallgren-Pettersson *et al.*, 1999], and sporadic cases have been reported frequently (63%). Six genes have been associated with NM, all encoding known components of skeletal muscle sarcomeric thin filaments: different disease genes have been identified: α -tropomyosin (*TPM3*), nebulin (*NEB*), *ACTA1*, β -tropomyosin (*TPM2*), muscle troponin T1 (*TNNT1*), and muscle cofilin 2 (*CFL2*). *NEB* and *ACTA1* appear to be the most common causes of NM [Wallgren-Pettersson and Laing, 2006] (Tab. 3). In many cases, there is no strict genotype/phenotype correlation, indicating clinical and genetic heterogeneity of the disease. In a few cases, mutations in *RYR1*

have also been associated with nemaline bodies. However, these nemaline bodies appeared together with central cores, indicating a mixed core-rod myopathy [Monnier *et al.*, 2000; Pallagi *et al.*, 1998; Scacheri *et al.*, 2000].

1.4.2.4 Centronuclear myopathy (CNM)

CNM is a rare CM morphologically characterized by numerous centrally located nuclei; additional but inconsistent histopathological features comprise a central zone either devoid of oxidative enzyme activity or with oxidative enzyme accumulation, radial strands surrounding the central area, type 1 fibre predominance and hypotrophy (Fig. 16). The clinical phenotype of CNM is highly variable. Proximal limb girdle, paraspinal muscles, ptosis and extraocular eye muscle have been reported in several patients; distal muscular weakness has been described rarely [Wallgren-Pettersson, 2000].

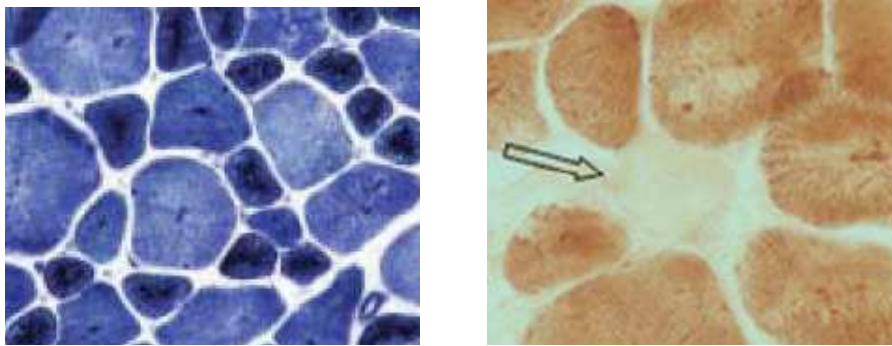


Fig. 16 Skeletal muscle fibers of patient with CNM. **A.** Type 1 fiber atrophy, central nuclei and radial sarcoplasmic strands are seen by NADH-TR staining (figure from Fujimura-Kiyono *et al.*, 2009). **B.** Presence of COX negative fibers underlined with the arrows (figure from Zanoteli *et al.*, 2009)

Genetic basis. CNM is associated with mutations in several genes, whose products are involved in endocytosis and membrane trafficking, and exists in X-linked (MIM 310400), autosomal-dominant (MIM 160150) and recessive (MIM 255200) forms. Mutations in the *MTM1* gene, which encodes myotubularin 1, have been identified in patients with the most severe form of CNM, inherited as X-linked trait [Laporte *et al.*, 1997; Laporte *et al.*, 1996] (Tab. 3). The autosomal recessive form has its onset in infancy or early childhood, whereas the autosomal dominant CNM has later onset in early adulthood and presents with mild weakness and slow progression. The dominant form of CNM is associated with mutations in the *DNM2* gene, which encodes dynamin-2 [Bitoun *et al.*, 2005], whereas the autosomal recessive form has recently been associated with mutations in the *BIN1* gene, which encodes amphiphysin 2 [Nicot *et al.*, 2007]. Recently, a heterozygous dominant missense *de novo* *RYR1* mutation (p.S4112L) was identified in a patient with histopathologic and clinical features of CNM [Jungbluth *et al.*, 2007].

1.4.2.5 Congenital neuromuscular disease with uniform Type 1 fibers (CNMDU1)

CNMDU1 is defined as a rare form of congenital myopathy characterized by the almost exclusive presence of Type 1 muscle fiber (>99%) without any specific structural changes [Oh *et al.*, 1983]. Clinically, CNMDU1 shares common features with congenital myopathy, including early onset, mild proximal muscle weakness.

Genetic basis. Sato *et al.* [2008] reported that 40% of patients with a diagnosis of CNMDU1 is associated with mutations in the C-terminal domain of RYR1, and suggested that CNMDU1 is allelic to central core disease. Recently, Fujimura-Kiyono *et al.*, [2009] reported indicated that CNMDU1 patients with RYR1 C-terminal mutations present clinical manifestations similar to those of CCD phenotype associated with RYR1 C-terminal mutations, regardless of the presence or absence of cores on muscle biopsy. Therefore they proposed that CCD and CNMDU are the same disease, and that the absence of cores may be attributed to muscle sampling, as the degree of affection could be different among muscles. Alternatively, cores may be formed in an age-dependent manner and in CNMDU1 cases and the muscle was biopsied before cores were formed.

1.4.2.6 Congenital fibre type disproportion (CFTD)

CFTD is a subtype of congenital myopathy in which consistent type 1 fibre hypotrophy (compared to type 2 fibres) is the main histological abnormality. Clinical phenotypes show hypotonia and diffuse weakness that may improve with age; other clinical features can include facial, bulbar, respiratory weakness, low body weight, multiple joint contractures, scoliosis, long, thin face, and high-arched palate. Ophthalmoplegia, cardiac disease, and mental retardation are rare.

Genetic basis. Mutations in three genes (*TPM3*, *SEPN1*, *ACAT1*) are associated with CFTD. Clarke *et al.*, [2008] identified *RYR1* as the fourth gene associated with CFTD. In fact, they found in a CFTD patient a compound heterozygosity of a missense mutation, and a nonsense (silencing) mutation in the *RYR1* gene.

1.4.3 Molecular mechanisms in RYR1-related core myopathies

Zhou *et al.*, [2007] suggested potential molecular mechanisms implicated in the marked phenotypic variability observed in core myopathies associated with dominant and recessive RYR1 mutations. Dominant RYR1 mutations were mainly found in the C-terminal and rarely in the central domain of *RYR1* gene [Zhou *et al.*, 2007; Wu *et al.*, 2006]. Most dominant CCD-related RYR1 mutations localize to the M8/M10 loop surrounding the pore helix region (Du *et al.*, 2002), demonstrating the main role of this part of the protein in the pathogenesis of CCD; two dominant CCD mutations localized in or close to segment M6 implies the potential importance of this transmembrane domain for channel function and stability [Zhou *et al.*, 2007]. Most patients with dominant C-terminal mutations have the classical CCD phenotype (variable degrees of proximal weakness, respiratory or extraocular involvement, orthopaedic complications, and scoliosis), and showed a highly consistent pattern of

selective muscle involvement at magnetic resonance imaging (MRI) of muscle. Interestingly, patients carrying the same amino acid substitution show marked variation in age of onset and severity, suggesting either a nonstochastic distribution of mutant and wild-type RYR1 proteins or other modifying genetic factors. Most cases with dominant mutations had large cores, central or peripheral. Moreover, there isn't a direct correlation between muscle weakness and the propensity to develop cores in RYR1-related myopathies. In fact, in one family harbouring a seven amino acid deletion (p.C4883_Y4889del) and characterized by profound muscle weakness, clear cores were not present at the light microscopy level, although they were identified on electron microscopy performed on the second muscle biopsy from the affected mother 30 years after the first, non-diagnostic biopsy. Interestingly, the finding that dominant MHS-associated *RYR1* mutations may give rise to a congenital myopathy phenotype in the compound heterozygous or homozygous state suggests a combined deleterious effect on the tetrameric RYR1 protein [Zhou *et al.*, 2007].

In contrast to dominant *RYR1* gene mutations, recessive *RYR1* gene mutations were distributed throughout different domains of the protein, with variable clinical manifestations ranging from typical CCD phenotypes to generalized muscle weakness and wasting with associated external ophthalmoplegia, variable degrees of bulbar involvement and respiratory impairment. Some patients with typical CCD phenotype showed recessive *RYR1* gene mutations previously associated at the heterozygous state in MHS patients [Zhou *et al.*, 2007]. Recently, Carpenter *et al.*, [2009] described the segregation of a non-synonymous change in RYR1 (p.R3772Q) in three Asian families. Patients with this mutation at the heterozygous state were typed MHS, whereas the patients with this mutation at the homozygous state were both MHS and affected by myopathy.

Moreover, Zhou *et al.*, [2006] showed that the *RYR1* gene may undergo epigenetic allele silencing during human development and that some CCD patients had a monoallelic expression in skeletal muscle but not in other tissues. The monoallelic expression can unveil the presence of an apparently recessive mutation. This epigenetic mechanism is likely due to genomic imprinting. However, although it has been demonstrated that monoallelic expression of the *RYR1* gene is associated with DNA methylation, the regulatory elements of this *RYR1* monoallelic expression have not been localized yet. Similar epigenetic modifications of *RYR1* expression could account for both the reduced penetrance and the phenotypic heterogeneity of RYR1-linked muscle diseases [Zhou *et al.*, 2006]. This mechanism may also account for the observation that several mutations affect the amount of mutant RYR1 proteins in skeletal muscle [Zhou *et al.*, 2006]. While the amount of expressed RYR1 protein was normal in patients with a typical CCD phenotype, a marked reduction of RYR1 protein in muscle biopsies from patients with more severe clinical phenotypes (generalized muscle weakness and wasting and external ophthalmoplegia) was observed. In these patients, a heterozygous *RYR1* gene missense mutation was expressed on the background of a second non-transcribed allele, suggesting *RYR1* epigenetic silencing as an important aetiological mechanism in RYR1-related congenital myopathies [Zhou *et al.*, 2006a]. Monnier *et al.*, [2008] reported nine non-consanguineous families affected by recessive forms of congenital myopathies with cores and moderate to very severe phenotypes and for which quantitative defects of RYR1 were evidenced in muscles. Mutations were identified on both alleles for all the affected patients, in particular null mutation was present in at least one allele and a missense mutation on the second allele. Null alleles resulted either from frameshift,

splicing, or nonsense mutations and generated either unstable mRNA or unstable RYR1 protein. The degree of severity of the clinical presentation depended on the functional expression of the second mutant allele. Therefore, in the families reported by Monnier *et al.*, [2008] the loss of RYR1 expression was caused by mutations of the *RYR1* gene that affected either the stability of the transcript or the protein processing and did not involve epigenetic silencing that has been proposed by Zhou *et al.*, [2006] to explain monoallelic expression of *RYR1*.

Zhou *et al.*, [2006b] reported three families with clinical features of core myopathies and with compound heterozygous substitutions in the *RYR1* gene. Functional properties of these RYR1 mutants were studied on myotubes carrying endogenous mutations. In one family the presence of the p.A1577T/ p.G2060C substitutions *in trans* leads to a decrease in the amount of RYR1 expressed in skeletal muscle, without noticeably affecting the functional properties of the recombinant RYR1 ion channel. The relative amount of the RYR1 protein in the muscle biopsy from one patient of the family was significantly decreased. Zhou *et al.*, [2006b] proposed that the concomitant presence of both substitutions leads to a decrease in the stability of the RYR1 homotetramer causing a partial depletion of RYR1 channels in the skeletal muscle tissue of the patient. In an other family the compound p.R109W/p.M485V substitutions *in cis* also reduced the endogenous RYR1 expression level in muscle, but affected also the ability of recombinant channels expressing both substitutions to conduct Ca^{2+} . In the third family the p.S71Y and p.N2283H mutations do not lead to a significant reduction in RYR1 protein content, but affected both channel stability and activity. The clinical phenotypes of patients from the two families, where partial depletion of RYR1 channels, was found, were more severe compared with the patient from the third family.

Rossi *et al.*, [2007] reported the identification of a novel *RYR1* mutation resulting in a premature truncation of the RYR1 protein, RYR1^{R4837fsX4839}, in a MH proband. The histological analysis of muscle biopsy of the patient showed a clear prevalence of type 1 fibres (about 95%) and central core lesions in about 80% of fibres. This mutation was also found in two daughters of the proband with the same histological changes in skeletal muscle fibres, but both typed MHN by IVCT. However, neither the proband nor the two daughters exhibited myopathy, indicating that the central core lesions observed were sub-clinical and do not adversely affect muscle function. Studies of Ca^{2+} release and Ca^{2+} dependence of [³H]ryanodine binding showed that the homozygotic expression of RYR1^{R4836fsX4838} in HEK293 cells resulted in non-functional RYR1 channels and the expression of RYR1^{wt}/RYR1^{R4836fsX4838} resulted in channels with overall functional properties similar to those of wild-type RYR1 channels. Homozygotic expression of mutated channels exhibited negligible [³H]ryanodine binding at different Ca^{2+} concentrations indicating that the truncation either results in a constitutively closed channel or a marked disruption in the ryanodine-binding site. Sucrose-density gradient analysis of recombinant RYR1^{wt}, RYR1^{R4836fsX4838} and RYR1^{wt}/RYR1^{R4836fsX4838} channels expressed in HEK293 cells suggested that the heterotetrameric channels were likely less stable than homotetrameric wild-type RYR1 channels. The effects of the RYR1^{R4836fsX4838} truncation on E-C coupling RYR1 in skeletal myotubes, probably due to the reduced stability/assembly of these channels, may predispose individuals to MHS, although with only a low degree of penetrance (MHS status of the proband but not his two carrier daughters). This variable degree of penetrance for MHS might arise from

differences between individuals with regard to wild-type:mutant stoichiometry, presence or absence of other modifying genes, or a combination of both.

1.4.4 Risk of MH associated with core myopathies

Some *RYR1* mutations are associated with the coexistence of MH and CCD phenotypes: MH triggering drugs are contraindicated in patients with CCD carrying these mutations. In fact, many CCD patients, that have developed clinical episodes of MH, were typed MHS by IVCT [Shuaib *et al.*, 1987; Robinson *et al.*, 2006]. However, some patients with diagnosis of CCD were typed MHN by IVCT [Halsall *et al.*, 1996; Curran *et al.*, 1999]. Since genotype-phenotype correlations are insufficient, it may be more appropriate to assume MH susceptibility in CCD patients and prefer the nontriggering anesthetics unless the patient was typed MHN.

Patients with MmD linked to mutations in the *RYR1* gene may be at risk of MH reactions as it has been reported in few cases [Koch *et al.*, 1985; Osada *et al.*, 2004]; minicores on muscle biopsy have also been noticed in few MHS subjects, but without clinical features of a congenital myopathy [Barone *et al.*, 1999; Guis *et al.*, 2004]. The functional effects of MmD-associated *RYR1* mutations have been studied in HEK293 cells and in immortalized lymphocytes [Zorzato *et al.*, 2007]: some of these mutations result in increased triggered Ca^{2+} release whereas others do not. Moreover, there is considerable overlap between CCD and MmD, in the some patients with CCD present multiple cores or minicores on histochemical staining of muscle biopsy samples, and a time-related change in the morphology from minicores to cores has been described [Ferreiro *et al.*, 2002b]. Although there is no definitive evidence to absolutely contraindicate volatile anesthetics in MmD, it may be appropriate to advise caution in patients with MmD with a *RYR1* etiology.

The association between typical NM (patients who exclusively present rod bodies) and MH is rather unlikely, because there are no reports in which patients with NM developed a severe MH crisis or were tested as MHS by IVCT. Some NM patients exhibit the histological feature of cores and rods in the same muscle biopsy; in these patients the nemaline bodies may be a secondary feature of CCD. The nontriggering anesthetics are preferred, since the CCD itself may represent the major risk factor for MH reactions [Davis *et al.*, 2003; Scacheri *et al.*, 2000; Monnier *et al.*, 2000].

As a pragmatic approach, the nontriggering anesthetics could be preferred in patients with core myopathy with a *RYR1* etiology [Klingler *et al.*, 2009]. Table 3 summarizes the genes involved in the core myopathy, underlying their genetic heterogeneity.

2 AIMS OF THE WORK AND EXPERIMENTAL DESIGN

The aims of this study were:

- 1) the screening of the *RYR1* gene for the identification of sequence variants in 24 MHS subjects, one CCD patient and one patient with minicores;
- 2) the molecular characterization of the sequence variants identified;
- 3) functional characterization of the RYR1 mutated channels.

In order to reach this aims we used the following experimental design:

- 1)
 - genomic DNA extraction
 - amplification of the 106 exons of the *RYR1* gene
 - denaturing high performance liquid chromatography (dHPLC) analysis of the amplicons
 - direct sequencing of the amplicons with an altered dHPLC elution profile;
- 2)
 - analysis of changes in charge, polarity or structure introduced by the amino acid replacements
 - analysis of the conservation of the amino acid residues replaced across homologous proteins by BLASTP
 - segregation of the sequence variants in families by restriction analysis or by direct DNA sequencing
 - absence/presence of the sequence variants identified in 100 normal chromosomes of the same ethnic group by dHPLC analysis

Regarding the insertion-variant identified:

- *in silico* protein structure prediction (Garnier and Octanol softwares)
 - transcription analysis
 - m-RNA semi-quantitative analysis
- 3)
 - infection of the lymphoblastoid cells derived from patients carrying the sequence variants with Epstein Barr virus (EBV)
 - proton and calcium release measurements in response to the RYR1 activator 4-CmC in immortalized B lymphocytes derived from patients by the metabolic microphysiometry assay and the flow cytometry, respectively.

3 MATERIALS AND METHODS

3.1 Patients

Twenty-four unrelated MHS subjects including 16 probands, who experienced an MH event during anesthesia, were enrolled in this study. The MHS status was assessed by the IVCT according to the protocol devised by the EMHG [European Malignant Hyperpyrexia Group, 1984; Ørding *et al.*, 1997]. One patient was referred with myopathy and minicores and one patient with CCD. Informed consent was obtained for each patient according to a procedure established by the local Bioethics Institutional Committee.

3.2 Genomic DNA extraction

Genomic DNA was extracted with the “Nucleon” procedure (Amersham, UK) from peripheral blood samples and from immortalized lymphoblastoid cells.

Blood samples (3-10 ml) were collected in sodium EDTA tubes and the cells were lysed adding 4 volumes of Reagent A (10 mM Tris-HCl, 320 mM sucrose, 5 mM MgCl₂, 1% (v/v) Triton X-100, pH 8.0) to the blood sample. The mix was stirred for 4 min at room temperature and centrifuged at 1300 x g for 5 min.

Immortalized B-lymphocytes (1 x 10⁷ cells) were centrifuged at 600 x g for 5 min at 4°C and the pellet was resuspended and lysed in 1 ml Reagent A. The mix was left on ice for 5 min and centrifuged at 1300 x g for 5 min.

The cellular pellet derived from blood samples or from immortalized cells was resuspended in 2 ml of Reagent B (400 mM Tris-HCl, 60 mM EDTA, 150 mM NaCl, 0.1% SDS, pH 8.0) and transferred to a 15 ml screw capped propylene centrifuge tube. Sodium perchlorate solution (1 ml) was added and mixed to perform the deproteinisation. DNA was extracted adding chloroform (2 ml) and mixing by inversion. Nucleon resin was added and centrifuged at 1300 x g for 3 min. The upper phase was transferred to a clean tube and 2 volumes of absolute ethanol were added and mixed by inversion until the precipitate appears. Precipitated DNA was hooked out using a heat-sealed Pasteur pipette. DNA was placed directly into Tris EDTA (10 mM Tris-HCl, 1 mM EDTA, pH 8) buffer. The DNA concentration was determined by the absorbance at 260 nm (A₂₆₀) ($\epsilon^{0,1\%} = 20$). The ratio of the readings at 260 nm and 280 nm (A₂₆₀/A₂₈₀) provides an estimate of the purity of DNA with respect to contaminants that absorb in the UV, such as protein. Pure DNA has an A₂₆₀/A₂₈₀ ratio of 1.8-2.0.

3.3 Polymerase chain reaction (PCR)

PCR is a standard method to amplify DNA fragments [Mullis *et al.*, 1987]. We used the Amplitaq DNA Polymerase (Applied Biosystems), a thermostable DNA polymerase, and we prepared a PCR master mix under the standard conditions listed below (Tab. 4).

Tab. 4 PCR amplification protocol.

Reagents	Final concentration
10X PCR Buffer	1X
dNTPs	0.8 mmol/l
MgCl ₂	1.5 mmol/l
Forward Primer	0.4 µg/ml
Reverse Primer	0.4 µg/ml
DNA template	40 ng/µl
Taq DNA Polymerase	0.02 U/µl
Final Volume	50 µl

We performed the PCR amplifications with Applied Biosystems GenAmp PCR System 9600. In order to avoid nonspecific amplifications we used the touchdown cycling condition (Tab. 5) [Roux *et al.*, 1994]. The PCR amplification conditions for each *RYR1* exon are shown in the table 6.

Tab. 5 Touch-down cycling condition; Ta (annealing temperature).

	Initial Denaturation	94°C	5'
14 c y c l e s	Denaturation	94°C	20"
	Annealing	Ta + 7° C with Δ -0.5°C for each cycle	40"
	Elongation	72°C	45"
25 c y c l e s	Denaturation	94°C	20"
	Annealing	Ta	40"
	Elongation	72°C	45"
	Final elongation	72°C	7'

Tab. 6 Primer sequences, Ta (annealing temperature) of the PCR reactions, PCR product size (bp) and temperatures of the dHPLC analysis for each *RYR1* gene exon.

exon	forward primer	reverse primer	Ta	amplicon size (bp)	dHPLC temperatures
1	GGGAGTCCTGGTCCAATG	CTCAGAGACCACCAGCAAGC	47 °C	362	62 °C, 63 °C, 64 °C
2	TGTGGTATCCGGGCCAGGCC	CACCTCCTTTCAGACTCCCAGAACC	59 °C	269	59 °C, 64 °C, 65 °C
3	CTCAAGAGTGTGGGCATCC	GCCCTAAACGACCCCTGG	48 °C	276	62 °C, 63 °C, 64 °C
4	TGGAGAGTCCGGGATCTGTGC	GAGGTCAGCCTCCTTCTAGCAGGC	59 °C	195	63 °C, 65 °C
5	GAGTGCAACCTCGGTGGCGTGG	TCTCATGCTTGCCCTGGCGTTCTGC	61 °C	255	63 °C, 64 °C
6	GGCAGTGATAGGAGTGTGGGCC	ACCTGGGAGCAGGAGAACCGC	61 °C	264	61 °C, 62 °C
7	CTCGCCACCCTGCAATCG	TATGCCTGAAGGGCAACATTAAGGG	61 °C	217	62 °C, 64 °C
8	TCCAGCCTCCCAATTGACCAACTTCC	TCATAGGGTCCCAGCCCTCCACG	61 °C	198	62 °C, 63 °C
9	ATTCGGGGAGCTGAACCC	CTTCCCCTCAAGACCTTTTCTGTCC	52 °C	207	61 °C, 62 °C, 63 °C
10	GGGGTCTCTGACTCCCCTTGGC	AGTGCAGGCTGGGCTGGGACGGG	64 °C	257	64 °C
11	GCTCCCCTGCTAAACACAG	CCTGGAAGTCAAGCATTCTCC	61 °C	279	60 °C, 61 °C, 63 °C, 64 °C
12	GGGCAAGTGCAGAACTCAAGTC	TTAGACAAGGGTGTGGGCAAC	52 °C	231	62 °C, 64 °C, 65 °C
13	CGTTGCGGCAGTTAGCGC	GCCCACAGGCCCGCTCCG	58 °C	285	64 °C, 65 °C
14	AGACAAGGAAGGGAGGGCCTGG	GGTGTGATCCAATAGGACTGGG	59 °C	265	60 °C
15	CCAGTCTGACTCCCCTGAGAACACC	TGCCCAGAATGAGAGTTGAAGCG	59 °C	244	61 °C, 62 °C, 63 °C
16	GAGGCTTGTGGAGGGATGG	GGAGGAGCAGAGTTCTGGAGCCC	61 °C	261	61, 62 °C
17	CAGGGTCTTCTGTAGACCTGCC	CTGGGTCAGATGTTGAGAGCC	60 °C	226	60 °C, 61 °C
18 (I)	TTGGCTCTCTCTCTGCCTCTCCG	TCATCGCCGACCCCGTTGCC	58 °C	258	64 °C, 65 °C
18 (II)	AGCTCAGGCCACCCACTTGCG	GACTTAGAAATGCTGGGGTCAATGG	59 °C	202	63 °C, 65 °C
19	TGGTCTGTGGGACCTGTGACG	GGTCTGAGACTGGCCGTGG	61 °C	282	63 °C, 64 °C
20	TGATCCCCATTGTCTTCTTACCC	CCTCGCCAGAAAACCTTTGCAGG	60 °C	278	62 °C, 63 °C
21	ATGGTGGGAAAGGGGTGCT	ATGACCCCTGACCTCCAACC	54 °C	375	61 °C, 63 °C, 64 °C, 65 °C
22	GTGGGGAGTGGGAAGGAAAG	AATCCCTGTCCCCTCCATCC	54 °C	275	61 °C, 62 °C, 63 °C
23	TGGAGACCCTGAGGCCGTGG	TCGACCTCCCAGCCCTTAGC	58 °C	243	63 °C, 64 °C, 65 °C
24 (I)	GCAGAGCCCGAAAGTGGAGGTGAGG	TGCTGCGCTTGGTGGCTTCATCC	64 °C	341	64 °C, 66 °C, 67 °C
24 (II)	CAGGGCTGGAGCTACAGCGCAGTG	ATCGGGCTGGGTCAGAGTTGG	64 °C	235	64 °C, 65 °C, 66 °C
25 (I)	CCAACTCTCGATGTCTTGGGATC	CGCATCTCGCCTGTGGTGAC	54 °C	190	60 °C, 61 °C, 62 °C
25 (II)	CGCATCTTCCGGGCAGAGAAATCC	TGGGAGAGACCACAGGACCTGGCAG	66 °C	217	63 °C, 64 °C, 65 °C
26	CCTTATCTCTCCATTCTCTGTGTG	AGAAGGGCAGTGCAGGGTTG	54 °C	308	61 °C, 62 °C, 64 °C
27	CCAACTCTCCATCCCTACCTCC	AGCACTGTGGAAGGAAGGAGC	58 °C	362	62 °C, 63 °C, 64 °C
28 (I)	TATGGCCTAATGGTGGCTCCGTGTG	TTGCCGTTCTCTGCCTCGCTCC	55 °C	376	63 °C, 64 °C, 65 °C
28 (II)	GCACTTCCGCTGCACTGC	CAGGTTACTGTGGTTGCCTACTTG	49 °C	341	62 °C, 63 °C, 66 °C, 67 °C
29	ATATTGCGGTGGGAGGGCTGGGC	GGGCAGCTACTGGGACTGTCACAC	66 °C	291	61 °C, 62 °C, 64 °C
30	GGGACCCGAGTCCCTGACTTC	AGCTCTGACTGCCTCCTGCCCTC	64 °C	279	61 °C, 63 °C, 64 °C
31	TTCCGGGAGCTTGGGAAAGGG	TCCTGGGATGCTGGGACATGATGC	60 °C	300	60 °C, 61 °C, 62 °C, 63 °C
32	CCTCCCTCCAGCCCACCCGTTTG	CCCCACATCTCCTGCCTCAGCTG	68 °C	194	61 °C, 62 °C
33	CTGGAAGTGGTGTGGTGGGACAGAG	AGGGGCACTGAGTGGGACCCAG	62 °C	371	63 °C, 64 °C, 65 °C
34 (I)	GATGCAGGAGGCTCATTATCTGTG	GAAGTGGTACTCCAACCTCCCGG	64 °C	427	63 °C, 65 °C
34 (II)	GGAAGGAGCACAGAAAATGG	TTTTGGGAATGTGGGAGAAG	52 °C	357	62 °C, 63 °C, 64 °C
35	GGCCAGGGCTGATGATG	TCCCCTGCTGAGGACGAAG	58 °C	426	60 °C, 61 °C
36	TTCAAGGAAGTCTGATGGTCTC	GATGTTGAGGTTGGGTTAGACAG	60 °C	318	62 °C, 63 °C,

37	TCTCAGAGTTCCTGCTTTG	CCGATACTGTAGAGGGTTGT	46 °C	269	58 °C
38	TGCACAAATAATGAGTGTGTAAGT	AGGCATGGGGCTACCCAC	53 °C	282	59 °C, 60 °C, 61 °C
39	CCATGTGCCGACCTGCCCTGCATG	GGGCCAGAAGTTGGGAAGGGAATG	68 °C	424	63 °C, 64 °C, 65 °C
40	CGCTGTCACAGTGGTGGCTATGGC	AGCTCCCCAGCACCTGCCCTGG	62 °C	220	66 °C
41	CAGGGGAGGAGGCAGCCACAGAG	GGAGTGTGTTGTAATGAGTGAGC	58 °C	286	62 °C, 63 °C, 64 °C
42	TACAGACCAGAGGAGGCACCTGATCC	AGGTGTCCAAGCAGCCGGG	61 °C	279	63 °C, 64 °C, 65 °C
43	GCTGAGCCCCAGGAGGAAGGTGG	GGAGGTGTGTGACCAGTGACTCCG	61 °C	259	63 °C, 64 °C
44	CATGAGACCCCTTTCCCCATGCG	GGCGGGTTGCCCTATTGAGG	61 °C	256	65 °C, 66 °C
45	TGCCTCCCAACCCACCCACCTTC	TGCCTGCCCTCCCTCCCATCTCG	61 °C	183	63 °C, 64 °C, 65 °C
46	GCTCTACCCTCCTGTGTGTAAGGG	GCATCACTCCTTCGCCAAGTTCC	61 °C	252	62 °C, 63 °C
47(I)	GGTGACAGGGGATGGAACCTTGCCG	TGTCGGGCAGAACCCACGTC	64 °C	231	60 °C, 63 °C, 64 °C
47(II)	CATCCTTCGTGCCGACCACAAG	TGCTGCTCTACCGTGACCCATCTCC	64 °C	216	63 °C, 64 °C
48	TGTGCAGCGGGCTGATGTCC	TGCCCCACCTGAAGCCTGC	64 °C	288	64,2 °C, 65,2 °C
49	GATTCTACATCTTGTGATTGTCCC	GTAGGAGGGAAGAGCAAACCAAGTGG	58 °C	187	62 °C, 63 °C
50	TGCCTGCCATTGCTGGTGCC	TTGCAGAACCTTCTCCTCTGAAC	57 °C	315	59 °C, 62 °C
51	GGGAGGAGGGCTGATGATTGCAGTG	CAGCAGATGTTGGAGCTGGGGTTCC	70 °C	343	60 °C, 61 °C, 63 °C
52	CGGCCTGTGAGACCCCTCAAGTG	GGGCCTCAGGGAAGAACCAGGTC	66 °C	269	61 °C
53	TGTCTCGGCTCCTCCAGGG	ATTGCCTCACTCCTCCCGAATC	58 °C	246	58 °C, 59 °C, 61 °C
54	TGGTCAGGGTTTTCTGCTTTG	TCTCTCTCCATCCCTTCCC	48 °C	307	60 °C, 61 °C
55	GTGGAGGGGTAGAATGGAC	AGCTCCTGCTTCTTCTCCG	48 °C	328	60 °C, 61 °C, 62 °C
56	GGGGGCTGGCATCCTCTGAA	CGGTGAATCCACGGGGTAGC	50 °C	172	61 °C, 62 °C, 63 °C
57	GCAAGCAATGTTCCGTTATTTC	TTAGCTCCTCCCTCTGGTT	45 °C	396	62 °C, 63 °C, 64 °C
58	GAGGGGAGAAGGTAAGTG	AGGGGAGGACGGATTGAGAG	51 °C	395	61 °C, 62 °C
59	ATTTCCCAACTCTGCTCCCA	GAGATAAAGGGTCCAATGAG	45 °C	238	60 °C, 61 °C
60	CCCCTATTGGACCTTTAT	TCAGTCCCGGGTACACTAGG	49 °C	320	60 °C, 61 °C, 62 °C
61	CTGTCTCGTCTCCTTGGC	ATAGGTCTGTCTCTCCACT	48 °C	335	59 °C, 60 °C, 61 °C
62	AGGAAGAGAGCGGTTGGGG	GGCAGCGGGGAACATCAG	50 °C	256	61 °C, 62 °C, 63 °C
63	GCCCACTCCACCATCATC	CCACACATTCAAACACCAG	52 °C	430	61 °C, 62 °C, 63 °C
64	CTGCTTGCTCTTCCCACTG	CATCTACCCTGCTTTTACC	50 °C	285	63 °C, 64 °C
65	GGGAGGAGCCGTTTCTATG	CCCAGCCCAGCCACTAC	50 °C	317	63 °C, 64 °C, 65 °C
66 (I)	TAGTTGGGTTGGAGGGTGAG	TGAGGTGGTCAGAGGTGACA	58 °C	410	58 °C, 59 °C, 62 °C
66 (II)	CCCAACAGTGTGGAGGAGAT	TGACCCTGGTCTTTTGATG	56 °C	468	62 °C, 63 °C, 64 °C
67	GAGATGCTGTTTGGGAGTCG	AGATCAGATGGGGCTGGAG	50 °C	400	63.8 °C, 64.8 °C
68	GAAACCCATCCCTCTGAC	CACAAAGTTCTGCTCTCGC	54 °C	327	63 °C, 64 °C
69	AGGAGCTGTTCAGGATGGTG	GAGATGGGAGGAGGGAGAAG	48 °C	449	60 °C, 61 °C, 62 °C
70	CCTTCTCAGGTCTCAGAGAA	GGGTGGGGAACAGAAGCAGG	48 °C	302	61 °C, 62 °C, 63 °C
71	CCTGGGGTGTGGATGATG	GGGCTCAGTGGCATTGTGG	54 °C	330	64 °C, 65 °C
72	AAAACCTCTCAGTCTCTGG	GTAATGCTCAAACCTTCACTA	50 °C	254	59 °C, 60 °C
73	TCACCCATTGAGTCTCCCA	AGACCCACCCACATCCTTG	54 °C	342	64 °C
74	TTCTTCTGCCGTGTGAGTC	GTGCTTCCCGACCTCCCAT	49 °C	373	61 °C, 62 °C, 63 °C, 64 °C
75	GAGAGTCTGGAGAATGGAGG	GCCCTACTTTGGTTCTACTC	54 °C	370	61 °C, 62 °C
76	AAACCTCTCCCAAGTCTC	CCCAGATTGCTGGGACTACA	51 °C	293	61 °C, 62 °C, 63 °C
77	AGAGTGTGGGATTACAGGC	ACAAAGCAGACCCCTCCATC	58 °C	259	61 °C
78	ATTTCCCTCTCCACCTGC	TGCTCTGTGAACACATGCTG	49 °C	250	61 °C, 62 °C
79	TGAGAATGTGAGGGGAAAG	CAAACCACAGGCATTGAGGG	48 °C	284	61 °C, 62 °C, 63 °C
80	TGGCTGTTTTTCTGGTGGTG	GGAGAAACTGGGAGTCACAC	50 °C	226	60 °C, 61 °C, 62 °C
81	CAGGTAACAGAGGCAAAGGG	AAGAGCAGAATCAGAACTGG	48 °C	265	59 °C, 60 °C

82	GCTAAATGGGTGGTTTCTGG	GGAGGAATCCCAAAGGAAGA	52 °C	347	59 °C, 60 °C
83	GCCTTTCTCTCTGTGGGTTG	GGGGAAAGTGAAGCTTAGGG	48 °C	418	59 °C, 60 °C, 61 °C, 62 °C
84	CAGTGTCTTTGGAGTGGCAG	GGCCGAAACTAATTCAGTC	52 °C	306	61 °C, 62 °C, 63 °C
85	CTGGCATAACAATAGGAACTC	CCGAGTAGTACCAGTAGAAG	48 °C	313	58 °C, 59 °C, 63 °C, 64 °C
86	CACGGTTCAGGTGTGACTTG	GCGCCCTACCTGGATGTA	50 °C	221	61 °C, 62 °C, 63 °C
87	CTGGGGCGGGAGTGGGAAG	CCCGGAAGCAGGTGGATGGA	59 °C	239	63 °C, 64 °C
88	GTAGGTGAGGAGGGGAGAA	CCCTCACTCCTGGGTGTTA	52 °C	182	61 °C, 62 °C
89	CGACCTGACATCATTAGC	CAAACAAGGAAAGTGAAG	46 °C	532	60 °C, 61 °C, 63 °C
90	GAATTGAGGCTCTCCAGGTCACC	TCTGAGGGTGCAGGAAGTGAAG	62 °C	467	62 °C, 64 °C
91(I)	GCGGTGACCCCTGTAGCTG	AGGCTGCGGTAGCTGAGGCC	50 °C	405	64 °C, 65 °C, 67 °C
91(II)	CCGGAGACCGACGAGGACGA	CTCGTCGCTGGTGGGTGCGG	61 °C	390	64 °C, 70 °C, 71 °C, 72 °C
91(III)	TGCTCTGGGCTCGCTGTTT	GTGTGTGTCTCCACCCAGCC	55 °C	453	61 °C, 66 °C, 68 °C
92	AAAGGAGATGAGAGGAGCAGG	CTACTCTAGGAGGGAGGCAGT	56 °C	214	63 °C, 64 °C, 65 °C
93	GCCCTTGGTGAATGTTTTG	GGTTCTTCTTAGAGACGAGC	54 °C	350	61 °C, 62 °C
94	TTTGATTGCAGGTAATGATGGGATG	CCCTGAAATCTGATAGGGGCTGAGC	58 °C	262	59 °C, 60 °C, 61 °C
95	CCAGTCCAATCTCGGGAATGGAG	CACCCAGCCAATAAGCCCTTGC	59 °C	385	60 °C, 61 °C, 62 °C, 63 °C
96	TGCTGAGACTATGGTCCAGCCAAGG	ATTACAGGTGTGAGCCACCGTGCC	61 °C	315	62, 63 °C
97	TGTCGTGGCTGACAGCTCTGATCCC	TGCCCAAGGTACACACCAAGCAAG	62 °C	216	60 °C, 61 °C
98	TGCACCTCCCATTCTCAC	GAGAGATGCTTGTGATGACAGACTC	45 °C	320	63 °C, 64 °C
99	ATCACAGCCACAATGAGCG	GGAGTCATTCTTTGGTCAGG	52 °C	303	62 °C, 63 °C, 64 °C
100	TACCCTCCAGAGTGCTCCTCG	GTTTCAGTCCCTGTGGCTTACC	59 °C	379	61 °C, 62 °C, 63 °C
101(I)	TAGAGCCACAGGGACTGAACCG	CTTGTGTAGAAGTTCGCGGAAGAAG	58 °C	187	62 °C, 63 °C, 64 °C
101(II)	TGATGACCGTGGGCCTTCTG	TATTAAGTCTTCAACAGATGCGAG	49 °C	192	61 °C, 62 °C
102	CGAATGAATGAGTGACCAAGTGTGC	TTGACACCCGAGAGGTGACTTGCC	63 °C	344	61 °C, 62 °C, 63 °C
103	GAGGGCAAGCCCTGGAGGTAGGTAGC	GCAAGAGACATCAGAGTGGAGGCC	61 °C	232	61 °C, 62 °C
104	GGAGGATATGGAGGTAGGTCATGTC	AGTACCCCACTGCTGGCTATTG	58 °C	270	61 °C, 62 °C, 63 °C
105	TTGGGCAACATAGCAAGACTTC	CTTTTTACTGCCACCTACTGAC	54 °C	231	58 °C, 59 °C
106(I)	CAACAGAGCAACACCTGTG	ACTAAGGGGCTTGTGTGAG	54 °C	254	57 °C, 58 °C, 59 °C
106(II)	AAGAGAGATGTTGGGATTC	GAAACAATCTCGGATGTCC	50 °C	269	58 °C, 60 °C, 61 °C, 62 °C

Each amplification reaction was checked by agarose gel electrophoresis with ethidium bromide staining. DNA molecular weight Marker IX (Roche) was used to determine the sizes of amplified fragments.

3.4 Denaturing High Performance Liquid Chromatography (dHPLC)

dHPLC is an ion-pair reversed-phase high-performance liquid chromatography (IP-RP-HPLC) technique. It identifies sequence variants based on detection of heteroduplex formation between mismatched nucleotides in double-stranded PCR amplified DNA. Sequence variation creates a mixed population of heteroduplexes and homoduplexes during reannealing of wild-type and mutant DNA. When this mixed population is analysed by dHPLC under partially denaturing temperatures, the heteroduplexes elute from the column earlier than the homoduplexes because of their reduced melting temperature [Sivakumaran *et al.*, 2003].

dHPLC analysis was performed using the WAVE system 3500 (Transgenomic, Omaha, NE). PCR samples from patients were mixed with equimolar amounts of the

wild type amplicon, denaturated at 95°C for 5 min and then cooled at room temperature to allow heteroduplexes to form if a mutation is present in the sample from the patient. Aliquots of each mixture (5-8 µL) were loaded onto a preheated C18 reverse-phase column (DNASep 4.5 x 50 mm; Transgenomic). To enhance the probability of detecting sequence variations of the PCR products by dHPLC, we analysed the PCR products for heteroduplexes using two or three partially denaturing temperatures selected from the predicted fragment melting profile generated by the WaveMaker 4.1.40 software (Transgenomic). The temperatures of the analysis for each *RYR1* exon amplicon are showed in table 6.

3.5 DNA sequence

Amplicons with an altered dHPLC elution profile compared to that obtained from a wild-type amplicon were directly sequenced with dye-terminator chemistry (Applied Biosystems) using an ABI3100 automated sequencer (Applied Biosystems, USA). Nucleotide substitutions were numbered on the cDNA sequence (GeneBank NM_000540.2) and on the genomic sequence (AC011469.6, AC067969.1, AC005933.1 accession numbers) using the Mutalyzer program [Wildelman *et al.*, 2008].

3.6 EBV-transformed B-lymphocytes

In order to obtain stable lymphoblastoid cell lines, human B lymphocytes were infected with the Epstein-Barr virus (EBV), according to standard procedures [Neitzel, 1986].

3.6.1 Production of the Epstein-Barr Virus

The source of EBV was the marmoset cell line, B95-8, which is chronically infected with the virus and can secrete viral particle into the culture medium. B95-8 cells were cultured at $1-3 \times 10^6$ cells/ml in RPMI medium (R 0883, Sigma-Aldrich), supplemented with 10% fetal bovine serum (FBS) (CH30160,03, Hyclone) and 1% L-glutamine (G7513, Sigma-Aldrich) at 37°C, 5% CO₂. In order to stimulate the B95-8 cells to secrete the EBV in the culture medium, the cells were plated at 2×10^5 cells/ml and cultured for 3-4 weeks at 33°C, 5% CO₂. The cell suspension cultures were centrifuged at 1300 x g for 10 min. These supernatants were filtered with a 0,22 mm pore diameter filter (Millipore) and aliquots were frozen at -80°C.

3.6.2 Mononuclear cell isolation

Peripheral blood mononuclear cells were isolated by Ficoll-Hypaque density centrifugation. Peripheral blood was diluted 1:1 with Phosphate Buffered Saline (PBS) and 7 ml of diluted blood were layered carefully on top of 3 ml Ficoll-Hypaque. After centrifugation for 30 min at 750 x g at room temperature, the upper layer was removed and the mononuclear cell layer was collected from the interface. The cells were transferred to a 15 ml test tube and 10 ml of PBS were added. The cells were centrifuged for 10 min at 250 x g at room temperature. The cell pellet was washed 2 times with PBS and the cell number was determined in a Burker counting chamber. The cells were transformed with EBV or stored in liquid nitrogen.

3.6.3 EBV infection of human B lymphocytes

For infection with EBV, mononuclear cells were suspended at $1,6 \times 10^7$ cells in culture medium containing 50% of the EBV supernatant [Neitzel *et al.*, 1986]. Medium was replenished twice weekly, and the cultures were monitored for signs of transformation (increased cell growth, cell aggregates, or clumping), which were generally apparent within 3 to 8 weeks in successful cultures. Transformed cultures were grown to approximately 1×10^7 cells/ml, cryopreserved in heatsealed borosilicate glass ampules (~ 5 million viable cells for each ampule) and stored in liquid nitrogen.

One of the problems of EBV-transformed cell lines is the instability of the cells derived. Therefore each transformed cell line was cloned. Cell suspensions were diluted to a concentration of ~ one cell per 0,5 ml of culture medium. The cells were plated into 96-well plates, adding 100 μ l of medium per well. The cultures were grown until ~ 10^3 cells/well, then transferred to a 24-well plate. Clones were expanded into flasks and stored in liquid nitrogen. All the EBV-immortalized lymphoblastoid cells carrying the *RYS1* gene variants were analyzed to verify the presence of the nucleotide substitutions.

3.7 RNA extraction from EBV-immortalized B-Lymphocytes

Total cellular RNA was extracted from EBV-immortalized B-lymphocytes using QIAamp RNA Blood Mini kit (52304, Qiagen). The kit provides a silica-based membrane and a specialized high-salt buffering system that allows RNA species longer than 200 bases to bind to the QIAamp membrane.

Immortalized cells (1×10^7 cells) were centrifuged at $400 \times g$ for 10 min at 4°C and the pellet was lysed in 600 μ L Buffer RLT that immediately inactivate RNases, allowing the isolation of intact RNA. The lysate was homogenated by a brief centrifugation through a QIAshredder spin column, then 1 volume of 70% ethanol was added to the column and the sample was transferred to a QIAamp spin column. During a brief centrifugation step RNA is bound to the silica membrane. To eliminate the contaminants, the column was washed first with 700 μ L of Buffer RW1 and then by 500 μ L of Buffer RPE. RNA was eluted in 30 μ l or more of RNase-free water and stored at -80°C . RNA concentration and purity were determined by measuring in a spectrophotometer the absorbance at 260 nm ($\epsilon^{0.1\%} = 20$). Pure RNA has an A260/A280 ratio of 1.9–2.1. The quality and integrity of RNA were verified by agarose gel electrophoresis.

3.8 cDNA synthesis

The SuperScript III first-strand synthesis system (18080-051, Invitrogen) was used to synthesize first-strand cDNA from total RNA extracts. The reaction was performed as follows: - 2,5 μ g RNA were denatured at 65°C for 5 min in a mixture containing 5 ng/ μ L of random hexamer primers and 1 mM of dNTPs (10 μ L final volume) and then placed on ice for 1 min; - 10 μ L of the cDNA Synthesis Mix (20 mM of dithiothreitol, 2 \times RT Buffer and 20 U/ μ L of SuperScript III reverse transcriptase) were added to 10

μ L RNA/primers/dNTPs mixture and incubated at 25°C for 10 min to anneal the primers to the RNA template; - cDNA was synthesized at 50°C for 50 min and then the reaction was terminated at 85°C for 5 min; - finally RNA was removed incubating synthesized cDNA with 2 U/ μ L of RNase H at 37°C for 20 min; cDNA was stored at - 20°C or used immediately for PCR.

3.9 Semi-quantitative PCR

Semi-quantitative PCR reactions were performed using a Perkin Elmer 9600 thermocycler with the following mix: 1,5 μ L cDNA, 0,2 U/ μ L of AmpliTaq polymerase, 0.1 mM of dNTPs mix, 1 \times buffer AmpliTaq, 1,5 mM MgCl₂ and 0,2 ng/ μ L of each primer. To avoid genomic DNA amplification in the PCR reaction, primers were designed over the intron splice junctions (Tab. 7). The housekeeping β -ACTIN gene was used as a control for variations in the RNA input.

Tab. 7 Sequences of the primer used for semi-quantitative RT-PCR. The forward primers were labeled with one fluorescent dyes, PET and VIC for the *RYS1* and the β -ACTIN genes, respectively.

Gene	Forward (F) and reverse (R) primers (5'-3')	Location	Gene Bank Accession No.	Product size(bp)
<i>RYS1</i>	F PET-tcacatgtacgtgggtgtcc R gcacttggtctccatattcctc	c.14788-14807 c.14987-15007	NM 000540	220
β -ACTIN	F VIC-cgtcttcccctccatcgt R tgtggcgtacaggtctttg	c.171-188 c.954-973	NM 001101.3	803

Reaction conditions used for semi-quantitative RT-PCR are shown in table 8. The amount of amplicons in subsequent PCR cycles was evaluated by capillary electrophoresis.

Tab. 8 Reaction conditions used for semi-quantitative RT-PCR of *RYS1* and β -ACTIN genes.

Initial Denaturation		95°C	5'
25 c y c l e s	Denaturation	95°C	20"
	Annealing	54°C	40"
	Elongation	72°C	45"
Final elongation		72°C	7'

3.10 Capillary Gel electrophoresis (CGE)

CGE is a technique that allows high-resolution separation of nucleic acids. The most important advantage of CGE, when compared to other liquid-phase separation techniques, is the analysis speed combined with the high separation efficiency [Smith and Nelson, 2003].

RT-PCR products were separated on the ABIPRISM 3130 Genetic Analyzer. The matrix file (spectral calibration) was generated using a 5-dye system (FAM, VIC, PET, and LIZs standards). 1 μ L of the amplified product and 0.5 μ L of GeneScanTM-500 LIZ size standard were added to 12 μ L of deionized Hi-DiTM Formamide (Applied Biosystems), denatured at 95°C for 5 min, and then chilled on ice for 3 min. Samples were injected for 10 s at 3 kV and subjected to electrophoresis at 15 kV for 25 min using the POP-7 polymer at 60°C. The data were collected using the ABIPRISM 3130 Data Collection Software application v1.1. Electrophoresis results were analyzed using ABIPRISM GeneScans Analysis Software v3.7.1.

3.11 Proton release assay

The increase in the extracellular acidification rate of immortalized lymphoblastoid cells in response to 4-CmC is mainly due to the activation of the RYR1 channel and has been used to characterize the functional defect of RYR1 mutant channels [Zullo *et al.*, 2009, see appendix]. We measured proton release using the Cytosensor[®] microphysiometer (Molecular Devices, San Diego) as described [Zullo *et al.*, 2009; Klingler *et al.*, 2002]. All experiments were carried out with repeated cycles of 9 min applications of 4-CmC (C55402, Sigma-Aldrich) with a stepwise increase from 200 μ M to 1000 μ M, followed by a 9-min washout. The stock solutions of 10 mM 4-CmC (C55402, Sigma-Aldrich) were prepared for the experiments with the Cytosensor[®].

3.12 Calcium release assay

The principle of flow cytometric Ca²⁺ flux measurement is based on changes in fluorescence intensity or emission wavelength of a fluorophore following chelating of calcium ions. The fluorescence intensity of fluo-3 increases upon binding Ca²⁺ and that of Fura Red decreases; the Fluo-3/Fura Red fluorescence signal ratio allows a ratiometric analysis of Ca²⁺ fluxes [Bailey *et al.*, 2006].

EBV-immortalized B-lymphocytes were incubated with two Ca²⁺ sensitive fluorophores, Fluo-3 AM and Fura-Red AM, for ratiometric analysis of Ca²⁺-release [Minta *et al.*, 1989; Novak and Rabinovitch, 1994]. Fluo-3 and Fura Red dyes were used at concentration of 2,6 μ M and were excited at 488 nm and the two emission signals were detected at 530/30 nm (Fluo-3) and 610/20 nm (Fura Red). The incubation was performed at 37°C, 5% CO₂ for 30 min in the Iscove's medium supplemented with 0.1% BSA and 1% L-Glutamine. The cells were washed once and resuspended in HBSS medium without Ca²⁺, 1mM EGTA at 1x10⁶ cells/ml. A BD FACSAria cell sorter was used to measure Ca²⁺ fluxes in response to 4-CmC and thapsigargin (TG); the measurement was done at 37°C. Forward angle scatter signals (FSC), an indicator of cell size, and side angle scatter signals (SSC), an indicator of cell granularity, were displayed on a linear scale, with the forward scatter

adjusted to gate cells from debris (Fig. 17 A). Fluo-3 and fura-Red fluorescence values are recorded and displayed on a logarithmic scale (Fig. 17 B). For each experiment, the fluo-3/fura-red values were recorded for 2 min before the addition of the triggering agents to obtain the baseline. Cells were then exposed to 4-CmC or TG and the cellular responses were analyzed over a period of 5 min (Fig. 17 C). To obtain a kinetic analysis of the response to the triggering agents, we splitted in 50 gates the dot plot display of fluo-3/fura-red values *versus* time (Fig. 17 D). The fluo-3/fura-red mean values for each gate were calculated using the Becton-Dickinson analysis software (Fig. 17 E).

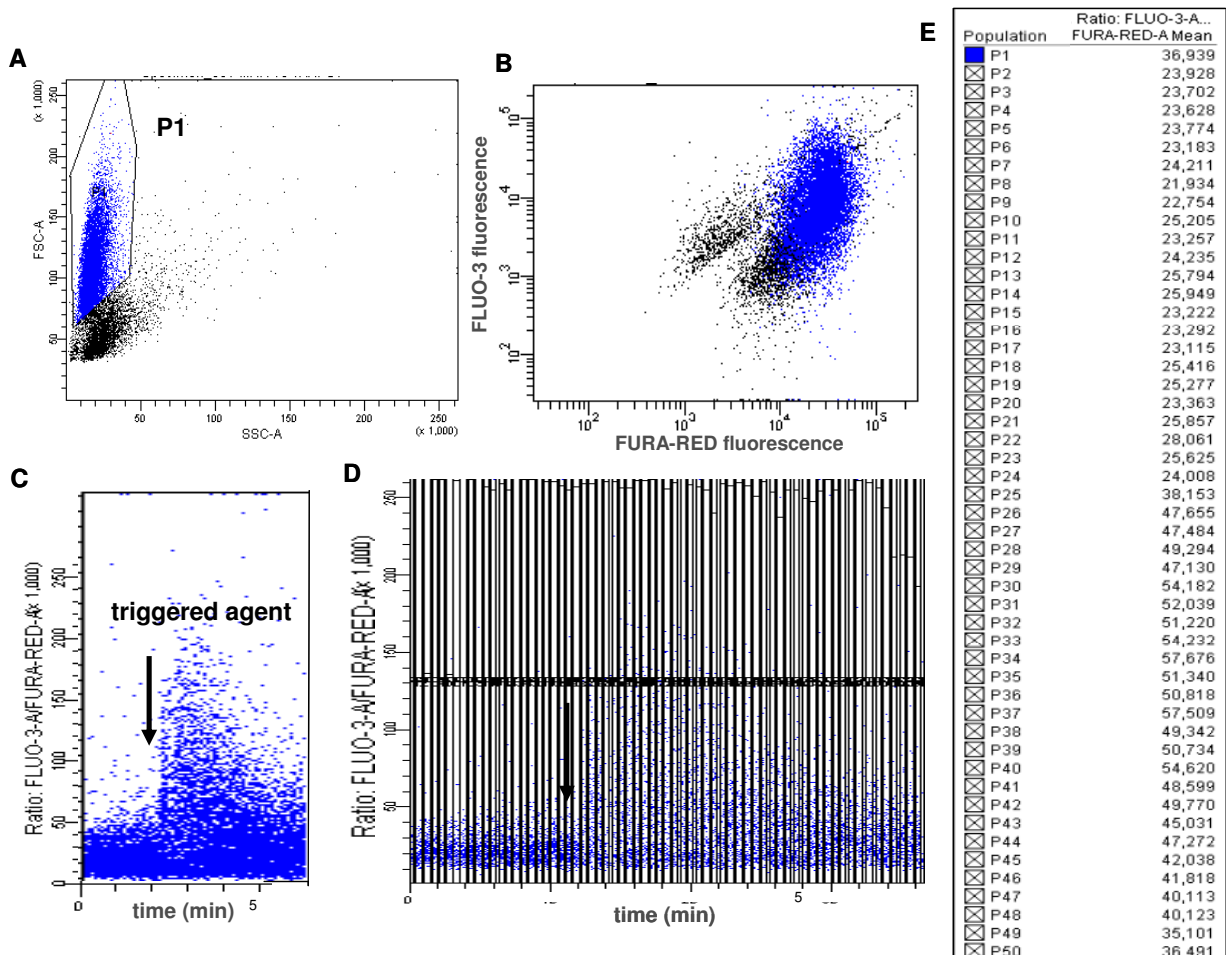


Fig. 17 A. Forward angle scatter signals was plotted *versus* side angle scatter signals and P1 gate was drawn to rule out debris. **B.** Fluo-3 fluorescence values were plotted *versus* fura-red fluorescence values, on a logarithmic scale. **C.** The cellular responses were analyzed as ratio between fluo-3 and fura-red fluorescence value over a period of 7 min; the arrow indicates the administration of triggering agent. **D.** The dot plot display of the fluo-3/fura-red fluorescence values *versus* time was splitted in 50 gates to perform a kinetic analysis. **E.** Values of fluo-3/fura-red mean values calculated for each gate.

The cellular responses to the drug (4-CmC or TG) were measured by integrating the Fluo-3/Fura Red fluorescence signals by SigmaPlot program. Lymphoblastoid cells from normal subject responded to 4-CmC by increasing the Fluo-3/Fura Red fluorescence signals (Fig. 18).

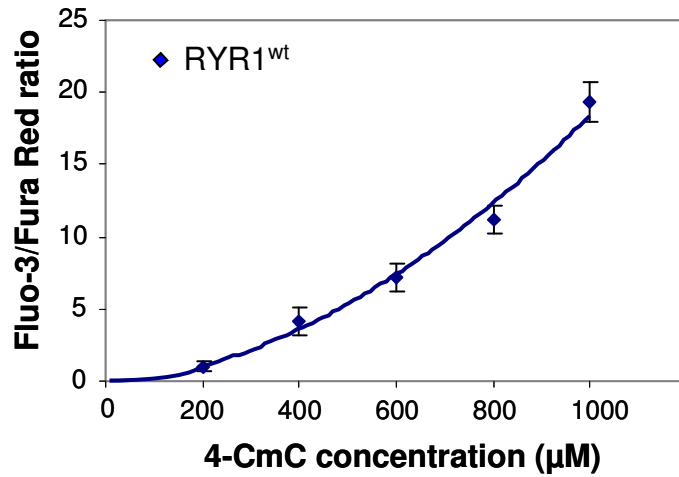


Fig. 18 Increase of Fluo-3/Fura Red fluorescence mean signals in the control B-lymphocytes stimulated with different concentrations of 4-CmC. Error bars show the propagation of the SEM.

3.13 Statistical analysis

Results are reported as means and standard error of the mean (SEM) of at least three independent experiments. Significance of the differences between groups was evaluated by the Mann-Whitney test. Differences were considered to be significant when $P < 0.05$.

4. RESULTS

d-HPLC screening of the 106 exons of the *RYR1* gene was performed in 24 MHS subjects, one CCD patient and one with minicores. Sequencing of amplicons with altered d-HPLC elution profiles revealed 14 sequence variants, an *in-frame* insertion variant (Tab. 9) and several known and novel polymorphisms (Tab. 10). Some results have been already published [Zullo *et al.*, 2009, see appendix]. For each novel sequence variant identified we performed the molecular characterization (see 4.1) and we characterized the effect of nine *RYR1* variants on the channel function (see 4.2). The mutation rate was 57%, considering the known mutations and the putative causative variants identified in this study, each in a single patient, with the exception of the CCD patient who bears a double *RYR1* variant.

Tab. 9 *RYR1* sequence variants identified in 24 MHS subjects, one CCD patient and one MmD patient screened.

Exon	Nucleotide change	Amino acid change	Role of mutation	References
15	c.1589G>A	p.R530H	MHS c.m.*	Robinson <i>et al.</i> 2006
17	c.1840C>T	p.R614C	MHS c.m.	Robinson <i>et al.</i> 2006
39	c.6488G>C	p.R2163P	MHS c.m.*	Robinson <i>et al.</i> 2006
39	c.6502G>A	p.V2168M	MHS c.m.	Robinson <i>et al.</i> 2006
40	c.6635T>A	p.V2212D	MHS p.c.m.	Galli <i>et al.</i> 2006
43	c.7025A>G	p.N2342S	MHS c.m.*	Robinson <i>et al.</i> 2006
44	c.7035C>A	p.S2345R	MHS p.c.m.	This thesis
44	c.7112A>G	p.E2371G	MHS c.m.*	Zullo <i>et al.</i> 2009 and this thesis
46	c.7355G>C	p.R2452P	MHS p.c.m.	Zullo <i>et al.</i> 2009
46	c.7361G>A	p.R2454H	MHS c.m.	Robinson <i>et al.</i> 2006
63	c.9293T>A	p.S3098I	CCD c.m.	This thesis
85	c.11708G>A	p.R3903Q	MHS/ MmD p.c.m	Galli <i>et al.</i> 2006/ Zullo <i>et al.</i> 1009
91	c.12700G>C	p.V4234L	MHS p.c.m.	Robinson <i>et al.</i> 2006
95	c.13990T>C	p.C4664R	MHS c.m.*	Zullo <i>et al.</i> 2009 and this thesis
102	c.14772-14773ins TAGACAGGGTGTGCTCTGTTGCCCTTCTT	p.F4924-V4925ins RPAVAVLPFF	CCD p. c.m.	This thesis

c.m.: causative mutation; c.m.*: causative mutation demonstrated in this study; p.c.m: putative causative mutation. Nucleotide numbering reflects cDNA numbering based on cDNA Ref Seq: NM_000540.2, with +1 corresponding to the A of the ATG translation initiation codon in the reference sequence. The initiation codon is codon 1.

Tab. 10 Polymorphisms detected in the patient population screened.

Nucleotide change		Location	Amino acid	Ref SNP ID (NCBI)	References
genomic	cDNA				
g.27135G>T	c.165+35G>T	Intron 2			Zullo <i>et al.</i> 2009
g.28716G>A	c.270+27G>A	Intron 3		rs3745843	
g.30855C>T	c.573C>T	Exon 7	p.D191	rs892054	
g.30876A>G	c.594A>G	Exon 7	p.L198	rs12985668	
g.30952_30953insC	c.631+39_40insC	Intron 7			Zullo <i>et al.</i> 2009
g.35004T>C	c.1077T>C	Exon 11	p.A359	rs10406027	
g.41447T>C	c.1441-24T>C	Intron 13		rs7254832	
g.41778G>A	c.1668G>A	Exon 15	p.S556	rs2288888	
g.41811G>C	c.1672+29G>C	Intron 15		rs2288889	
g.44559C>G	c.2167+30C>G	Intron 18		rs2071086	
g.45499C>T	c.2286C>T	Exon 19	p.P762	rs3745847	
g.49592A>G	c.2678-67A>G	Intron 20		rs2304148	
g.52376G>A	c.2920G>A	Exon 24	p.V974M		Zullo <i>et al.</i> 2009 and this thesis
g.52399G>A	c.2943G>A	Exon 24	p.T981	rs2228069	
g.52435C>T	c.2979C>T	Exon 24	p.N993	rs2228070	
g.55276C>T	c.3456C>T	Exon 26	p.I1152	rs11083462	
g.61548T>C	c.4161-6T>C	Intron 28		rs55845760	
g.64095C>T	c.4443C>T	Exon 30	p.N1481		Zullo <i>et al.</i> 2009
g.72251C>T	c.5360C>T	Exon 34	p.P1787L	rs34934920	
g.75487A>G	c.5622A>G	Exon 35	p.E1874		Robinson <i>et al.</i> 2006
g.75714C>G	c.5814+35C>G	Intron 35		rs16972654	
g.76880A>G	c.6039A>G	Exon 37	p.K2013	rs2228068	
g.78776G>T	c.6178G>T	Exon 38	p.G2060C	rs35364374	
g.80697C>T	c.6384C>T	Exon 39	p.Y2128		Zullo <i>et al.</i> 2009
g.80871C>T	c.6548+10C>T	Intron 39			Zullo <i>et al.</i> 2009
g.82501C>T	c.6599C>T	Exon 40	p.A2200V		Robinson <i>et al.</i> 2006
g.85932C>T	c.7089C>T	Exon 44	p.C2363	rs2228071	
g.85941C>T	c.7098C>T	Exon 44	p.P2366	rs2229147	
g.86189C>T	c.7260C>T	Exon 45	p.H2420	rs12973632	
g.86794G>T	c.7324-48G>T	Intron 45			Zullo <i>et al.</i> 2009
g.87112G>T	c.7500G>T	Exon 47	p.A2500	rs2228072	
g.87139G>A	c.7527G>A	Exon 47	p.V2509	rs2071088	
g.87236C>G	c.7614+10C>G	Intron 47		rs2960323	
g.89143C>T	c.7863C>T	Exon 49	p.H2621	rs2229142	
g.89152C>T	c.7872C>T	Exon 49	p.R2624	rs1469698	
g.89234A>G	c.7926+28A>G	Intron 49		rs1469699	
g.90506G>A	c.7977G>A	Exon 50	p.T2659	rs2229144	
g.90953_90955delCCT	c.8068-30_32delCCT	Intron 50		rs10532729	
g.91034T>C	c.8118T>C	Exon 51	p.I2706	rs2960340	
g.91106T>C	c.8190T>C	Exon 51	p.D2730	rs2915951	
g.91571G>A	c.8337G>A	Exon 53	p.E2779	rs2915952	

Nucleotide change		Location	Amino acid	Ref SNP ID (NCBI)	References
genomic	cDNA				
g.91610G>A	c.8376G>A	Exon 53	p.R2792		Zullo <i>et al.</i> 2009 and this thesis
g.91662A>G	c.8400+28A>G	Intron 53		rs2915953	
g.92216C>T	c.8541+34C>T	Intron 54		rs2960342	
g.92219T>G	c.8541+37T>G	Intron 54		rs2960343	
g.92221G>C	c.8541+39G>C	Intron 54			Zullo <i>et al.</i> 2009
g.92236A>G	c.8541+52A>G	Intron 54		rs2915954	
g.92586T>C	c.8589T>C	Exon 55	p.S2863	rs2229146	
g.92620G>A	c.8616+7G>A	Intron 55			Zullo <i>et al.</i> 2009
g.92635G>C	c.8616+22G>C	Intron 55			Zullo <i>et al.</i> 2009
g.92672C>T	c.8617-35C>T	Intron 55		rs2960344	
g.92673T>C	c.8617-34T>C	Intron 55			Zullo <i>et al.</i> 2009
g.92810T>G	c.8692+28T>G	Intron 56		rs2960345	
g.92960_92961insTCA	c.8693-105_104insTCA	Intron 56		rs35973146	
g.92996A>T	c.8693-69A>T	Intron 56			Zullo <i>et al.</i> 2009
g.93055G>C	c.8693-10G>C	Intron 56		rs2915958	
g.93205T>A	c.8816+16T>A	Intron 57		rs2915959	
g.93231A>C	c.8816+42A>C	Intron 57		rs2960346	
g.94097_94098insC	c.8932+34_35insC	Intron 58		rs5828009	
g.97960G>A	c.9172+114G>A	Intron 61			Zullo <i>et al.</i> 2009 and this thesis
g.98287C>T	c.9173-21C>T	Intron 61		rs2960338	
g.98321A>G	c.9186A>G	Exon 62	p.P3062	rs2071089	
g.98704G>A	c.9457G>A	Exon 63	p.G3153R		Zullo <i>et al.</i> 2009
g.102442G>A	c.9674G>A	Exon 65	p.R3225Q		Zullo <i>et al.</i> 2009
g.105619C>T	c.10188C>T	Exon 67	p.D3396	rs2229145	
g.105655C>T	c.10218C>T	Exon 67	p.Y3406		Robinson <i>et al.</i> 2006
g.105697G>A	c.10259+7G>A	Intron 67			Zullo <i>et al.</i> 2009
g.109668G>T	c.10440+122G>T	Intron 69			Zullo <i>et al.</i> 2009
g.8585C>T	c.10687-7C>T	Intron 72		rs2960354	
g.9458A>G	c.10938-86A>G	Intron 74		rs6508806	
g.15671C>G	c.11266C>G	Exon 79	p.Q3756E	rs4802584	
g.17914C>T	c.11608+201C>T	Intron 83			Zullo <i>et al.</i> 2009
g.24356T>A	c.11754T>A	Exon 85	p.T3918	rs45613041	
g.11427C>T	c.13317C>T	Exon 91	p.A4439		Robinson <i>et al.</i> 2006
g.16392C>G	c.13671C>G	Exon 94	p.S4557	rs35959206	
g.32386G>T	c.15021+37G>T	Intron 105			Zullo <i>et al.</i> 2009 and this thesis

Nucleotide location was determined using the Mutalyzer program [Wildelman *et al.*, 2008] from the genomic sequences AC011469.6 (from intron 2 to intron 69), AC067969.1 [(from intron 72 to exon 85) and AC0059333.1 (from exon 91 to intron 105) and from cDNA sequence Ref Seq: NM_000540.2 (nucleotides were numbered on cDNA with +1 corresponding to the A of the ATG translation initiation codon in the reference sequence. The initiation codon is codon 1).

4.1 Molecular characterization of sequence variants

Nine sequence variants [c.1589G>A (p.R530H), c.1840C>T (p.R614C), c.6488G>C (p.R2163P), c.6502G>A (p.V2168M), c.6635T>A (p.V2212D), c.7025A>G (p.N2342S), c.7361G>A (p.R2454H), c.11708G>A (p.R3903Q) and c.12700G>C (p.V4234L)] were previously associated with MHS status [Robinson *et al.*, 2006], among which three (p.R614C, p.V2168M, p.R2454H) were found to be MH-causative (www.emhq.org), and one, p.R530H, was reported [Robinson *et al.*, 2006] as a personal communication without characterization data. The p.R3903Q sequence variant was found at the homozygous status in a patient who had myopathy associated to altered distribution of oxidative enzymes and minicores in muscle (biopsy analysis, Dr. F. Cornelio, Milan, Italy, personal communication). Five missense changes, c.7112A>G (p.E2371G), c.7035C>A (p.S2345R), c.7355G>C (p.A2452P), c.9293T>A (p.S3098I) and c.13990T>C (p.C4664R) (Tab. 9), are novel sequence variants; these were absent in more than 100 alleles of MHN subjects and resulted in changes of amino acid residues conserved in all the RYR isoforms of various species. We also identified the variants c.2920G>A (p.V974M) and c.9674G>A (p.R3225Q) (Tab.10), each detected also in one MHN individual, and c.9457G>A (p.G3153R) and c.6599C>T (p.A2200V), which did not segregate with the MHS phenotype in the pedigrees we analyzed. Therefore, these sequence variants are probably polymorphisms (Tab. 10). The variants p.E2371G and p.R2452P occurred in two single MHS subjects, whereas p.R530H, p.S2354R and p.C4664R segregated with the disease in the family (Fig. 19). Family NA-15, in which p.C4664R segregated with the MHS phenotypes, also carried the p.R3225Q substitution, and subject II:2 had both sequence variants (Fig. 19 B). Moreover, we identified in a CCD patient, besides the variant p.S3098I, also a novel insertion variant c.14772_14773insTAGACAGGGTGTGCTCTGTTGCCCTTCTT (p.F4924_V4925insRQGVALLPFF); this variant was not detected in 100 alleles of MHN subjects and affect a protein region highly conserved across homologous RYR isoforms from different species. The segregation of the double RYR1 variant, p.S3098I and p.F4924_V4925insRQGVALLPFF, was not investigated because of the absence of DNA samples from relatives.

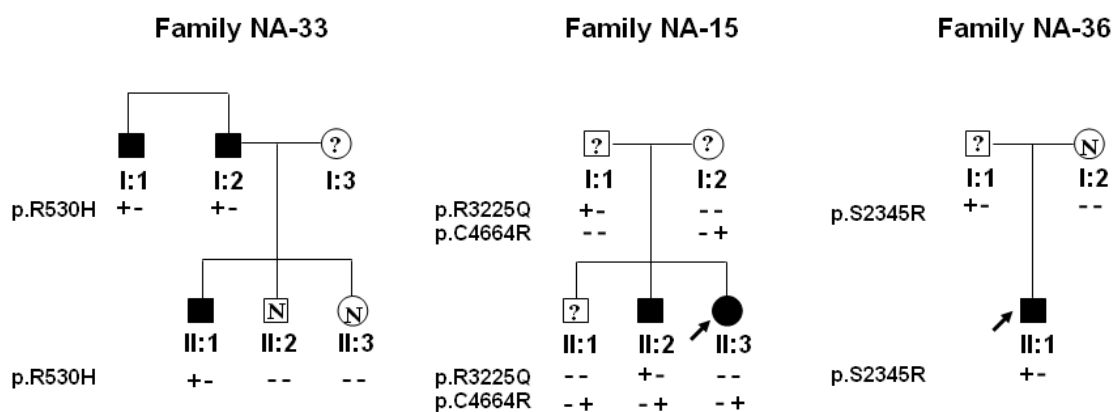


Fig. 19 Pedigrees of families NA-33 (A), NA-15 (B) and NA-36 (C) showing the segregation of RYR1 sequence variants, which are listed on the left of each panel. Solid symbols: MHS individuals identified by the IVCT; N: individuals MHN typed by the IVCT; ?: untested members of the pedigree; +/-: presence or absence of the sequence variants. The arrow indicates the index case who experienced an MH episode.

4.1.1 Molecular characterization of the double variant S3098I and F4924_V4925insRQGVALLPFF.

The c.14772_14773insTAGACAGGGTGTGCTCTGTTGCCCTTCTT variant, identified in the *RYR1* exon 102 of the CCD patient, results in the *in-frame* insertion of 10 amino acid (aa) residues (F4924_V4925insRQGVALLPFF). The DNA sequence analysis revealed the presence of two overlapping sequences due to the heterozygous status of the insertion. We confirmed the presence of this variant by two ARMS reactions with two insertion-specific primer pairs designed to amplify the allele with insertion. As expected, we obtained amplification products only in the samples from the CCD patient (Fig. 20).

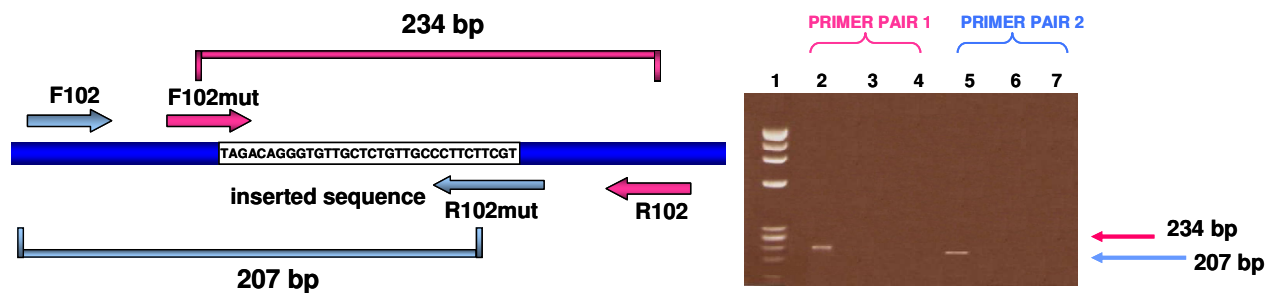


Fig. 20 ARMS-PCR system. **A.** Primers design and scheme of PCR products. **B.** Agarose gel electrophoresis of ARMS PCR products. Lane 1: DNA molecular weight Marker IX (Roche) Lanes 2, 5: PCR samples from the CCD patient; lanes 3, 6: PCR samples from wild type DNA; lanes 4, 7: mock.

Interestingly, we found that the 30-nt inserted sequence corresponds to an inverted and complementary sequence of 25 bp located at the *RYR1* intron 105. To study the probable mechanism generating this mutational event, we sequenced the entire *RYR1* genomic region spanning from intron 102 to exon 106. Since no deletion of the transposed sequence was found in the CCD patient, we ruled out a conservative transposition event. Moreover, we did not find any nucleotide substitution in the mutated DNA which could have generated rearrangement breakpoints. Thus, we hypothesized that this insertion variant could have arisen from a replicative transposition involving the intron sequence replication, and its inversion and transfer to the new site (Fig. 21).

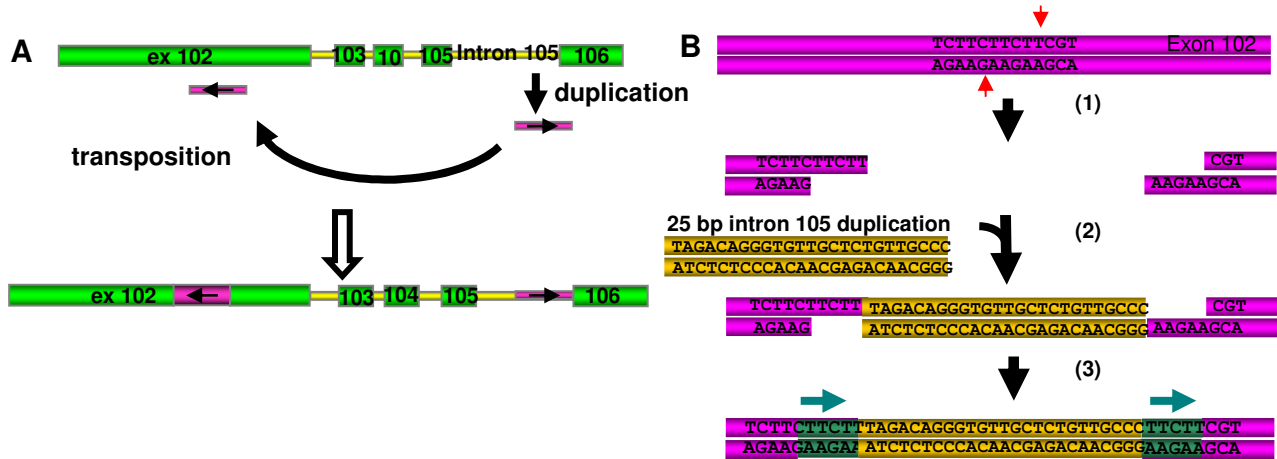
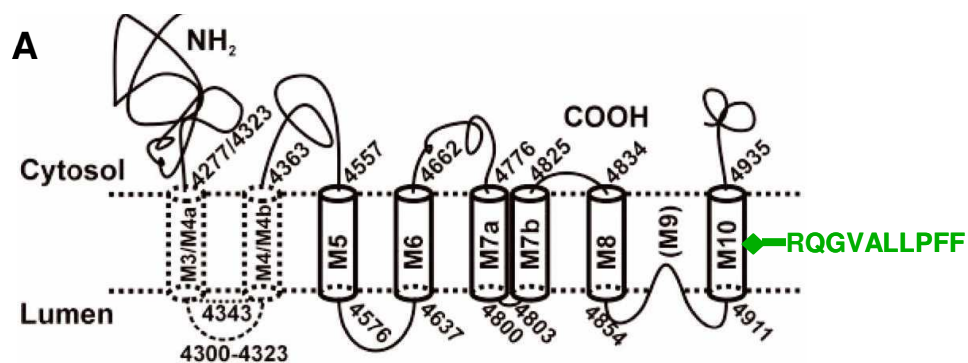


Fig. 21 **A.** Transposition scheme. A 25 bp sequence from the intron 105 (TAGACAGGGTGTGCTCTGTTGCC) was duplicated and inserted in the exon 102 of the *RYR1* gene. **B.** Hypotized insertion mechanism: 1) 5' protruding cut in the exon 102; 2) 25 bp duplicated sequence insertion; 3) fill-in synthesis and generation of 5 bp direct repeats (TTCTT). As result of this insertion event, 30 nucleotides were added to the exon 102 sequence.

Effects of F4924_V4925insRQGVALLPFF insertion on the structure of the RYR1 channel. To shed light on the possible structural changes introduced in the RYR1 channel by the insertion variant, we analyzed the effect of this insertion on the RYR1 structure by using 3D prediction softwares. The 10 aa insertion, F4924_V4925insRQGVALLPFF, lies in the M10 transmembrane segment (aa Val4914-Ile4937) of the RYR1 structure model proposed by Zorzato [Du *et al.*, 2002] (Fig. 22). Secondary structure prediction by the Emboss' Garnier software and the analysis of hydropathy by the Octanol software showed that the insertion causes an interruption in an α -helix structure (Fig. 23 A and B) and modifies the hydropathy plot of the M10 segment (Fig. 23 C and D).



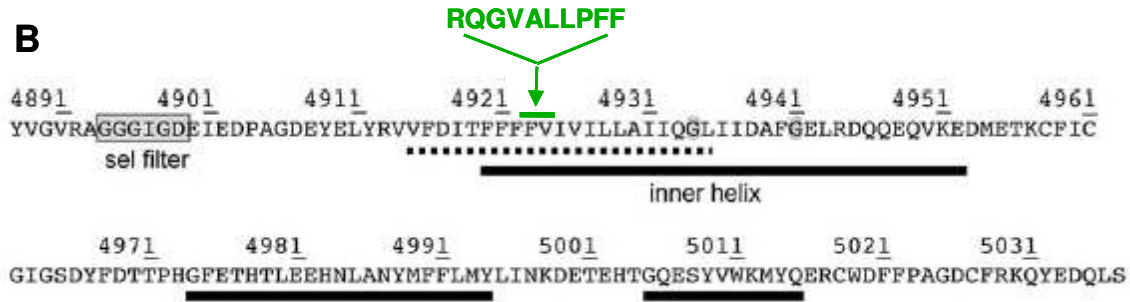


Fig. 22 Predicted structure of the RYR1 C-terminal region. The insertion-variant (in green) identified is located at the M10 domain (**A**), an α -helix adjacent to the predicted channel pore (**B**). **A**. Transmembrane topology of rabbit skeletal muscle RYR1 in Du model [figure modified from Du *et al.*, 2002]. **B**. Secondary Structure Prediction. Predicted regions of hydrophathy (dashed line) and a helix (continuous line) for the C-terminal region of RYR1. The position of the selectivity (sel) filter is also indicated. The G residues (highlighted in gray) are possible points of flexibility (figure modified from Samsò *et al.*, 2009).

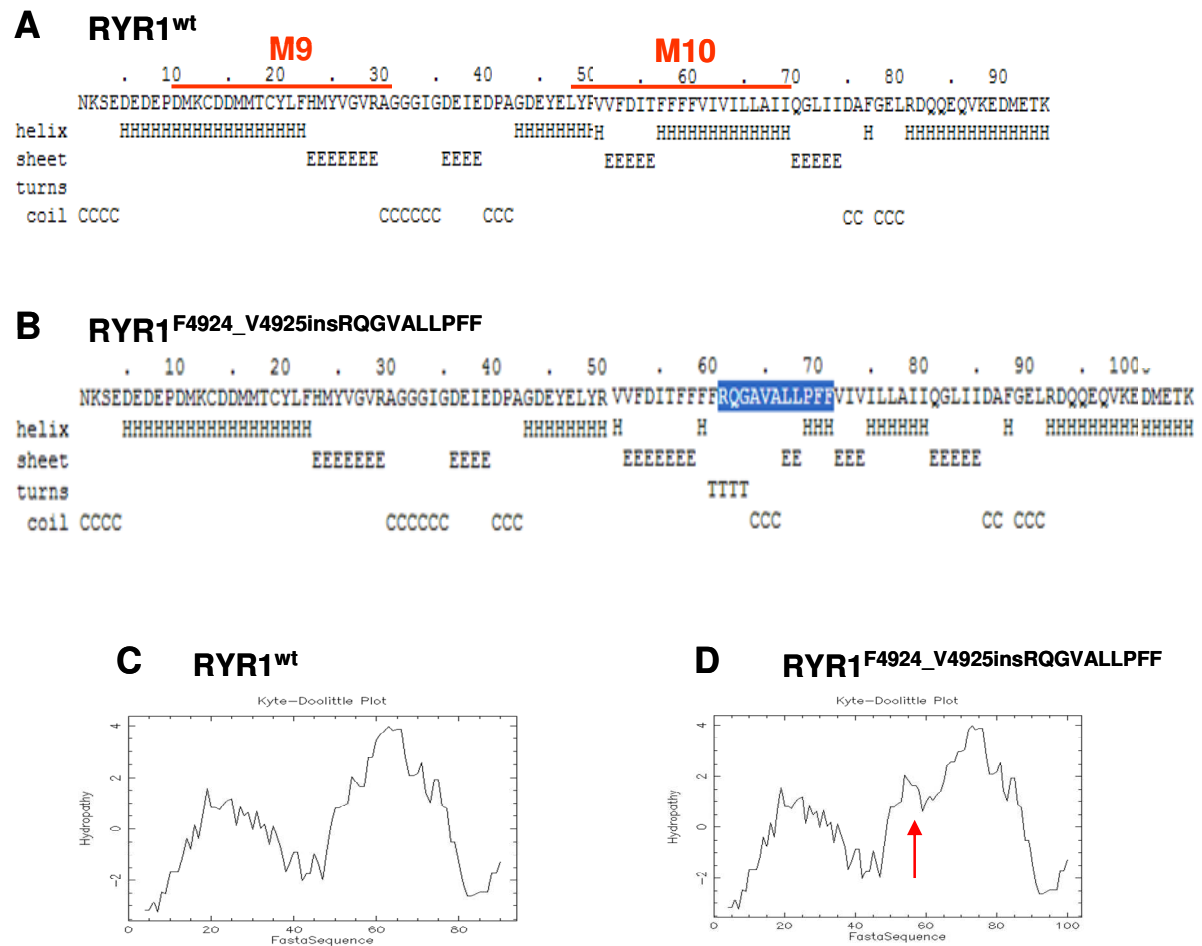


Fig. 23 Secondary structure prediction of the M9-M10 domains in RYR1^{wt} (**A**, **C**) and RYR1^{F4924_V4925insRQGVALLPFF} (**B**, **C**). Emboss' Garnier software (**A**, **B**): the M10 segment in the mutated channel shows an interruption in α -helix-structure. Octanol software (**C**, **D**): the insertion mutation modifies the hydrophathy profile of the mutated channel. The arrow indicates the insertion site.

Transcription analysis. Quantitative defects of *RYR1* gene expression have been reported in some patients with core myopathy [Monnier *et al.*, 2008; Zhou *et al.*, 2006 a; Zhou *et al.*, 2006 b]. Therefore, we examined the allelic expression of the *RYR1* gene in the CCD patient. Total cellular RNA was extracted from the CCD patient and from wild type immortalized B-lymphocytes. cDNA was synthesized from RNA and used as template for the amplification of an *RYR1* fragment (c.14658-14877, cDNA numbering) containing the insertion site. The amplicons from the CCD patient cDNA, separated by capillary gel electrophoresis, revealed two peaks of 220 bp and 250 bp, corresponding to the expected lengths of the wild type and mutated *RYR1* alleles, respectively. The peak of the mutated *RYR1* allele was about 16% than wild type allele revealing an unbalanced allelic expression in the CCD patient (Fig. 24).

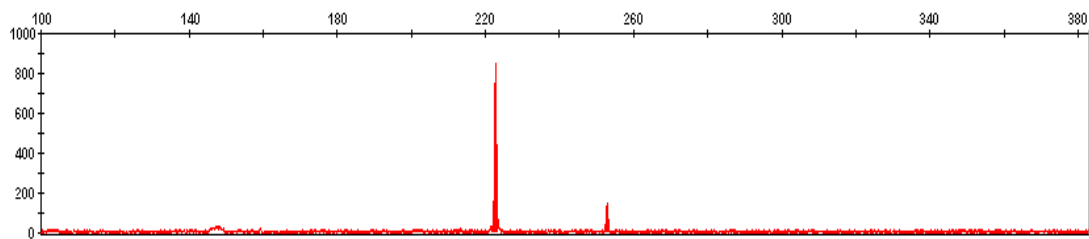


Fig. 24 Capillary gel electrophoresis analysis of the amplicons derived from the CCD patient cDNA. The cDNA region amplified contains the insertion site. The electropherogram shows two peaks at 220 bp and 250 bp, corresponding to the products from the wild type and the mutated alleles, respectively.

The unbalanced allelic expression was confirmed by sequence analysis of c.9269-9564 (containing the 3098 codon) and c. 14658-14877 amplicons. Both the electropherograms showed the presence of two-overlapping sequences, deriving from the mutated and wild type alleles, but the peaks from the mutated sequences are lower than those from the wild type sequences. The instability of the mutated transcript was illustrated by the disequilibrium between the levels of the wild type and the mutated sequences of the cDNA in comparison with the gDNA (Fig. 25). This data indicate that the double variant generated an unstable mRNA in the CCD patient.

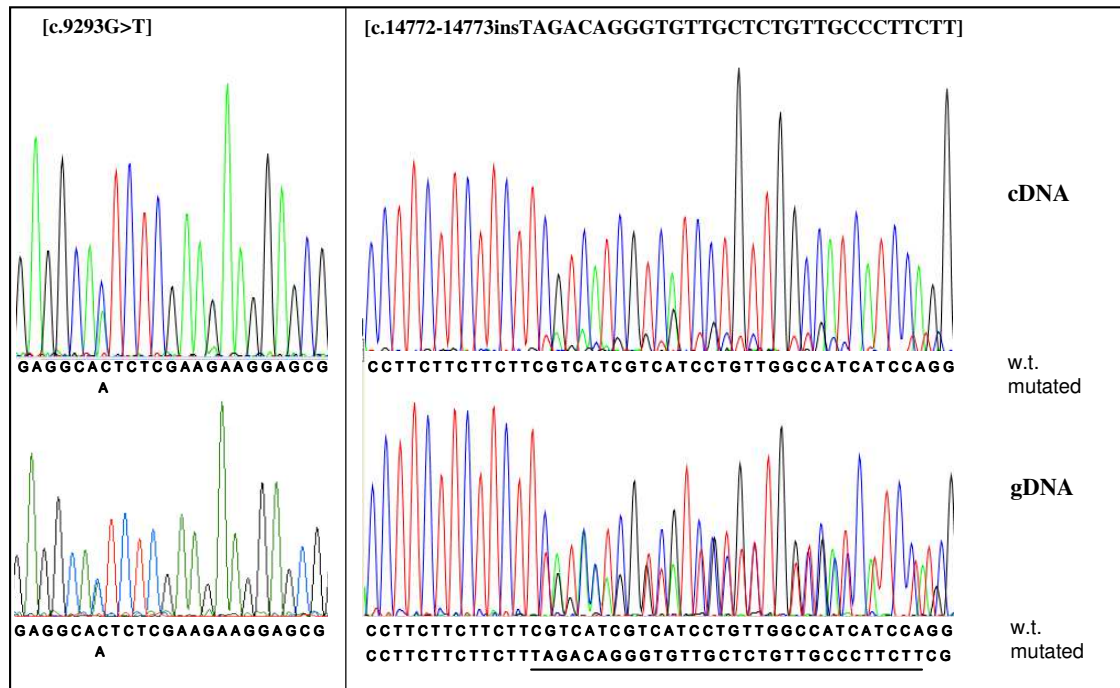


Fig. 25 Sequence analysis of exon 63 (left side) and exon 102 (right side) regions from cDNA (upper side) and genomic DNA (lower side). The c.9293G>T variant is shown as non coding sequence obtained using the reverse primers. The c.14772_14773ins TAGACAGGGTGTGCTCTGTTGCCCTTCTT variant is shown as coding sequence obtained using the forward primers. The nucleotide sequences are shown below the chromatogram peaks. The insertion is underlined.

To determine whether the two sequence variants lay on a common or on a different haplotype allele, we performed the allele discrimination by amplifying hemizygous cDNA segments from a heterozygous template, with allele specific oligonucleotides (ASO) [Michalatos-Beloin *et al.*, 1996]. Conventional approaches to haplotyping require the use of several generations to reconstruct haplotypes within a pedigree, but in our case DNA samples from relatives were not available. Since the transcription analysis revealed that the allele with insertion was expressed at a very low level, we designed an ASO reverse (wt-ASO-R) that anneals specifically to the allele without the insertion. The specificity of wt-ASO-R was checked by using this primer to amplify both the genomic DNA (g.30726-30853) and cDNA (c.14657-14784) from the CCD patient and from a control subject (Fig. 26 A). In any case, only one product of 127 bp, corresponding to the size of the PCR product from the wild type allele, was obtained for the mutated and control sequences, confirming that the primer doesn't amplify the allele carrying the 30-nt insertion. Therefore, the wt-ASO-R was employed in a long-range RT-PCR to amplify a 6878 bp fragment (c.7906-14784, containing the 3098 codon and the sequence corresponding to the exon 102) (Fig. 26 B). The long-range PCR products were used as template for the amplification of a shorter fragment containing the 3098 codon (c.9269-9564) and the sequence analysis showed the presence of the G nucleotide at the position 9293 (Fig. 26 C). Therefore, the allele without insertion, selected in the ASO long-range RT-PCR, codifies for serine 3098. In conclusion, the missense variant in the exon 63 is located *in cis* with the insertion variant.

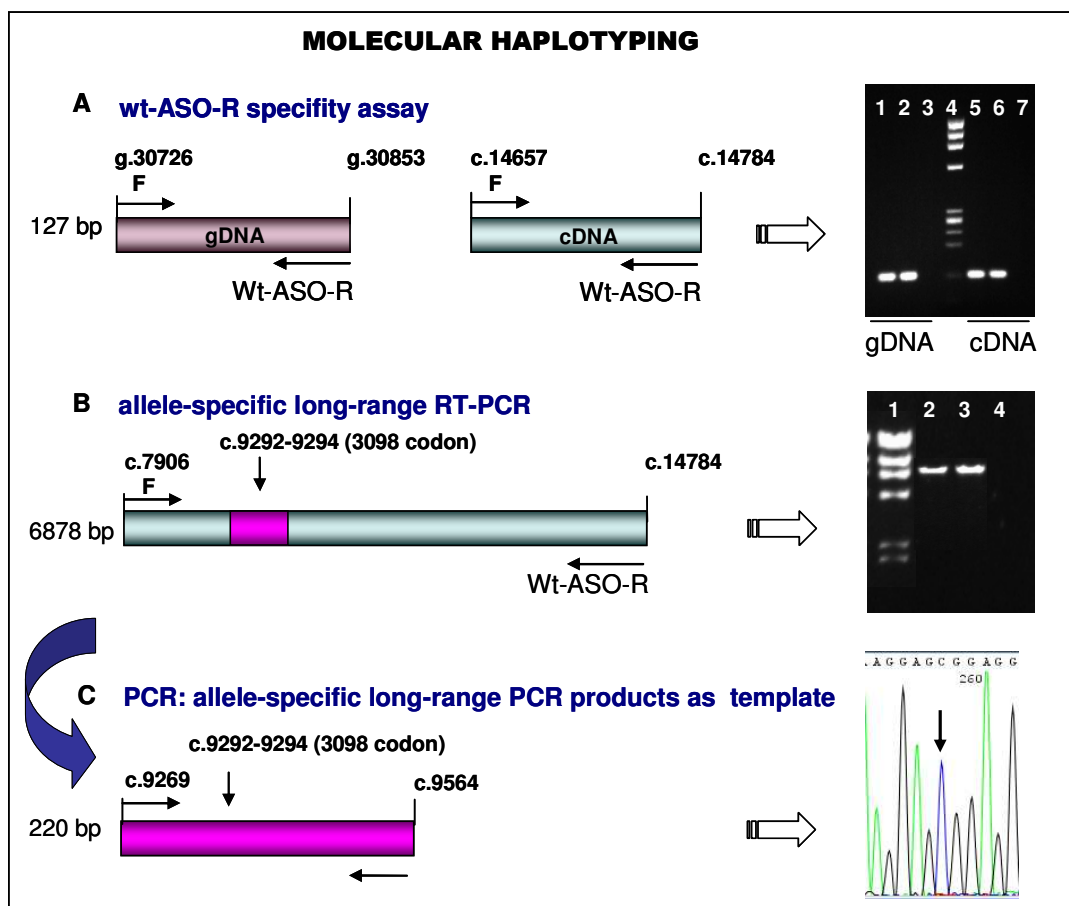
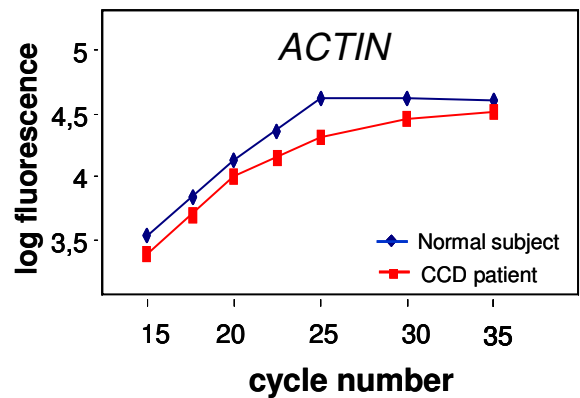
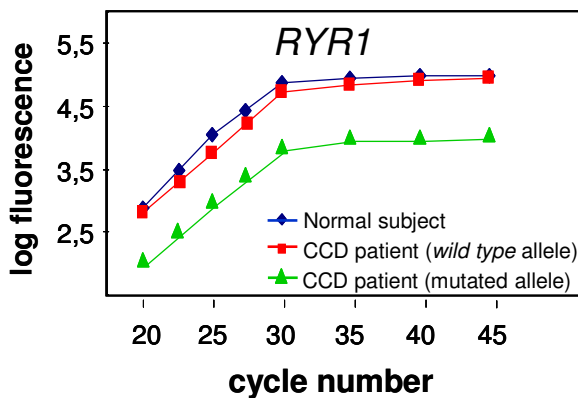


Fig. 26 *RYR1* molecular haplotyping of the CCD patient. **A.** wt-ASO-R specificity assay. **Left.** Scheme of the PCR. **Right.** Agarose gel electrophoresis. Lane 1: PCR reaction from the wild type genomic DNA; lane 2 : PCR reaction from the CCD patient genomic DNA; lane 4: DNA molecular weight Marker IX (Roche); lane 5: PCR reaction from the wild type cDNA; lane 6: PCR reaction from the CCD patient cDNA; lanes 3, 7: mock reactions. **B.** **Left** Scheme of the allele-specific long-range PCR. **Right.** Agarose gel electrophoresis. Lane 1: DNA molecular weight Marker II (Roche); lane 2 : PCR reaction from the wild type cDNA; lane 3: PCR reaction from the CCD patient cDNA; lane 4: mock reaction. **C.** **Left.** Scheme of nested PCR using the allele-specific long-range products as a template. **Right.** DNA sequence of the amplicon derived from the CCD patient (complementary strand).

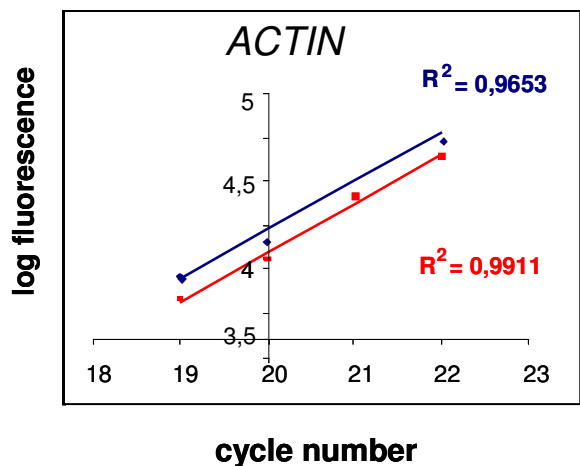
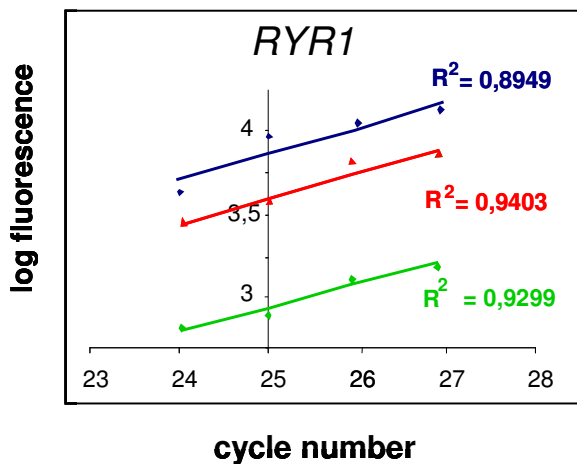
m-RNA semi-quantitative analysis. To analyze the expression levels of each *RYR1* allele identified in the CCD patient we performed a semi-quantitative analysis of mRNA, isolated from B-lymphocytes of the CCD patient and of a control subject, by using the RT-PCR according to Breljak *et al.* [Breljak *et al.*, 2005]. We carried out kinetic analysis on *RYR1* and β -*ACTIN* cDNAs, as a reference gene, by amplifying PCR products over different number of PCR cycles. The PCR products were separated by capillary gel electrophoresis. PCR reactions were exponential between 24-27 and 19-22 cycles for *RYR1* and β -*ACTIN* genes, respectively (Fig. 27 A). The logarithm of the fluorescence signals for each gene was plotted *versus* the corresponding number of PCR cycles of the exponential phase; the data points were processed by linear regression analysis [Breljak *et al.*, 2005]. The expression levels of *RYR1* and β -*ACTIN* genes in samples from the CCD patient and from the control were derived from the intercept of the regression line with the Y-axis (after 25 and 20 cycles for *RYR1* and β -*ACTIN* genes, respectively; Fig. 27 B). The fluorescence

values at the intercept of the regression line with the Y-axis represent the mRNA levels. The total levels of *RYR1* mRNA in the CCD patient (normalized versus β -*ACTIN*) are about 89% of the control (normalized versus β -*ACTIN*), and the wild type allele represents the 76% and the mutated allele with the insertion about 13% (Fig. 27 C). Interestingly, the expression of *RYR1* gene in the CCD patient is about 89% of the control, although the mutated allele is very low expressed (about 16%, Fig. 25).

A



B



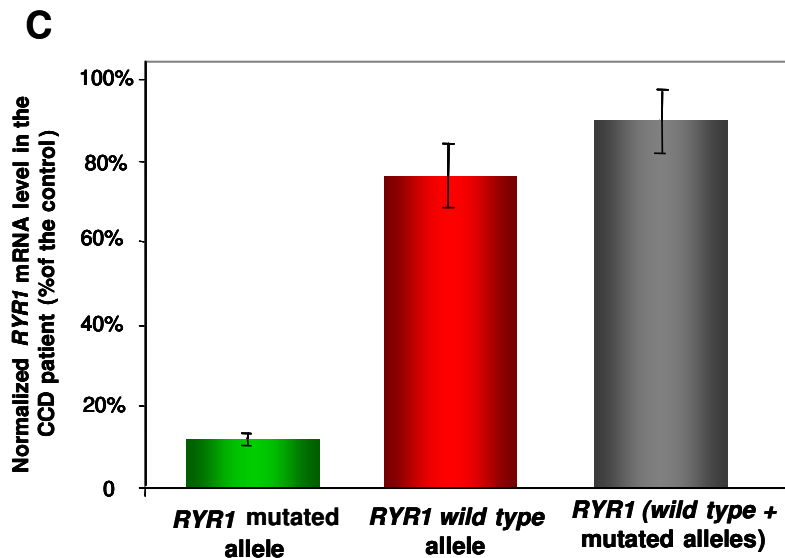


Fig. 27 Relative quantification of *RYR1* mRNA. RNAs isolated from B-lymphocytes were reverse transcribed and the RT-PCR products were analyzed by the capillary gel electrophoresis. **A.** The log of fluorescence signals for the *RYR1* and β -*ACTIN* genes (left and right, respectively) were plotted against the number of PCR cycles. RNAs from the CCD patient and from the control were analyzed. **B.** The logarithm of the fluorescence signals for each gene was plotted *versus* the corresponding number of PCR cycles of the exponential phase; the expression levels of *RYR1* and β -*ACTIN* genes in samples from the CCD patient and the control were derived from the intercept of the regression line with the Y-axis (25 and 20 cycles for the *RYR1* and β -*ACTIN* genes, respectively). **C.** *RYR1* mRNA level in the CCD patient (normalized *versus* β -*ACTIN* gene) are expressed as percentages of the control. Each experiment was performed in triplicates. Error bars show the propagation of the SEM.

4.2 Functional characterization of sequence variants

We characterized the functional alterations caused by nine *RYR1* sequence variants in EBV-immortalized lymphoblastoid cells by:

- a metabolic assay based on the measurements of proton release in response to the RYR1 activator 4-CmC [Zullo *et al* 2009, see appendix];
- flow cytometry based on the measurements of calcium release in response to the RYR1 activator 4-CmC.

Proton release measurements. The increased acidification rate of lymphoblastoid cells in response to 4-CmC was characterized and reported to be mainly due to RYR1 activation [Zullo *et al.*, 2009; Zullo *et al.* 2007; Zullo, 2006]. Therefore, this assay can be used to analyze the activity of RYR1 in this cellular system. B-lymphocytes from patients with RYR1^{Arg530His} (subject II:1 of family NA-33, Fig. 19), RYR1^{R2163P} (proband of family NA-3 [Fortunato *et al.*, 2000]), RYR1^{N2342S}, RYR1^{S2345R} (proband of family NA-36, Fig. 19), RYR1^{E2371G}, RYR1^{R2454H} and RYR1^{C4664R} variants were available and were immortalized with EBV. As for the RYR1^{C4664R} variant, three cell lines, MHS5, MHS6 and MHS7, were prepared from subjects II:1, II:2 and II:3, respectively, of family NA-15 (Fig. 19). Two cell lines were used as controls, named MHN1 from an unrelated MHN subject and MHN10 from subject II:2 of family NA-33 (Fig. 19). Metabolic responses to 4-CmC were significantly higher in the cell lines harboring RYR1 channels with the sequence variants located at the N-terminus and at the central regions of the protein than in wild-type RYR1 cell lines (Fig. 28). On the

contrary, the metabolic responses to 4-CmC were lower in the three cell lines carrying RYR1^{C4664R} than in controls (Fig. 28). However, the response to 800 μ M 4-CmC of the MHS6 cell line with two substitutions, p.R3225Q and p.C4664R, each transmitted from one parent (Fig. 28), did not significantly differ from controls. The basal metabolism was unaffected, since the acidification rate of all the three cell lines expressing RYR1^{C4664R} recorded in the absence of 4-CmC was indistinguishable from that of the MHN control cells (data not shown). Mutations in the C-terminal membrane-spanning domain have been reported to show a smaller TG induced increase in cytosolic [Ca²⁺], in the absence of external Ca²⁺, than controls [Treves *et al.*, 2008; Lynch *et al.*, 1999]. This result has been taken to indicate Ca²⁺ store depletion due to “leaky” mutant RYR1 channels, since the signal obtained with the SERCA blocker reflects the size of the rapidly releasable intracellular Ca²⁺ stores [Tilgen *et al.*, 2001]. To determine if the RYR1^{C4664R} variant reacts in a similar way, we analyzed the acidification response of the MHS5 cell line to the TG. The early increase (in the first 2 min) after treatment with the SERCA pump blocker was about 50% lower (data not shown) in this cell line than in the control. This result is consistent with partial Ca²⁺ store depletion in the cell line expressing RYR1^{C4664R}, as confirmed by Ca²⁺ release measurements (see calcium release measurement).

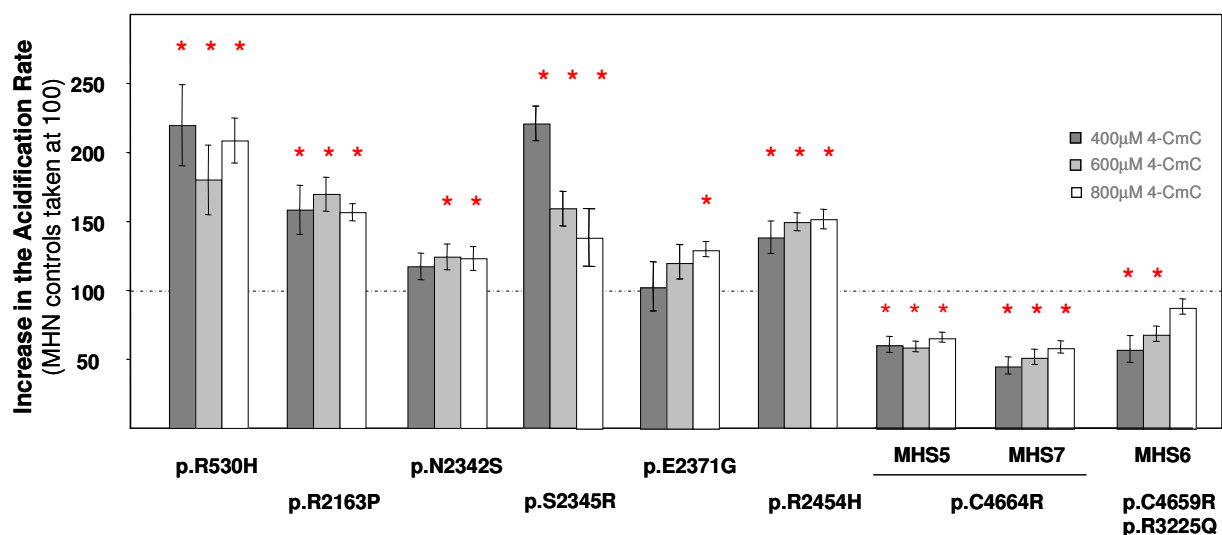


Fig. 28 Increase in the acidification rate of RYR1 variants. The increase in the acidification rate value of lymphoblastoid cells from normal subjects is taken as 100. Cell lines carrying RYR1 variants p.R530H, p.R2163P, p.N2342S, p.S2345R, p.E2371G, p.R2454H, p.C4664R and p.C4664R/p.R3225Q were stimulated with 400 μ M, 600 μ M or 800 μ M 4-CmC as indicated. Each block of three bars corresponds to a cell culture preparation derived from a RYR1 variant patient as indicated. MHS5, MHS7 and MHS6 correspond to three different cell lines (see text). Error bars show the propagation of the SEM; asterisks indicate responses significantly different ($P < 0.05$) from the controls.

Calcium release measurements. The Ca²⁺ responses to 4-CmC of B lymphocytes derived from MHS and control individuals showed significant differences [Girard *et al.*, 2001; Sei *et al.*, 2002]. In the human B cell line, Ca²⁺ release in response to 4-CmC can be a sensitive indicator of RYR1 function since RYR1-mediated Ca²⁺ signals can be pharmacologically distinguished from other intracellular sources in human B cells, as the IP3-sensitive stores and the mitochondrial stores [McKinney *et*

al., 2006]. We investigated the Ca^{2+} release in response to the stimulation with 4-CmC and TG in immortalized B-lymphocytes carrying $\text{RYR1}^{\text{C4664R}}$, $\text{RYR1}^{\text{S3098I/F4924_V4925insRQGVALLPFF}}$, and MHN control cell lines using a flow cytometric technique. The Ca^{2+} fluxes were measured by integrating the ratio of the Fluo-3/Fura Red fluorescence signals.

B-lymphocytes carrying the $\text{RYR1}^{\text{C4664R}}$ mutated channel revealed a 4-CmC (to 600, 800 and 1000 μM)- and a TG-triggered Ca^{2+} release significantly lower than the control cells showing that the Ca^{2+} stores of the cell line expressing $\text{RYR1}^{\text{C4664R}}$ are partially depleted. In particular, the TG-triggered Ca^{2+} release in $\text{RYR1}^{\text{C4664R}}$ channel is about 50% lower than in the control. Therefore the p.C4664R variant leads to a leaky channel, since the Ca^{2+} stores are partially depleted. (Fig. 29). These data confirmed the results obtained by proton release assay (see Proton release measurements) [Zullo *et al.*, 2009].

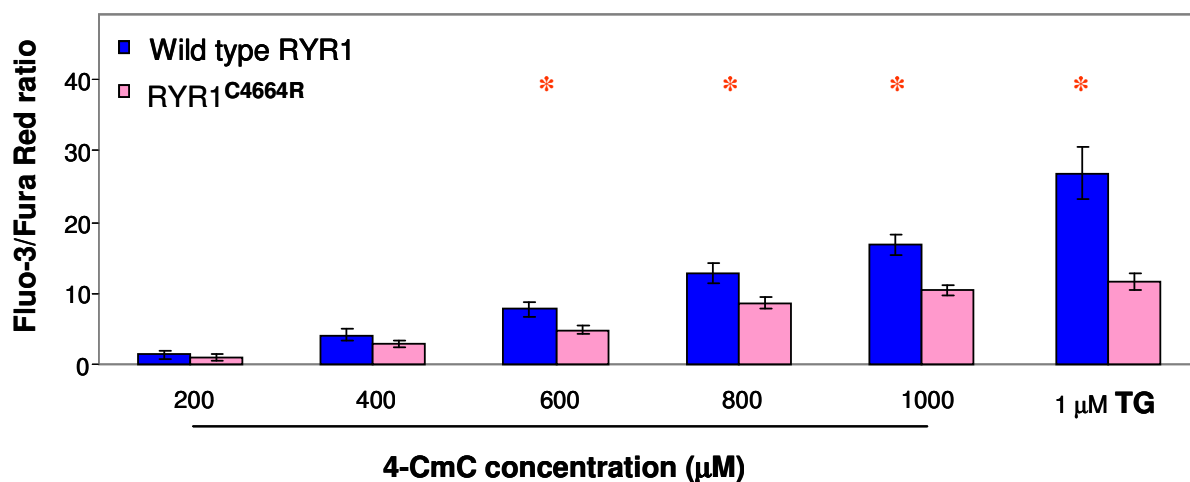


Fig. 29 Fluo-3/Fura Red fluorescence signals ratio in response to 4-CmC or to TG. Cell lines carrying RYR1 variant p.C4664R (pink) and control cells (blue) were stimulated with 4-CmC (200 μM to 1000 μM) or 1 μM TG. Ca^{2+} release were measured by integrating the ratio of the Fluo-3/Fura Red fluorescence signals. Experiments were carried out at least 7 times. Error bars show the propagation of the SEM; asterisks indicate responses significantly different ($P < 0.05$) from the controls.

B-lymphocytes expressing the $\text{RYR1}^{\text{S3098I/F4924_V4925insRPAVALPFF}}$ channel showed a 4-CmC (600, 800 and 1000 μM)-triggered Ca^{2+} release significantly higher than the control cells (Fig. 30). Moreover, the TG-triggered Ca^{2+} release was not significantly different from the control cells (Fig. 30), indicating that the RYR1 mutated channel is not a leaky channel.

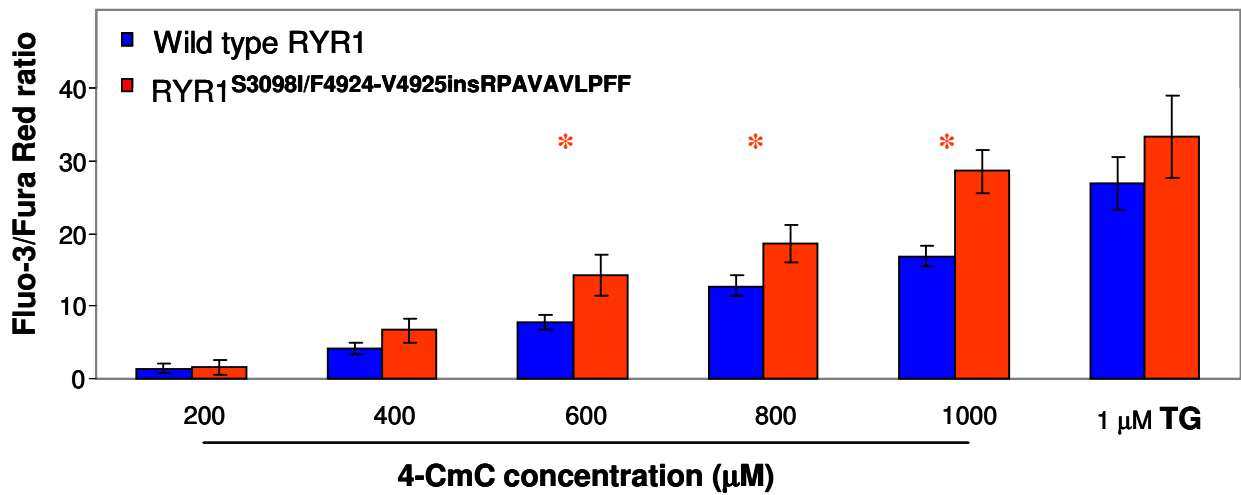


Fig. 30 Fluo-3/Fura Red fluorescence signals ratio in response to 4-CmC or to TG. Cell lines carrying RYR1^{S3098I/F4924-V4925insRPAVAVLPPF} (red) and control cells (blue) were stimulated with 4-CmC (200 μM to 1000 μM) or 1 μM TG. Ca²⁺ release were measured by integrating the ratio of the Fluo-3/Fura Red fluorescence signals. Experiments were carried out at least 8 times. Error bars show the propagation of the SEM; asterisks indicate responses significantly different (P<0.05) from the controls.

5. DISCUSSION

RYR1 gene screening showed that no *RYR1* sequence variant is prevalent in MHS subjects and families from southern Italy. We examined the function of RYR1 channel variants in EBV-immortalized lymphoblastoid cells by proton or calcium release assays. RYR1 is expressed in human B lymphocytes where it functions as a Ca²⁺-release channel during the B-cell receptor–stimulated Ca²⁺ signaling process [Sei *et al.*, 1999], and Ca²⁺ homeostasis is altered in B cells of MHS individuals [Sei *et al.*, 2002; Girard *et al.*, 2001]. The increase in the acidification rate of immortalized lymphoblastoid cells in response to 4-CmC is mainly due to the activation of the RYR1 calcium channel, and this assay can be used to analyze the activity of RYR1 [Zullo *et al.*, 2009]. The metabolic responses of mutant RYR1 channels analyzed in this study were of two types, i.e. increase or decrease of proton release rate compared with the wild-type channel. The response seems to depend on the location of the mutation. The metabolic response was higher in RYR1 channels with mutations located in the N-terminal and the central regions of the protein, and these higher metabolic responses can account for the MHS phenotype. On the contrary, 4-CmC-induced activation was significantly lower in the cell lines harboring the RYR1^{C4664R} mutated channel, and our results obtained by two different methods, proton and calcium release assays, indicate that p.C4664R leads to a leaky channel with depletion of intracellular stores. The p.C4664R mutation is located at the C-terminal region of the protein in the M6 transmembrane segment [Zorzato *et al.*, 1990]. Other mutations at the C-terminus of RYR1 and associated with the CCD phenotype have been reported to lead to channels that are non- or hypo-reactive to chemical stimulation [Brini *et al.*, 2005; Ducreux *et al.*, 2004; Tilgen *et al.*, 2001; Lynch *et al.*, 1999]. In contrast, the p.T4826I mutation, associated to the MHS phenotype, was reported to have a higher 4-CmC and caffeine sensitivity compared to the wild-type RYR1 in transfected human myotubes [Yang *et al.*, 2003]. The p.C4664R mutation has been identified in an MH family (Fig. 19) and no signs of myopathy compatible with CCD were found in the medical history of the patients. However, a core myopathy could develop late in the life. In fact, recently was reported a patient (77 years old) with a novel *RYR1* mutation (G40V) associated with pathologic features of a core myopathy and onset of symptoms at 60 years [Jungbluth *et al.*, 2009]; therefore, patients with MH mutations may develop overt skeletal muscle involvement later in life.

We identified in a CCD patient the compound p.S3098I/p.F4924_V4925insRQGVALLPFF substitutions *in cis*. Most dominant CCD-related RYR1 mutations are localized to the M8/M10 loop surrounding the pore helix region (Du *et al.*, 2002), that is involved in the channel function and regulation. The insertion variant identified is located at the M10 domain of the RYR1 channel and it could have arisen from a replicative transposition (Fig. 21). The double variant generated an unstable mRNA in the B-lymphocytes of the CCD patient: the mutated allele is expressed at 16% in comparison with the wild-type allele. Interestingly, the total *RYR1* gene expression in the CCD patient is about 89% of the control, although the mutated allele is very low expressed (Fig. 25). This finding indicates a positive regulation of the wild-type allele transcription of the *RYR1* gene in the B-lymphocytes of the CCD patient. B-lymphocytes expressing the RYR1^{S3098I/F4924-V4925insRPAVAVLPFF} channel showed a 4-CmC-triggered Ca²⁺ release significantly higher than the control cells (Fig. 30). Moreover, the TG-triggered Ca²⁺ release was not significantly different

from the control cells (Fig. 30), indicating that the RYR1 mutated channel is not a leaky channel. Some *RYR1* gene mutations identified in CCD patients generate channels that are excessively leaky to Ca^{2+} and lead to depletion of SR Ca^{2+} stores; other *RYR1* gene mutations identified in CCD patients generate channels with a deficit in E-C coupling, i.e., a reduced voltage-gated release in the absence of detectable store depletion [Dirksen and Avila, 2002]. The RYR1^{S3098I/F4924-V4925insRPAVAVLPFF} mutated channel displayed hyperactivation by chemical stimulation in lymphoblastoid cells. This behaviour is usually associated with the MHS phenotype. Although the MH susceptibility was not investigated in this CCD patient, the CCD condition is frequently associated with the MH susceptibility. The future prospective of this work is the study of the E-C coupling of the RYR1^{S3098I/F4924-V4925insRPAVAVLPFF} mutated channel in transfected myotubes to investigate if the development of the myopathy in this patient could be ascribed to an altered E-C coupling.

RYR1-related diseases present genetic, phenotypic and histopathological overlaps and marked phenotypic variability, therefore molecular and functional studies of novel sequence variants of *RYR1* gene contribute to clarify genetic basis and molecular mechanisms in RYR1-related disease.

REFERENCES

- Anderson A A, Brown R L, Polster B, Pollock N, Stowell K M. Anesthesiology. Identification and biochemical characterization of a novel ryanodine receptor gene mutation associated with malignant hyperthermia. 2008; 108: 208-215.
- Anderson AA, Treves S, Biral D, Betto R, Sandonà D, Ronjat M, Zorzato F. The novel skeletal muscle sarcoplasmic reticulum JP-45 protein. Molecular cloning, tissue distribution, developmental expression, and interaction with alpha 1.1 subunit of the voltage-gated calcium channel. *J Biol Chem.* 2003; 278:39987-39992.
- Anetseder M, Hager M, Muller CR, Roewer N. Diagnosis of susceptibility to malignant hyperthermia by use of a metabolic test. *Lancet.* 2002; 359:1579-1580.
- Avila G, Dirksen R T. *J. Gen. Physiol.* Functional effects of central core disease mutations in the cytoplasmic region of the skeletal muscle ryanodine receptor. 2001; 118: 277-290.
- Bannister RA, Grabner M, Beam KG. The alpha(1S) III-IV loop influences 1,4-dihydropyridine receptor gating but is not directly involved in excitation-contraction coupling interactions with the type 1 ryanodine receptor. *J Biol Chem.* 2008; 283: 23217-23223.
- Barone V, Massa O, Intravaia E, Bracco A, Di Martino A, Tegazzin V, Cozzolino S, Sorrentino V. Mutation screening of the RYR1 gene and identification of two novel mutations in Italian malignant hyperthermia families. *J Med Genet.* 1999; 36:115-118.
- Beard NA, Sakowska MM, Dulhunty AF, Laver DR. Calsequestrin is an inhibitor of skeletal muscle ryanodine receptor calcium release channels. *Biophys J.* 2002; 82:310-320.
- Bendahan D, Guis S, Monnier N, Kozak-Ribbens G, Lunardi J, Ghattas B, Mattei J P, Cozzone P J. Comparative analysis of in vitro contracture tests with ryanodine and a combination of ryanodine with either halothane or caffeine: a comparative investigation in malignant hyperthermia. *Acta Anaesthesiol Scand.* 2004; 48:1019-1027.
- Bitoun M, Maugendre S, Jeannet PY, Lacène E, Ferrer X, Laforêt P, Martin JJ, Laporte J, Lochmüller H, Beggs AH, Fardeau M, Eymard B, Romero NB, Guicheney P. Mutations in dynamin 2 cause dominant centronuclear myopathy. *Nat Genet.* 2005; 37:1207-1209.
- Bleunven C, Treves S, Jinyu X, Leo E, Ronjat M, De Waard M, Kern G, Flucher BE, Zorzato F. SRP-27 is a novel component of the supramolecular signalling complex involved in skeletal muscle excitation-contraction coupling. *Biochem J.* 2008; 411:343-349.
- Blayney LM, Jones JL, Griffiths J, Lai FA. A mechanism of ryanodine receptor modulation by FKBP12/12.6, protein kinase A, and K201. *Cardiovasc Res.* 2009

Brandt A, Schleithoff L, Jurkat-Rott K, Klinger W, Baur C, Lehmann-Horn F. Screening of the ryanodine receptor gene in 105 malignant hyperthermia families: novel mutations and concordance with the in vitro contracture test. *Hum Mol Genet.* 1999; 8: 2055–2062.

Brandt NR, Caswell AH, Wen SR, Talvenheimo JA. Molecular interactions of the junctional foot protein and dihydropyridine receptor in skeletal muscle triads. *J Membr Biol.* 1990; 113:237-251.

Breljak D, Ambriovic-Ristov A, Kapitanovic S, Cavec T, Gabrilovac J. Relative Quantification of mRNA, *Food Technol. Biotechnol.* 2005;43: 379–388.

Brini M, Manni S, Pierobon N, Du GG, Sharma P, MacLennan DH, Carafoli E. Ca²⁺ signaling in HEK-293 and skeletal muscle cells expressing recombinant ryanodine receptors harboring malignant hyperthermia and central core disease mutation. *J Biol Chem.* 2005; 280: 15380-15389.

Brinkmeier H, Krämer J, Krämer R, Iazzo PA, Baur C, Lehmann-Horn F, Rüdel R. Malignant hyperthermia causing Gly2435Arg mutation of the ryanodine receptor facilitates ryanodine-induced calcium release in myotubes. *Br J Anaesth.* 1999; 83: 855-861.

Brillantes AMB, Ondrias K, Scott A, Kobrinsky E, Ondriasova E, Moschella MC, Jayaraman, T, Landers M, Ehrlich BE and Marks AR. Stabilization of calcium release channel (ryanodine receptor) function by FK506-binding protein. *Cell.* 1994; 77:513-523.

Buck E, Zimanyi I, Abramson JJ, Pessah IN. Ryanodine stabilizes multiple conformational states of the skeletal muscle calcium release channel. *J Biol Chem.* 1992; 267:23560-23567.

Carmignac V, Salih MA, Quijano-Roy S, Marchand S, Al Rayess MM, Mukhtar MM, Urtizberea JA, Labeit S, Guicheney P, Leturcq F, Gautel M, Fardeau M, Campbell KP, Richard I, Estournet B, Ferreiro A. C-terminal titin deletions cause a novel early-onset myopathy with fatal cardiomyopathy. *Ann Neurol.* 2007; 61:340-351.

Carpenter D, Robinson RL, Quinnell RJ, Ringrose C, Hogg M, Casson F, Booms P, Iles DE, Halsall PJ, Steele DS, Shaw MA, Hopkins PM. Genetic variation in RYR1 and malignant hyperthermia phenotypes. *Br J Anaesth.* 2009; 103:538-548.

Chen SR, Li X, Ebisawa K, Zhang L. Functional characterization of the recombinant type 3 Ca²⁺ release channel (ryanodine receptor) expressed in HEK293 cells. *J Biol Chem.* 1997; 272:24234-24246.

Ching LL, Williams AJ, Sitsapesan R. Evidence for Ca²⁺ activation and inactivation sites on the luminal side of the cardiac ryanodine receptor complex. *Circ Res.* 2000; 87:201-206.

Clarke N, Monnier N, Smith R, Waddell L, Cooper S, Lunardi J, North K. PW14-171 compound heterozygous mutations in RYR1 associated with CFTD with extreme fibre size disproportion. 30 International Congress of Myology. 2008.

Copello J A, Barg S, Sonnleitner A, Porta M, Diaz-Sylvester P, Fill M, Schindler H, and Fleischer S. Differential activation by Ca^{2+} , ATP and caffeine of cardiac and skeletal muscle ryanodine receptors after block by Mg^{2+} . *J Membr Biol.* 2002; 187:51-64.

Cornea RL, Nitu F, Gruber S, Kohler K, Satzer M, Thomas DD, Fruen BR. FRET-based mapping of calmodulin bound to the RyR1 Ca^{2+} release channel. *Proc Natl Acad Sci U S A.* 2009; 106: 6128-33.

Curran JL, Hall WJ, Halsall PJ, Hopkins PM, Iles DE, Markham AF, McCall SH, Robinson RL, West SP, Bridges LR, Ellis FR. Segregation of malignant hyperthermia, central core disease and chromosome 19 markers. *Br J Anaesth.* 1999; 83:217-222.

Davis MR, Haan E, Jungbluth H, Sewry C, North K, Muntoni F, Kuntzer T, Lamont P, Bankier A, Tomlinson P, Sanchez A, Walsh P, Nagarajan L, Oley C, Colley A, Gedeon A, Quinlivan R, Dixon J, James D, Müller CR, Laing NG. Principal mutation hotspot for central core disease and related myopathies in the C-terminal transmembrane region of the RYR1 gene. *Neuromuscul Disord.* 2003; 13:151-157.

Denborough MA, Dennett X, Anderson RM. Central-core disease and malignant hyperpyrexia. *Br Med J.* 1973; 1:272-273.

Denborough MA, Lovell RRH. Anaesthetic deaths in a family. *Lancet.* 1960; 276:45.

Deufel T, Sudbrak R, Feist Y, Rübsam B, Du Chesne I, Schäfer K L, Roewer N, Grimm T, Lehmann-Horn F, Hartung E J, Müller C R. Discordance in a malignant hyperthermia pedigree, between the in vitro contracture test phenotypes and haplotypes for the MHS1 region of chromosome 19q12–13.2, comprising the C1840T transition in the RYR1 gene. *Am J Hum Genet* 1995; 56: 1334–1342.

Dirksen RT, Avila G. Altered ryanodine receptor function in central core disease: leaky or uncoupled Ca^{2+} release channels? *Trends Cardiovasc Med.* 2002; 12: 189-197.

Donoso P, Beltran M, Hidalgo C. Luminal pH regulated calcium release kinetics in sarcoplasmic reticulum vesicles. *Biochemistry.* 1996; 35:13419-13425.

Donoso P, Prieto H, Hidalgo C. Luminal calcium regulates calcium release in triads isolated from frog and rabbit skeletal muscle. *Biophys J.* 1995; 68:507-515.

Du GG, Sandhu B, Khanna VK, Guo XH, MacLennan DH. Topology of the Ca^{2+} release channel of skeletal muscle sarcoplasmic reticulum (RyR1). *Proc Natl Acad Sci USA.* 2002; 99:16725-16730.

Dubowitz V, Sewry CA. Muscle biopsy – A practical approach 3rd edition. Baillière Tindall/W.B. Saunders London. 2006.

Dubowitz V, Pearse AG. Oxidative enzymes and phosphorylase in centralcore disease of muscle. *Lancet*. 1960; 2:23-24.

Ducreux S, Zorzato F, Ferreiro A, Jungbluth H, Muntoni F, Monnier N, Muller CR, Treves S. Functional properties of ryanodine receptors carrying three amino acid substitutions identified in patients affected by multi-minicore disease and central core disease, expressed in immortalized lymphocytes. *Biochem J*. 2006; 395:259-266.

Eng GD, Epstein BS, Engel WK, McKay DW, McKay R. Malignant hyperthermia and central core disease in a child with congenital dislocating hips. *Arch Neurol*. 1978; 35:189-197.

European Malignant Hyperpyrexia Group. A protocol for the investigation of malignant hyperpyrexia (MH) susceptibility. *Br J Anaesth*. 1984; 56:1267-1269.

Fananapazir L, Dalakas MC, Cyran F, Cohn G, Epstein ND. Missense mutations in the beta-myosin heavy-chain gene cause central core disease in hypertrophic cardiomyopathy. *Proc Natl Acad Sci USA*. 1993; 90:3993-3997.

Fardeau M, Tome F. Congenital myopathies. In *Myology*. Edited by Engel AG, Franzini-Armstrong C. New York. 1994. 1487–1533.

Feng W, Tu J, Yang T, Vernon PS, Allen PD, Worley PF, Pessah IN. Homer regulates gain of ryanodine receptor type 1 channel complex. *J Biol Chem*. 2002; 277:44722-44730.

Fessenden JD, Perez CF, Goth S, Pessah IN, Allen PD. Identification of a key determinant of ryanodine receptor type 1 required for activation by 4-chloro-m-cresol. *J Biol Chem*. 2003; 278: 28727-28735.

Ferreiro A, Quijano-Roy S, Pichereau C, Moghadaszadeh B, Goemans N, Boönnemann C, Jungbluth H, Straub V, Villanova M, Leroy JP, Romero NB, Martin JJ, Muntoni F, Voit T, Estournet B, Richard P, Fardeau M, Guicheney P. Mutations of the selenoprotein N gene, which is implicated in rigid spine muscular dystrophy, cause the classical phenotype of multiminicore disease: reassessing the nosology of early-onset myopathies. *Am J Hum Genet*. 2002a; 71:739-749.

Ferreiro A, Monnier N, Romero NB, Leroy JP, Boönnemann C, Haenggeli CA, Straub V, Voss WD, Nivoche Y, Jungbluth H, Lemainque A, Voit T, Lunardi J, Fardeau M, Guicheney P. A recessive form of central core disease, transiently presenting as multi-minicore disease, is associated with a homozygous mutation in the ryanodine receptor type 1 gene. *Ann Neurol*. 2002b; 51:750-759.

Ferreiro A, Estournet B, Chateau D, Ferreiro A, Estournet B, Château D, Romero NB, Laroche C, Odent S, Toutain A, Cabello A, Fontan D, dos Santos HG, Haenggeli CA, Bertini E, Urtizberea JA, Guicheney P, Fardeau M: Multi-minicore disease –

searching for boundaries: phenotype analysis of 38 cases. *Ann Neurol.* 2000; 48:745-757.

Fill M and Copello JA. Ryanodine receptor calcium release channels. *Physiol Rev.* 2002; 82:893-922.

Fischer D, Herasse M, Ferreiro A, Barragan-Campos HM, Chiras J, Viollet L, Maugendre S, Leroy JP, Monnier N, Lunardi J, Guicheney P, Fardeau M, Romero NB. Muscle imaging in dominant core myopathies linked or unlinked to the ryanodine receptor 1 gene. *Neurology.* 2006; 67:2217-2220.

Fortunato G, Carsana A, Tinto N, Brancadoro V, Canfora G, Salvatore F. A case of discordance between genotype and phenotype in a malignant hyperthermia family. *Eur J Hum Genet.* 1999; 7:415-420.

Fortunato G, Berruti R, Brancadoro V, Fattore M, Salvatore F, Carsana A. Identification of a novel mutation in the ryanodine receptor gene (RYR1) in a malignant hyperthermia Italian family. *Eur J Hum Genet.* 2000; 8:149-152.

Frank JP, Harati Y, Butler IJ, Nelson TE, Scott CI. Central core disease and malignant hyperthermia syndrome. *Ann Neurol.* 1980; 7:11-17.

Franzini-Armstrong C, Kenney LJ, and Varriano-Marston E. The structure of calsequestrin in triads of vertebrate skeletal muscle: a deep-etch study. *J Cell Biol.* 1987; 5:49-56.

Furniss P. The etiology of malignant hyperpyrexia. *Proc R Soc Med.* 1971; 64:216-220.

Fujimura-Kiyono C, Racz G, Nishino I. Myotubular/centronuclear myopathy and central core disease. 2008; 56 325-332.

Gao L, Balshaw D, Xu L, Tripathy A, Xin C, Meissner G. Evidence for a role of the lumenal M3-M4 loop in skeletal muscle Ca^{2+} release channel (ryanodine receptor) activity and conductance. *Biophys J.* 2000; 79:828-840.

García J, Schneider MF. Suppression of calcium release by calcium or procaine in voltage clamped rat skeletal muscle fibres. *J Physiol.* 1995; 485: 437-445.

Gillard EF, Otsu K, Fujii J, Khanna VK, de Leon S, Derdemezi J, Britt BA, Duff CL, Worton RG, MacLennan DH: A substitution of cysteine for arginine 614 in the ryanodine receptor is potentially causative of human malignant hyperthermia. *Genomics.* 1991; 11:751-755.

Girard T, Cavagna D, Padovan E, Spagnoli G, Urwyler A, Zorzato F, Treves S . B-lymphocytes from malignant hyperthermia-susceptible patients have an increased sensitivity to skeletal muscle ryanodine receptor activators. *J. Biol Chem.* 2001; 276: 48077-48082.

Goebel H. Congenital myopathies in the new millennium. *J Child Neurol.* 2005; 20:94-101.

Goonasekera SA, Beard NA, Groom L, Kimura T, Lyfenko AD, Rosenfeld A, Marty I, Dulhunty AF, Dirksen RT. Triadin binding to the C-terminal luminal loop of the ryanodine receptor is important for skeletal muscle excitation contraction coupling. *J Gen Physiol.* 2007; 130:365-378.

Guo W, and Campbell K P. Association of triadin with the ryanodine receptor and calsequestrin in the lumen of the sarcoplasmic reticulum. *J Biol Chem.* 1995; 270:9027-9030.

Gurgel-Giannetti J, Zatz M, Vainzof M. Central core disease due to recessive mutations in RYR1 gene: is it more common than described? *Muscle Nerve.* 2007; 35:670-672.

Guis S, Figarella-Branger D, Monnier N, Bendahan D, Kozak-Ribbens G, Mattei JP, Lunardi J, Cozzone PJ, Pellissier JF. Multimimicore disease in a family susceptible to malignant hyperthermia: histology, in vitro contracture tests, and genetic characterization. *Arch Neurol.* 2004; 61:106-113.

Gyorke I and Gyorke S. Regulation of the cardiac ryanodine receptor channel by luminal Ca^{2+} involves luminal Ca^{2+} sensing sites. *Biophys J.* 1998; 75:2801-2810.

Gyorke I, Hester N A, Jones L R, and Gyorke S. The role of calsequestrin, triadin, and junctin in conferring cardiac ryanodine receptor responsiveness to luminal calcium. *Biophys J.* 2004; 86:2121-2128.

Hakamata Y, Nakai J, Takeshima H and Imoto K. Primary structure and distribution of a novel ryanodine receptor/calcium release channel from rabbit brain. *FEBS Lett.* 1992; 312:229-235.

Halsall PJ, Bridges LR, Ellis FR, Hopkins PM. Should patients with central core disease be screened for malignant hyperthermia? *J Neurol Neurosurg Psychiatry.* 1996; 61:119-121.

Herrmann-Frank A, Lüttgau HC, Stephenson DG. Caffeine and excitation-contraction coupling in skeletal muscle: a stimulating story. *J Muscle Res Cell Motil.* 1999; 20: 223-237.

Jacobson AR, Moe ST, Allen PD, Fessenden JD. Structural determinants of 4-chloro-m-cresol required for activation of ryanodine receptor type 1. *Mol Pharmacol.* 2006; 70: 259-266.

Jungbluth H, Lillis S, Zhou H, Abbs S, Sewry C, Swash M, Muntoni F. Late-onset axial myopathy with cores due to a novel heterozygous dominant mutation in the skeletal muscle ryanodine receptor (RYR1) gene. *Neuromuscul Disord.* 2009; 19: 344-347.

Jungbluth H. Central core disease orphanet. *J Rare Dis.* 2007; 15:2-25.

Jungbluth H, Lillis S, Zhou H, Abbs S, Sewry C, Swash M, Muntoni F. Late-onset axial myopathy with cores due to a novel heterozygous dominant mutation in the skeletal muscle ryanodine receptor (RYR1) gene. *Neuromuscul Disord.* 2009; 19: 344-7.

Jungbluth H, Zhou H, Sewry CA, Robb S, Treves S, Bitoun M, Guicheney P, Buj-Bello A, Bönnemann C, Muntoni F. Centronuclear myopathy due to a de novo dominant mutation in the skeletal muscle ryanodine receptor (RYR1) gene. *Neuromuscul Disord.* 2007; 17:338-345.

Jungbluth H, Sewry CA, Muntoni F. What's new in neuromuscular disorders? The congenital myopathies. *Eur J Paediatr Neurol.* 2003; 7: 23-30.

Jungbluth H, Zhou H, Hartley L, Halliger-Keller B, Messina S, Longman C, Brockington M, Robb SA, Straub V, Voit T, Swash M, Ferreira A, Bydder G, Sewry CA, Müller C, Muntoni F. Minicore myopathy with ophthalmoplegia caused by mutations in the ryanodine receptor type 1 gene. *Neurology* 2005; 65:1930-1935.

Jungbluth H, Beggs A, Bonnemann C, Bushby K, Ceuterick-de Groote C, Estournet-Mathiaud B, Goemans N, Guicheney P, Lescure A, Lunardi J, Muntoni F, Quinlivan R, Sewry C, Straub V, Treves S, Ferreira A. *Neuromuscul Disord.* 2004; 14:754-766.

Jungbluth H, Müller CR, Halliger-Keller B, Brockington M, Brown SC, Feng L, Chattopadhyay A, Mercuri E, Manzur AY, Ferreira A, Laing NG, Davis MR, Roper HP, Dubowitz V, Bydder G, Sewry CA, Muntoni F. Autosomal-recessive inheritance of RYR1 mutations in a congenital myopathy with cores. *Neurology.* 2002; 59:284-287.

Jungbluth H, Sewry C, Brown SC, Manzur AY, Mercuri E, Bushby K, Rowe P, Johnson MA, Hughes I, Kelsey A, Dubowitz V, Muntoni F. Minicore myopathy in children – A clinical and histopathological study of 19 cases. *Neuromuscul Disord.* 2000; 10:264-273.

Jurkat-Rott K, Lehmann-Horn F. Muscle channelopathies and critical points in functional and genetic studies. *J Clin Invest.* 2005; 115:2000-2009.

Jurkat-Rott K, McCarthy T, Lehmann-Horn F. Genetics and pathogenesis of malignant hyperthermia. *Muscle Nerve.* 2000; 23:4-17.

Jurynech MJ, Xia R, Mackrill JJ, Gunther D, Crawford T, Flanigan KM, Abramson JJ, Howard MT, Grunwald DJ. Selenoprotein N is required for ryanodine receptor calcium release channel activity in human and zebrafish muscle. *Proc Natl Acad Sci USA.* 2008; 105:12485-12490.

Kaindl AM, Ruschendorf F, Krause S, Goebel HH, Koehler K, Becker C, Pongratz D, Müller-Höcker J, Nürnberg P, Stoltenburg-Didinger G, Lochmüller H, Huebner A.

Missense mutations of ACTA1 cause dominant congenital myopathy with cores. *J Med Genet.* 2004; 41:842-848.

Kaus S J, Rockoff M A. Malignant hyperthermia. *Pediatr Clin North Am.* 1994; 41:221-237.

Klingler W, Rueffert H, Lehmann-Horn F, Girard T, Hopkins PM. Core myopathies and risk of malignant hyperthermia. *Anesth Analg.* 2009; 109:1167-1173.

Koch BM, Bertorini TE, Eng GD, Boehm R. Severe multicore disease associated with reaction to anaesthesia. *Arch Neurol.* 1985; 42:1204-1206.

Kossugue PM, Paim JF, Navarro MM, Silva HC, Pavanello RCM. XXVI Annual Meeting of European Malignant Hyperthermia Group. 2007; abs 21.

Illes D E, Lehmann F, Scherer S V, Olde Weghuis D, Suijkerbuijk R F, Heytens L, Mikala G, Schwartz A, Ellis F R, Stewart A, Deufel T, Wieringa B. Localization of the gene encoding the $\alpha 2/\delta$ subunits of the L-type voltage dependent channel to chromosome 7q and analysis of the segregation of flanking markers in MH susceptible families. *Hum Mol Genet.* 1994; 3:969-975.

Laporte J, Guiraud-Chaumeil C, Vincent MC, Mandel JL, Tanner SM, Liechti-Gallati S, Wallgren-Pettersson C, Dahl N, Kress W, Bolhuis PA, Fardeau M, Samson F, Bertini E and members of the ENMC International Consortium on Myotubular Myopathy. Mutations in the MTM1 gene implicated in X-linked myotubular myopathy. *Hum Mol Genet.* 1997; 6:1505-1511.

Laporte J, Hu LJ, Kretz C, Mandel JL, Kioschis P, Coy JF, Klauck SM, Poustka A, Dahl N. A gene mutated in X-linked myotubular myopathy defines a new putative tyrosine phosphates family conserved in yeast. *Nat Genet.* 1996; 13:175-182.

Larach MG. Standardization of the caffeine haloten muscle contracture test. North America Malignant Hyperthermia Group. *Anesth Analg.* 1989; 69:511-515.

Larach MG, Landis JR, Bunn JS, Diaz M. Prediction of malignant hyperthermia susceptibility in low-risk subjects. An epidemiologic investigation of caffeine halothane contracture responses. The North American Malignant Hyperthermia Registry. *Anesthesiology.* 1992; 76:16-27.

Lee EH, Song DW, Lee JM, Meissner G, Allen PD, Kim DH. Occurrence of atypical Ca^{2+} transients in triadin-binding deficient-RYR1 mutants. *Biochem Biophys Res Commun.* 2006; 351:909-914.

Lee EH, Rho SH, Kwon SJ, Eom SH, Allen PD, Kim do H. N-terminal region of FKBP12 is essential for binding to the skeletal ryanodine receptor. *J Biol Chem.* 2004; 18:26481-26488.

Lee JM, Rho SH, Shin DW, Cho C, Park WJ, Eom SH, Ma J, Kim DH. Negatively charged amino acids within the intraluminal loop of ryanodine receptor are involved in the interaction with triadin. *J Biol Chem*. 2004; 279:6994-7000.

Lehmann-Horn F, Jurkat-Rott K. Voltage-gated ion channels and hereditary disease. *Physiol Rev*. 1999; 79:1317-1371.

Leong P, and MacLennan DH. A 37-amino acid sequence in the skeletal muscle ryanodine receptor interacts with the cytoplasmic loop between domains II and III in the skeletal muscle dihydropyridine receptor. *J. Biol. Chem*. 1998; **273**: 7791–7794.

Levitt R, Olckers A, Meyers S, Fletcher J E, Rosemberg H, Isacs H, Meyers D A. Evidence for the localization of a malignant hyperthermia susceptibility, *locus* (MHS2) to human chromosome 17q. *Genomics*. 1992; 14:562-566.

Ludtke SJ, Serysheva II, Hamilton SL, Chiu W. The pore structure of the closed RyR1 channel. *Structure*. 2005; 13:1203-1211.

Lynch PJ, Tong J, Lehane M, Mallet A, Giblin L, Heffron JJ, Vaughan P, Zafra G, MacLennan DH, McCarthy TV. A mutation in the transmembrane/luminal domain of the ryanodine receptor is associated with abnormal Ca^{2+} release channel function and severe central core disease. *Proc Natl Acad Sci U S A*. 1999;96 :4164-9.

Ma J. Block by ruthenium red of the ryanodine-activated calcium release channel of skeletal muscle. *J Gen Physiol*. 1993; 102: 1031-1056.

Maximciuc AA, Putkey JA, Shamoo Y, Mackenzie KR. Complex of calmodulin with a ryanodine receptor target reveals a novel, flexible binding mode. *Structure*. 2006; 14: 1547-1556.

McCarthy T V, Healy J M, Heffron J J, Lehane M, Deufel T, Lehmann-Horn F, Farrall M, Johnson K. Localization of the malignant hyperthermia susceptibility *locus* to human chromosome 19q12-13.2. *Nature*. 1990; 343:562-564.

Messina S, Hartley L, Main M, Kinali M, Jungbluth H, Muntoni F, Mercuri E. Pilot trial of salbutamol in central core and multi-minicore diseases. *Neuropediatrics*. 2004; 35:262-266.

Meyers MB, Pickel VM, Sheu SS, Sharma VK, Scotto KW, Fishman GI. Association of sorcin with the cardiac ryanodine receptor. *J Biol Chem*. 1995; 270:26411-26418.

Michalatos-Beloin S, Tishkoff SA, Bentley KL, Kidd KK, Ruano G. Molecular haplotyping of genetic markers 10 kb apart by allele-specific long-range PCR. *Nucleic Acids Res*. 1996; 24: 4841-4843.

Monnier N, Marty I, Faure J, Castiglioni C, Desnuelle C, Sacconi S, Estournet B, Ferreiro A, Romero N, Laquerriere A, Lazaro L, Martin J, Morava E, Rossi A, Van Der Kooi A, De Visser M, Verschuuren C, Lunardi J. Null mutations causing depletion of

the type 1 ryanodine receptor (RYR1) are commonly associated with recessive structural congenital myopathies with cores. *Hum Mutat.* 2008; 0: 1-9.

Monnier N, Ferreiro A, Marty I, Labarre-Vila A, Mezin P, Lunardi J. A homozygous splicing mutation causing a depletion of skeletal muscle RYR1 is associated with multi-minicore disease congenital myopathy with ophthalmoplegia. *Hum Mol Genet.* 2003; 12:1171-1178.

Monnier N, Romero NB, Lerule J, Nivoche Y, Qi D, MacLennan DH, Fardeau M, Lunardi J. An autosomal dominant congenital myopathy with cores and rods is associated with a neomutation in the RYR1 gene encoding the skeletal muscle ryanodine receptor. *Hum Mol Genet.* 2000; 9:2599-2608.

Monnier N, Procaccio V, Stieglitz P, Lunardi J. Malignant hyperthermia susceptibility is associated with a mutation of α 1 subunit of human DHPR in skeletal muscle. *Am J Hum Genet.* 1997; 60:1316-1325.

Moore CP, Moore CP, Rodney G, Zhang JZ, Santacruz-Tolosa L, Strasburg G, Hamilton SL. Apocalmodulin and Ca^{2+} calmodulin bind to the same region on the skeletal muscle Ca^{2+} release channel. *Biochemistry.* 1999; 38:8532-8537.

Naguib M, Flood P, McArdle JJ, Brenner HR. Advances in neurobiology of the neuromuscular junction: implications for the anesthesiologist. *Anesthesiology.* 2002; 96:202-231.

Nakai J, Imagawa T, Hakamata Y, Shigekawa M, Takeshima H and Numa S. Primary structure and functional expression from cDNA of the cardiac ryanodine receptor/calcium release channel. *FEBS Lett.* 1990; 271:169-177.

Nicot AS, Toussaint A, Tosch V, Kretz V, Wallgren-Pettersson C, Iwarsson E, Kingston E, Garnier JM, Biancalana V, Oldfors A, Mandel JL & Jocelyn Laporte. Mutations in amphiphysin 2 (BIN1) disrupt interaction with dynamin 2 and cause autosomal recessive centronuclear myopathy. *Nat Genet.* 2007; 39:1134-1139.

North K. Congenital myopathies. In: Engle A, Franzini-Armstrong C, eds. *Myology: basic and clinical.* 3rd ed. New York: McGraw-Hill, 2004:1473-1533.

Oba T, Murayama T, Ogawa Y. Redox states of type 1 ryanodine receptor alter Ca^{2+} release channel response to modulators. *Am J Physiol Cell Physiol.* 2002; 282:684-692.

Oh SJ, Danon MJ. Nonprogressive congenital neuromuscular disease with uniform type 1 fiber. *Arch Neurol* 1983; 40: 147-50.

Oyamada , Oguchi K, Saitoh N, Yamazawa T, Hirose K, Kawana Y, Wakatsuki K, Tagami M, Hanaoka K, Endo M, Iino M. *Jpn. J. Pharmacol.* Novel mutations in C-terminal channel region of the ryanodine receptor in malignant hyperthermia patients. 2002; 88: 159-166

Ørding H, Brancadoro V, Cozzolino S, Ellis FR, Glauber V, Gonano EF, Halsall PJ, Hartung E, Heffron JJ, Heytens L, Kozak-Ribbens G, Kress H, Krivosic-Horber R, Lehmann-Horn F, Mortier W, Nivoche Y, Ranklev-Twetman E, Sigurdsson S, Snoeck M, Stieglitz P, Tegazzin V, Urwyler A, Wappler F. In vitro contracture test for diagnosis of malignant hyperthermia following the protocol of the European MH Group: Results of testing patients surviving fulminant MH and unrelated low-risk subjects. The European Malignant Hyperthermia Group. *Acta Anaesthesiol Scand*. 1997; 41:955-966.

Osada H, Masuda K, Seki K, Sekiya S. Multi-minicore disease with susceptibility to malignant hyperthermia in pregnancy. *Gynecol Obstet Invest*. 2004; 58:32-35.

Otsu K, Willard HF, Khanna VK, Zorzato F, Green NM and MacLennan DH. Molecular cloning of cDNA encoding the Ca^{2+} release channel (ryanodine receptor) of rabbit cardiac muscle sarcoplasmic reticulum. *J Biol Chem*. 1990; 265:13472-13483.

Pallagi E, Molnar M, Molnar P, Dioszeghy P. Central core and nemaline rods in the same patient. *Acta Neuropathol*. 1998; 96:211-214.

Paul-Pletzer K, Yamamoto T, Bhat MB, Ma J, Ikemoto N, Jimenez LS, Morimoto H, Williams P G, Parness J. Identification of a dantrolene-binding sequence on the skeletal muscle ryanodine receptor. *J Biol Chem*. 2002; 277:34918-34923.

Pirone A, Schredelseker J, Tuluc P, Gravino E, Fortunato G, Flucher B E, Carsana A, Salvatore F, Grabner M. Identification and functional characterization of the malignant hyperthermia mutation T1354S in the 1s subunit of the skeletal muscle voltage-gated calcium channel. XXVI Annual Meeting of European Malignant Hyperthermia Group; 2007, Siena.

Phillips MS, Fuji J, Khanna VK, DeLeon S, Yokobata K, de Jong PJ and MacLennan DH. The structural organization of the human skeletal muscle ryanodine receptor (RYR1) gene. *Genomics*. 1996; 34:24-41.

Quane KA, Healy JM, Keating KE, Manning BM, Couch FJ, Palmucci LM, Doriguzzi C, Fagerlund TH, Berg K, Ording H, Bendixen D, Mortier W, Linz U, Muller CR, McCarthy TV. Mutations in the ryanodine receptor gene in central core disease and malignant hyperthermia. *Nat Genet*. 1993; 5:51-55.

Qin J, Valle G, Nani A, Chen H, Ramos-Franco J, Nori A, Volpe P and Fill M. Ryanodine receptor luminal Ca^{2+} regulation: swapping calsequestrin and channel isoforms. *Biophys J*. 2009; 97:1961-1970.

Radermacher M, Rao V, Grassucci R, Frank J, Timmerman AP, Wagenknecht T. Cryo-electron microscopy and three-dimensional reconstruction of the calcium release channel/ryanodine receptor from skeletal muscle. *J Cell Biol*. 1994; 127:411-423.

Ramachandran S, Serohijos AW, Xu L, Meissner G, Dokholyan NV. A structural model of the pore-forming region of the skeletal muscle ryanodine receptor (RyR1). *PLoS Comput Biol.* 2009; 5:e1000367.

Reiken S, Lacampagne A, Zhou H, Kherani A, Lehnart SE, Ward C, Huang F, Gaburjakova M, Gaburjakova J, Rosemblyt N, Warren MS, He KL, Yi GH, Wang J, Burkhoff D, Vassort G, Marks AR. PKA phosphorylation activates the calcium release channel (ryanodine receptor) in skeletal muscle: defective regulation in heart failure. *J Cell Biol.* 2003; 160:919-928.

Richter M, Schleithoff L, Deufel T, Lehmann-Horn F, Herrmann-Frank A.. Functional characterization of a distinct ryanodine receptor mutation in human malignant hyperthermia-susceptible muscle. *J Biol Chem.*1997; 272: 5256-5260.

Robinson R, Carpenter D, Shaw MA, Halsall J, Hopkins P. Mutations in RYR1 in malignant hyperthermia and central core disease. *Hum Mutat.* 2006; 27:977-989.

Robinson RL, Anetseder MJ, Brancadoro V, van Broekhoven C, Carsana A, Censier K, Fortunato G, Girard T, Heytens L, Hopkins PM, Jurkat-Rott K, Klinger W, Kozak-Ribbens G, Krivosic R, Monnier N, Nivoche Y, Olthoff D, Rueffert H, Sorrentino V, Tegazzin V, Mueller CR. Recent advances in the diagnosis of malignant hyperthermia susceptibility: how confident can we be of genetic testing? *Eur J Hum Genet.* 2003; 11: 342-348.

Robinson R, Monnier N, Wolz W, Jung M, Reis A, Nuernberg G, Curran J, Monsieurs K. A genome wide search for susceptibility *loci* in three european malignant hyperthermia pedigrees. *Hum Mol Genet.* 1997; 6:953-961.

Rossi D, De Smet P, Lyfenko A, Galli L, Lorenzini S, Franci D, Petrioli F, Orrico A, Angelini C, Tegazzin V, Dirksen R, Sorrentino V. A truncation in the RYR1 gene associated with central core lesions in skeletal muscle fibres. *J Med Genet.* 2007; 44: e67.

Rossi D, Sorrentino V. Molecular genetics of ryanodine receptors Ca²⁺-release channels. *Cell Calcium.* 2002 ; 32: 307-319.

Rueffert H, Olthoff D, Deutrich C, Meinecke C D, Froster U G. Mutation screening in the ryanodine receptor 1 gene (RYR1) in patients susceptible to malignant hyperthermia who show definite IVCT results: identification of three novel mutations. *Acta Anaesthesiol Scand.* 2002; 46:692-698.

Salama G, Abramson J J, Pike G K. Sulphydryl reagents trigger Ca²⁺ release from the sarcoplasmic reticulum of skinned rabbit psoas fibres. *J Physiol.* 1992; 454:389-420.

Sambuughin N, Nelson T E, Jankovic J, Xin C, Meissner G, Mullakandov M, Ji J, Rosenberg H, Sivakumar K, Goldfarb L G. Identification and functional characterization of a novel ryanodine receptor mutation causing malignant hyperthermia in North American and South American families. *Neuromuscul Disord*. 2001; 11: 530-537.

Samsó M, Feng W, Pessah IN, Allen PD. Coordinated movement of cytoplasmic and transmembrane domains of RyR1 upon gating. *PLoS Biol*. 2009; 7:e85.

Samsó M, Wagenknecht T, Allen PD. Internal structure and visualization of transmembrane domains of the RyR1 calcium release channel by cryo-EM. *Nat Struct Mol Biol*. 2005; 12:539-544.

Samsó M, Shen X, Allen PD. Structural characterization of the RyR1-FKBP12 interaction. *J Mol Biol*. 2006; 356:917-927.

Samsó M and Wagenknecht T. Apocalmodulin and Ca²⁺-calmodulin bind to neighboring locations on the ryanodine receptor. *J Biol Chem*. 2002; 277:1349-1353.

Sanoudou D, Beggs AH. Clinical and genetic heterogeneity in nemaline myopathy - a disease of skeletal muscle thin filaments. *Trends Mol Med*. 2001; 7:362-368.

Sato I, Wu S, Ibarra MC, Hayashi YK, Fujita H, Tojo M, Oh SJ, Nonaka I, Noguchi S, Nishino I. Congenital neuromuscular disease with uniform type 1 fiber and RYR1 mutation. *Neurology*. 2008; 70: 99-100.

Scacheri PC, Hoffman EP, Fratkin JD, Semino-Mora C, Senchak A, Davis MR, Laing NG, Vedanarayanan V, Subramony SH. A novel ryanodine receptor gene mutation causing both cores and rods in congenital myopathy. *Neurology*. 2000; 55:1689-1696.

Sei Y, Brandom BW, Bina S, Hosoi E, Gallagher KL, Wyre HW, Pudimat PA, Holman SJ, Venzon DJ, Daly JW, Muldoon S. Patients with malignant hyperthermia demonstrate an altered calcium control mechanism in B lymphocytes. *Anaesthesiology*. 2002. 97: 1052–1058.

Sei Y, Gallagher KL, and Basile AS. Skeletal muscle type ryanodine receptor is involved in calcium signaling in human B lymphocytes. *J Biol Chem*. 1999; 274:5995-6002.

Serysheva II, Ludtke SJ, Baker ML, Cong Y, Topf M, Eramian D, Sali A, Hamilton SL, Chiu W. Subnanometer-resolution electron cryomicroscopy-based domain models for the cytoplasmic region of skeletal muscle RyR channel. *Proc Natl Acad Sci U S A*. 2008; 105:9610-9615.

Serysheva II, Orlova EV, Chiu W, Sherman MB, Hamilton SL, van Heel M. Electron cryomicroscopy and angular reconstitution used to visualize the skeletal muscle calcium release channel. *Nat Struct Biol*. 1995; 2:18-24.

Shen X, Franzini-Armstrong C, Lopez JR, Jones LR, Kobayashi YM, Wang Y, Kerrick WG, Caswell AH, Potter JD, Miller T, Allen PD, Perez CF. Triadins modulate intracellular Ca²⁺ homeostasis but are not essential for excitation-contraction coupling in skeletal muscle. *J Biol Chem*. 2007; 282:37864-37874.

Shuaib A, Paasuke RT, Brownell KW: Central core disease. Clinical features in 13 patients. *Medicine*. 1987; 66:389-396.

Smith A, Nelson RJ. Capillary electrophoresis of DNA. *Curr Protoc Nucleic Acid Chem*. 2003;10: 10.9.

Sorrentino V, Giannini G, Malzac P and Mattei MG. Localization of a novel ryanodine receptor gene (RYR3) to human chromosome 15q14-q15 by in situ hybridization. *Genomics*. 1993; 18:163-165.

Sudbrak R, Procaccio V, Curran J. Mapping of a further MH susceptibility *locus* to chromosome 3q 13.1. *Am J Hum Genet*. 1995; 56:684-691.

Sun J, Xu L, Eu J P, Stamler J S, Meissner G. Classes of thiols that influence the activity of the skeletal muscle calcium release channel. *J Biol Chem*. 2001 a; 276:15625-15630.

Sun J, Xin C, Eu JP, Stamler JS, Meissner G. Cysteine-3635 is responsible for skeletal muscle ryanodine receptor modulation by NO. *Proc Natl Acad Sci U S A*. 2001 b; 98:11158-11162.

Sutko JL, Airey JA, Welch W, Ruest L. The pharmacology of ryanodine and related compounds. *Pharmacol Rev*. 1997; 49:53-98.

Sutko, J.L., and J.A. Airey. Ryanodine receptor Ca²⁺ release channels: does diversity in form equal diversity in function? *Physiol Rev*. 1996; 76:1027-1071.

Takehima H, Komazaki S, Nishi M, Iino M, Kangawa K. Junctophilins: a novel family of junctional membrane complex proteins. *Mol Cell*. 2000; 6:11-22.

Takehima H, Nishimura S, Matsumoto T, Ishida H, Kangawa K, Minamino N, Matsuo H, Ueda M, Hanaoka M, Hirose T and Numa S. Primary structure and expression from complementary DNA of skeletal muscle ryanodine receptor. *Nature*. 1989; 339:439-445.

Tilgen N, Zorzato F, Halliger-Keller B, Muntoni F, Sewry C, Palmucci LM, Schneider C, Hauser E, Lehmann-Horn F, Müller CR, Treves S. Identification of four novel mutations in the C-terminal membrane spanning domain of the ryanodine receptor 1: association with central core disease and alteration of calcium homeostasis. *Hum Mol Genet*. 2001;10: 2879-2887.

Tijskens P, Jones L R, Franzini-Armstrong C. Junctin and calsequestrin overexpression in cardiac muscle: the role of junctin and the synthetic and delivery pathways for the two proteins. *J Mol Cell Cardiol*. 2003; 35:961-974.

Tong J, McCarthy TV, MacLennan DH. Measurement of resting cytosolic Ca^{2+} concentrations and Ca^{2+} store size in HEK-293 cells transfected with malignant hyperthermia or central core disease mutant Ca^{2+} release channels. *J Biol Chem.* 1999; 274: 693-702.

Tong J, Oyamada H, Demaureux N, Grinstein S, McCarthy TV, MacLennan DH. Caffeine and halothane sensitivity of intracellular Ca^{2+} release is altered by 15 calcium release channel (ryanodine receptor) mutations associated with malignant hyperthermia and/or central core disease. *J. Biol. Chem.* 1997; 272:26332-26339.

Treves S, Anderson AA, Ducreux S, Divet A, Bleunven C, Grasso C, Paesante S, Zorzato F: Ryanodine receptor 1 mutations, dysregulation of calcium homeostasis and neuromuscular disorders. *Neuromuscul Disord.* 2005; 15:577-587.

Treves S, Feriotto G, Moccagatta L, Gambari R, Zorzato F. Molecular cloning, expression, functional characterization, chromosomal localization, and gene structure of junctate, a novel integral calcium binding protein of sarco(endo)plasmic reticulum membrane. *J Biol Chem.* 2000; 275:39555-39568.

Treves S, Scutari E, Robert M, Groh S, Ottolia M, Prestipino G, Ronjat M, Zorzato F. Interaction of S100A1 with the Ca^{2+} release channel (ryanodine receptor) of skeletal muscle. *Biochemistry.* 1997; 36:11496-11503.

Tripathy A and Meissner G. Sarcoplasmic reticulum luminal Ca^{2+} has access to cytosolic activation and inactivation sites of skeletal muscle Ca^{2+} release channel. *Biophys J.* 1996; 70:2600-2615.

Urwyler A, Deufel T, McCarthy T, West S; European Malignant Hyperthermia Group. Guidelines for molecular genetic detection of susceptibility to malignant hyperthermia. *Br J Anaesth.* 2001; 86: 283-287.

von der Hagen M, Kress W, Hahn G, Brocke K S, Mitzscherling P, Huebner A, Muller-Reible C, Stoltenburg-Didingere G, Kaindl A M. Novel RYR1 missense mutation causes core rod myopathy. *Eur J Neurol.* 2008; 15: e31–e32.

Voss AA, Lango J, Ernst-Russell M, Morin D, Pessah IN. Identification of hyperreactive cysteines within ryanodine receptor type 1 by mass spectrometry. *J Biol Chem.* 2004; 279: 34514-34520.

Wagenknecht T and Samsò M. Three-dimensional reconstruction of ryanodine receptors. *Front Biosci.* 2002; 7:1464-1474.

Wagenknecht T, Radermacher M, Grassucci R, Berkowitz J, Xin HB, Fleischer S. Locations of calmodulin and FK506-binding protein on the three-dimensional architecture of the skeletal muscle ryanodine receptor. *J Biol Chem.* 1997; 272: 32463-32471.

Wagenknecht T, Grassucci R, Berkowitz J, Wiederrecht GJ, Xin HB and Fleischer S. Cryoelectron microscopy resolves FK506-binding protein sites on the skeletal muscle ryanodine receptor. *Biophys J*. 1996; 70:1709-1715.

Wallgren-Pettersson C. Congenital nemaline myopathy: a longitudinal study. In *Commentationes Physico Mathematicae*. University of Helsinki; 1990.

Wallgren-Pettersson C. 72nd ENMC International Workshop: myotubular myopathy. *Neuromuscul Disord*. 2000; 10:525-529.

Wallgren-Pettersson C, Laing NG: 138th ENMC Workshop: nemaline myopathy. *Neuromuscul Disord*. 2006; 16:54-60.

Wallgren-Pettersson C, Pelin K, Hilpela P, Donner K, Porfirio B, Graziano C, Swoboda KJ, Fardeau M, Urtizberea JA, Muntoni F, Sewry C, Dubowitz V, Iannaccone S, Minetti C, Pedemonte M, Seri M, Cusano R, Lammens M, Castagna-Sloane A, Beggs AH, Laing NG, de la Chapelle A. Clinical and genetic heterogeneity in autosomal recessive nemaline myopathy. *Neuromuscul Disord*. 1999; 9:564-572.

Wang S, Trumble W R, Liao H, Wesson C R, Dunker A K, and Kang C H. Crystal structure of calsequestrin from rabbit skeletal muscle sarcoplasmic reticulum. *Nat Struct Biol*. 1998; 5:476-483.

Wehner M, Rueffert H, Koenig F, Neuhaus J, Olthoff D. Increased sensitivity to 4-chloro-m-cresol and caffeine in primary myotubes from malignant hyperthermia susceptible individuals carrying the ryanodine receptor 1 Thr2206Met (C6617T) mutation. *Clin Genet*. 2002; 62: 135-146.

Wu S, Ibarra MCA, Malicdan MCV, Murayama K, Ichihara Y, Kikuchi H, Nonaka I, Noguchi S, Hayashi YK, Nishino I: Central core disease is due to RYR1 mutations in more than 90% of patients. *Brain*. 2006; 129:1470-1480.

Xia R, Stangler T, Abramson J. Skeletal muscle ryanodine receptor is a redox sensor with a well defined redox potential that is sensitive to channel modulators. *J Biol Chem*. 2000; 275:36556-36561.

Yamaguchi N, Xin C, Meissner G Identification of apocalmodulin and Ca²⁺-calmodulin regulatory domain in skeletal muscle Ca²⁺ release channel, ryanodine receptor. *J Biol Chem*. 2001; 276:22579-22585.

Zanoteli E, Vergani N, Campos Y, Vainzof M, Oliveira AS, d'Azzo A. Mitochondrial alterations in dynamin 2-related centronuclear myopathy. *Arq Neuropsiquiatr*. 2009; 67:102-104.

Zhang L, Franzini-Armstrong C, Ramesh V, And Jones L R. Structural alterations in cardiac calcium release units resulting from overexpression of junctin. *J Mol Cell Cardiol*. 2001; 33:233-247.

- Zhang L, Kelley J, Schmeisser G, Kobayashi Y M and Jones L R: Complex formation between junctin, triadin, calsequestrin, and the ryanodine receptor. Proteins of the cardiac junctional sarcoplasmic reticulum membrane. *J Biol Chem.* 1997; 272:23389-23397.
- Zhang Y, Chen HS, Khanna VK, De Leon S, Phillips MS, Schappert K, Britt BA, Browell AK, MacLennan DH. A mutation in the human ryanodine receptor gene associated with central core disease. *Nat Genet.* 1993; 5:46-50.
- Zhang M, Tanaka T, Ikura M. Calcium-induced conformational transition revealed by the solution structure of apo calmodulin. *Nature Struct Biol.* 1995; 2:758-767.
- Zhou H, Jungbluth H, Sewry CA, Feng L, Bertini E, Bushby K, Straub V, Roper H, Rose MR, Brockington M, Kinali M, Manzur A, Robb S, Appleton R, Messina S, D'Amico A, Quinlivan R, Swash M, Müller CR, Brown S, Treves S, Muntoni F. Molecular mechanisms and phenotypic variation in RYR1-related congenital myopathies. *Brain.* 2007; 130:2024-2036.
- Zhou H, Brockington M, Jungbluth H, Monk D, Stanier P, Sewry CA, Moore GE, Muntoni F. Epigenetic allele silencing unveils recessive RYR1 mutations in core myopathies. *Am J Hum Genet.* 2006a; 79:859-868.
- Zhou H, Yamaguchi N, Xu L, Wang Y, Sewry C, Jungbluth H, Zorzato F, Bertini E, Muntoni F, Meissner G, Treves S. Characterization of recessive RYR1 mutations in core myopathies. *Hum Mol Genet.* 2006b; 15:2791-2803.
- Zimanyi I, Buck E, Abramson JJ, Mack MM, Pessah IN. Ryanodine induces persistent inactivation of the Ca²⁺ release channel from skeletal muscle sarcoplasmic reticulum. *Mol Pharmacol.* 1992; 42:1049-1057.
- Zorzato F, Delbono O, Treves S, Nishi M, Takeshima H. Modulation of skeletal muscle excitation contraction coupling by protein components of the sarcoplasmic reticulum junctional face membrane. *IUPS.* 2009; Kyoto.
- Zorzato F, Jungbluth H, Zhou H, Muntoni F, Treves S. Functional effects of mutations identified in patients with multiminicore disease. *IUBMB Life.* 2007; 59:14-20.
- Zorzato F, Scutari E, Tegazzin V, Clementi E, Treves S. Chlorocresol: an activator of ryanodine receptor-mediated Ca²⁺ release. *Mol Pharmacol.* 1993; 44: 1192-11201.
- Zorzato F, Fuji J, Otsu K, Phillips M, Green NM, Lai FA, Meissner G, MacLennan DH. Molecular cloning of cDNA encoding human and rabbit forms of the calcium release channel (ryanodine receptor) of skeletal muscle sarcoplasmic reticulum. *J Biol Chem.* 1990; 265:2244-2256.
- Zucchi R and Ronca-Testoni S. The sarcoplasmic reticulum Ca²⁺ channel/ryanodine receptor: modulation by endogenous effectors, drugs and disease states. *Pharmacol Rev.* 1997; 49:1-51.

Zullo A. Identificazione e caratterizzazione funzionale di mutazioni del gene RYR1 associate all'Ipertermia maligna. 2006; PhD thesis University of Naples "Federico II".

Zullo A, Klingler W, De Sarno C, Ferrara M, Fortunato G, Perrotta G, Gravino E, Di Noto R, Lehmann-Horn F, Melzer W, Salvatore F, Carsana A. Functional characterization of ryanodine receptor (RYR1) sequence variants using a metabolic assay in immortalized B-lymphocytes. *Hum. Mutat.* 2009; 30:E575-90.

Zullo A, Klingler W, De Sarno C, Ferrara M, Fortunato G, Perrotta G, Gravino E, Di Noto R, Lehmann-Horn F, Melzen W, Salvatore F, Carsana A. Mutations in the *RYR1* gene and their functional characterization in immortalized B-lymphocytes by detection of proton release rate. XXVI Annual Meeting of European Malignant Hyperthermia Group; 20-23 Maggio 2007, Siena; abs 21.

APPENDIX

LIST OF PAPERS, ORAL COMUNICATIONS AND POSTERS

Zullo A, Klingler W, De Sarno C, Ferrara M, Fortunato G, Perrotta G, Gravino E, Di Noto R, Lehmann-Horn F, Melzen W, Salvatore F, Carsana A. Functional characterization of ryanodine receptor (RYR1) sequence variants using a metabolic assay in immortalized B-lymphocytes. *Hum Mutat.* 2009; 30: E575-90.

Zullo A, Klingler W, De Sarno C, Ferrara M, Fortunato G, Perrotta G, Gravino E, Di Noto R, Lehmann-Horn F, Melzen W, Salvatore F, Carsana A. Mutations in the *RYR1* gene and their functional characterization in immortalized B-lymphocytes by detection of proton release rate. XXVI Annual Meeting of European Malignant Hyperthermia Group; 20-23 Maggio 2007, Siena; abs 21.

Perrotta G, Zullo A, Puca A, Ferrara M, Langella M, Del Vecchio L, Salvatore F, Carsana A. Sequence variants of the RYR1 gene in a patient with Central Core Disease. SIBBM Seminar "Frontiers in Molecular Biology"; 4-6 Giugno 2009, Napoli; P1.32.

Perrotta G, Zullo A, De Sarno C, Ferrara M, Puca A, Langella M, Del Vecchio L, Carsana A, Salvatore F. A novel insertion mutation in C-terminal region of RYR1 in a Central Core Disease patient. Retreat del Dipartimento di Biochimica e Biotecnologie Mediche Università Federico II di Napoli; 4-5 Aprile 2008, Napoli; P76.

This work has been carried out at the Department of Biochemistry and Medical Biotechnology, University of Naples "Federico II" and the CEINGE Biotecnologie Avanzate, Naples.

